NTNU – Trondheim
Norwegian University of
Science and Technology

Vortex Induced Vibrations in Fish Farm Structural Elements

Therese Veland Wergeland

Marine Technology
Submission date: June 2015
Supervisor: Carl Martin Larsen, IMT

Norwegian University of Science and Technology
Department of Marine Technology

NTNU Trondheim
Norwegian University of Science and Technology
Faculty of Engineering Science and Technology
Department of MarineTechnology

M.Sc. Thesis 2015

for

Therese Wergeland

Vortex Induced Vibrations in Fish Farm Structural Elements

Fish farm structures are exposed to waves and currents, and all structural elements must be designed to survive expected load conditions during their lifetime. One type of dynamic response that normally is disregarded in design analyses is vortex induced vibrations (VIV). This type of response may, however, occur in the heavy ring that hangs beneath the net. The aim of the present project is to carry out VIV analysis for this part of a fish farm system.

The purpose of this ring is to limit the distortion of the net in strong currents. The cross-section of the ring is normally circular and made of plastic material. The eigenfrequencies and mode shapes will depend on the dimensions and material properties, but will also be strongly influenced by the axial forces in the ring. These forces must be determined by a global analysis of the total cage system, which therefore must be carried out prior to a VIV analysis of the ring.

The SIMA program system including RIFLEX and VIVANA can be used for static and dynamic analysis of fish farm systems and calculation of VIV. It is, however, difficult to define a good global model for fish farms by using RIFLEX. AQUASIM, developed by the company Aquastructures, is a tailor-made program for this type of structures, and is used by the company Aqualine for the design of fish farms. The present project is proposed by Aqualine, who will provide a global model for a typical fish farm. A free license for use of AQUASIM in the work is provided by Aquastructures.

The work may be carried out in steps as follows:

1. Literature study that should include a limited survey of fish farm structures and methods for calculation of vortex induced vibrations.

2. Define a case study and apply AQUASIM for global analyses of a typical cage system with varying current velocity

3. Define a local model of the weight ring including boundary conditions that replace the net structure. The local model should be used in RIFLEX for a static analysis prior to the VIV analyses in VIVANA.

The work may prove to be more extensive than anticipated. Some topics may therefore be left out after discussion with the supervisor without any negative influence on the grading.

The candidate should in her/his report give a personal contribution to the solution of the problem formulated in this text. All assumptions and conclusions must be supported by mathematical models and/or references to physical effects in a logical manner.

The candidate should apply all available sources to find relevant literature and information on the actual problem.

The report should be well organized and give a clear presentation of the work and all conclusions. It is important that the text is well written and that tables and figures are used to support the verbal presentation. The report should be complete, but still as short as possible.

The final report must contain this text, an acknowledgement, summary, main body, conclusions and suggestions for further work, symbol list, references and appendices. All figures, tables and equations must be identified by numbers. References should be given by author name and year in the text, and presented alphabetically by name in the reference list. Two copies of the report must be submitted unless otherwise agreed with the supervisor.

The supervisor may require that the candidate should give a written plan that describes the progress of the work after having received this text. The plan may contain a table of content for the report and also assumed use of computer resources.

From the report, it should be possible to identify the work carried out by the candidate and what has been found in the available literature. It is important to give references to the original source for theories and experimental results.

The report must be signed by the candidate, include this text, appear as a paperback, and - if needed - have a separate enclosure (memory stick or DVD/ CD) with additional material.

Contact person at Aqualine: Martin Søreide

Supervisor at NTNU: Professor Carl M. Larsen

Trondheim, February 2015

Carl M. Larsen

Deadline: June 2015

Preface

This work has been carried out at Department of Marine Technology at the Norwegian University of Science and Technology (NTNU) in cooperation with Aqualine. I wish to thank my supervisor, Professor Carl M. Larsen, for guiding me through the work on this thesis. His good spirits and open mindset have motivated me in good and tough times. Thanks to Aqualine for initiating and laying the basis for this thesis. It has been both challenging and interesting to dive into this topic.

I am very thankful to Aquastructures, who gave me access to their developed software, AquaSim.

It has been very time-consuming to learn the new software. Especially RIFLEX and VIVANA. VIVANA has just recently been implemented in SIMA, and I have experienced problems with the software. I thank Andreas Amundsen from MARINTEK a lot for helping me fixing many of my problems.

I am very excited about the opportunities that this topic has given me. I have attended several conferences and events related to the Norwegian aquaculture industry. I have learned a lot and made new professional contacts within this field.

Thanks to Dan whom I met in Patagonia during my travel in South America in 2013. He took the time to proofread my thesis on short notice.

I am grateful to my supportive fellow students and good friends, Marion and Annette. This semester would not have been the same without you.

Thanks to Trondheim for being such a great city to live and study in for the past five years!

Trondheim, June 10, 2015

Therese Wergeland

Summary

Norway produces over 14 million meals of salmon every day. This corresponds to an annual value of close to 40 billion NOK. The world's continuous population increase will require a substantial increase in food production. The aquaculture industry in Norway has a great potential for growth. But first, several challenges related to sustainability need to be solved. One of them is to prevent escapes from cages.

Fish cages are exposed to waves and currents, and all components should be designed to survive expected load conditions. A typical fish farm structure has a sinker ring hanging beneath the net to keep it stretched and distended when exposed to environmental loads. Due to currents, vibrations due to vortex shedding on the ring can occur.

To investigate this, the sinker ring has been modeled in RIFLEX and analyzed in VIVANA for different current velocities. VIVANA is a program developed to predict vortex induced vibrations (VIV) for slender marine structures. Some adjustments and improvements on the basis of analyses done with a full cage model in AquaSim were implemented in the model boundary conditions. Due to the geometry of the structure, the magnitude of the normal component of the velocity will vary significantly over the length of the ring. This can induce a multi-mode response where several frequencies can be excited.

A range of current velocities from 0.1-1.4 m/s was investigated. The results show that there will be no vortex induced vibrations for velocities lower than 0.7 m/s. The maximum vibration and stress amplitudes occur in the part of the ring located upstream. This is related to the axial forces in the ring. Due to tension in the ropes connecting the ring to the net, compressive forces will act in the ring. The compressive forces have the largest magnitude in the upstream part of the ring. This will also affect the ring's eigenfrequencies. Compression forces lead to reduced stiffness, which gives lower eigenfrequencies.

Compared to global cage analyses in AquaSim, the RIFLEX model slightly over predicts the axial forces in the ring. However, they follow the same trend. From a simple prediction of VIV made prior to the analyses, one should expect VIV to also occur at lower velocities. Further investigation of the problem should be performed before making final conclusions regarding the survivability of the sinker ring.

Sammendrag

Norge produserer over 14 millioner måltider laks hver dag. Dette tilsvarer en årlig verdi på nesten 40 milliarder kroner. Verdens befolkningsøkning vil kreve en betydelig økning av matproduksjonen i fremtiden. Oppdrettsnæringen i Norge har et enormt vekstpotensial, men før ytterligere vekst kan tillates, må flere utfordringer knyttet til bærekraft løses. En av dem er å hindre rømming fra merdene.

Merdene er utsatt for bølger og strøm, og alle komponenter må være designet for å tåle forventede belastninger. Et typisk oppdrettsanlegg har en bunnring hengende under nettet for å holde det utstrakt når det utsettes for miljøbelastninger. På grunn av strømninger, kan vibrasjoner på grunn av virvelavløsning på ringen oppstå.

For å undersøke dette, har bunnringen blitt modellert i RIFLEX og analysert i VIVANA for forskjellige strømhastigheter. VIVANA er et program utviklet for å beregne virvelinduserte vibrasjoner (VIV) for slanke marine konstruksjoner. Noen forbedringer på bakgrunn av analysene gjort med en global modell i AquaSim ble implementert i den lokale modellens grensebetingelser. På grunn av geometrien i konstruksjonen, vil størrelsen på normalkomponenten av hastigheten variere betydelig over lengden av ringen. Dette kan indusere en respons der flere moder kan være aktive og flere frekvenser kan bli eksitert.

Et intervall av strømhastigheter mellom 0.1 og 1.4 m/s har blitt analysert. Resultatene viser at det ikke vil oppstå virvelinduserte vibrasjoner for hastigheter som er lavere enn 0.7 m/s. De maksimale respons- og spenningsamplitudene opptrer i den delen av ringen som befinner seg oppstrøms. Det vil si, den delen som ligger nærmest strømkilden. Dette er relatert til aksialkreftene i ringen. På grunn av strekket i tauene som fester ringen til nettet, vil trykkrefter virke i ringen. Trykkreftene er størst oppstrøms. Dette vil også påvirke ringens egenfrekvenser. Trykkrefter fører til redusert stivhet, noe som gir lavere egenfrekvenser.

Sammenlignet med globalanalysene i AquaSim, gir RIFLEX-modellen litt høyere aksialkrefter i ringen. Sett bort i fra dette, følger kreftene den samme trenden. Fra en enkle håndberegninger av VIV utført i forkant av analysene, burde man forvente VIV også ved lavere hastigheter. Videre undersøkelser av problemet bør utføres før endelige konklusjoner angående overlevelsesevnen til bunnringen blir gjort.

Table of Contents

List of Figures

List of Tables

Nomenclature

Abbreviations

CF	Cross-Flow
IL	In-Line
NS	Norwegian Standard
PE	Poly-Ethylene
SN	Stress-Number of cycles
VIV	Vortex Induced Vibartions

Roman Symbols

Symbol	Unit	Definition
A	[m^2]	Area
A	[m]	Amplitude
C	[Ns/m]	Damping matrix
$C_{e,CF}$	[-]	Cross-flow excitation force coefficient
D	[m]	Diameter
E	[N/m^2]	E-modulus
f_0	[1/s],[Hz]	Eigenfrequency in still water
f_v	[1/s],[Hz]	Vortex shedding frequency
f_{osc}	[1/s],[Hz]	Oscillation frequency/Response frequency
f^	[-]	Non-dimensional frequency
$F_{e,CF}$	[N]	Cross-flow excitation force
I	[m^4]	Moment of inertia
k	[N/m]	Stiffness
K	[N/m]	Stiffness matrix
m	[kg]	Mass
m_a	[kg]	Added mass
m	[kg/m]	Mass per length
M	[kg]	Mass matrix
R	[N]	Excitation force matrix
Re	[-]	Reynolds number
St	[-]	Strouhal number
T_v	[s]	Vortex shedding period
U	[m/s]	Current velocity
U_r	[-]	Reduced velocity
X	[N]	Excitation force matrix

Greek symbols

Symbol	Unit	Definition
α	[degrees]	Angle between the horizontal plane and the connection ropes
ρ	[kg/m^3]	Density of sea water
ω_n	[rad/s]	Eigenfrequency for mode n

1 Introduction

1.1 Background and motivation

The world's population passed 7 billion in 2011 and is expected to increase to more than 9 billion in 2050 (United Nations: Department of Economic and Social Affairs, 2012). Developing countries will account for the largest growth. In order to meet the population increase and the economic growth, food production has to increase by 70 percent by 2050 (Olafsen et al., 2012). Close to 1.2 million tons of salmon were produced in Norway in 2013. This is equivalent to 14 million meals of salmon every day (Nærings- og fiskeridepartementet, 2015). Aquaculture is an efficient way to produce food, both in terms of area and feed. Aquaculture has a great potential to grow, and to become one of the world's most valuable food resources. In Norway alone, a fivefold increase in salmon production from 2010 is predicted to be possible by 2050 (Olafsen et al., 2012).

Before further growth can be allowed, challenges related to escapes from cages, salmon lice, impact on wild fish, pollution, and fish feed need to be solved. A Norwegian standard, NS 9415 (Standard Norge, 2009) with technical requirements for marine fish farms has been developed to reduce the risk of escapes from cages.

Whether a location for fish farming is good is strongly connected with the current conditions in the area. Currents provide a constant supply of fresh seawater, which is important for fish welfare. In order to limit the distortion of the fish cage when exposed to environmental loads like waves and currents, a sinker ring is attached to the bottom of the net pen. Ocean currents can induce vibrations in the ring due to vortex shedding. These vibrations are called vortex induced vibrations, and are abbreviated VIV. This phenomenon is discussed in further detail in Chapter 2. VIV is an important source of fatigue damage accumulation. If the sinker ring fails, it can damage the net pen. This must be avoided in order to prevent fish escapes.

The price of oil has been a widely discussed topic this year. From June 2014 to June 2015, the oil price dropped from 115 (Qvale, 2014) to 63 USD (DN.no, 2015) per barrel. The related recession in the Norwegian oil and gas market has led to discussion of aquaculture as one of the most promising industries to eventually replace the oil and gas industry. This has been a great motivation for the work in this thesis.

1.2 Aquaculture in Norway

The term *aquaculture* refers to *"the breeding, rearing, and harvesting of plants and animals in all types of water environments including ponds, rivers, lakes, and the ocean." (NOAA Fisheries)*

In Norway, aquaculture is based on fish farming in the ocean. The most common species are salmon and rainbow trout. Rearing of white fish like cod and halibut also exists. Norway is the world's largest producer of Atlantic salmon (Laksefakta.no, 2014). In 2013, more than a million tons of salmon were produced. This had a value of almost 40 billion NOK (ssb.no, 2014). Overall, the aquaculture industry including suppliers constitutes around 20 000 effort-years (Laksefakta.no, 2014).

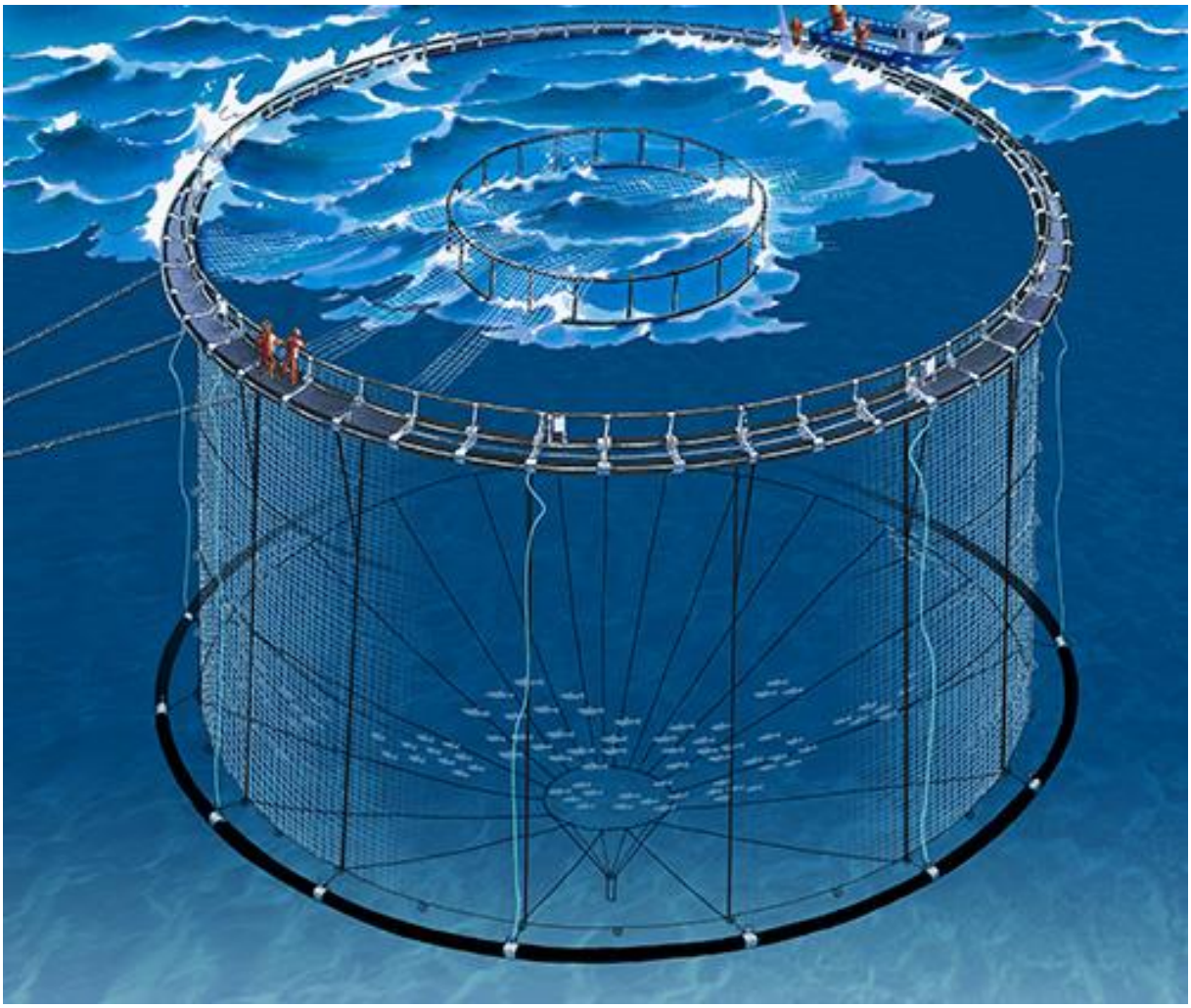

Figure 1-1 Illustration of a fish farm structure (aqualine.no)

Figure 1-1 shows a sketch of a typical fish cage. This is a traditional circular plastic collar cage with a weight ring to keep the net pen distended in waves and currents. Rectangular steel cages are also widely used.

1.2.1 Terminology

Definitions related to aquaculture and fish farm structures that are extensively used in this thesis are explained here.

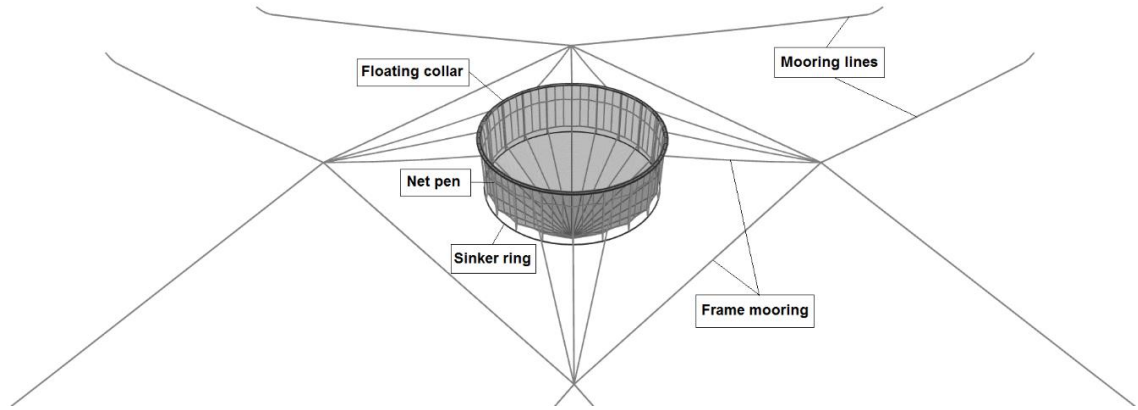

Figure 1-2 Main components of a traditional fish cage

Floating Collar

The floating collar is the floating element attached to the net pen. The floating collar can either be a circular ring made of high-density polyethylene (HDPE) or a rectangular hinged steel frame. Other options also exist, but are not commonly used. Traditionally, the steel frame was widely used. However, as a consequence of the Norwegian standard NS9415, plastic floating collars have largely taken over (Rosten et al., 2011). A plastic floating collar usually exists of two flotation rings.

Net Pen

The net pen is usually made of nylon. There are two "shapes" that are used: the cone net with a weight at the bottom and the normal net, which is cylindrical and is kept distended with a sinker tube at the bottom.

Sinker Ring

The sinker ring is a weight ring placed at the bottom of the net pen. The sinker ring together with the floating collar keep the net pen stretched and distended.

Mooring

The mooring system of a plastic floating collar is very complex. The floating collar is first moored in a frame, then to the seabed (Rosten et al., 2011). Because the floating collar has a very low horizontal stiffness, the framework is necessary to absorb the mooring forces. A steel collar can be directly moored to other collars or the seabed. The mooring system for a plastic collar is shown in Figure 1-2, and the mooring system for a full plant of cages is shown in Figure 1-3.

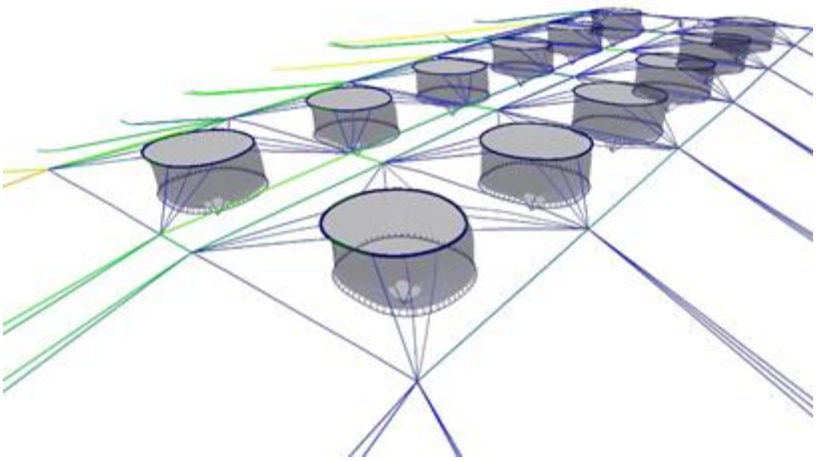

Figure 1-3 A fish farm plant with 12 cages (aqualine.no)

1.2.2 Future Perspectives

Today's fish farms are located near shore protected from the harsh environments that the open ocean can offer. Traditional structures are so-called open cages. Open cages are defined as cages where water flows in and out of the unit without being processed (Rosten et al., 2011). In other words, the fish is in direct contact with the surrounding environment. This form of farming has large risks both for the fish and the environment. Salmon lice are found naturally in the sea in the northern hemisphere (Laksefakta.no, 2014). The lice can cause infections and discomfort for the fish, but will not affect the food safety or quality of the meat. Escapes of fish can affect the genetic material of wild fish. Waste and sediments from the cages cause pollution of the environment close to the farm sites.

One option to completely eliminate the problems with escapes and salmon lice is to move the fish farms on shore. Another option is to develop solutions for closed cages in the sea. This is very challenging because of the large forces to which the cages are exposed.

The research project "Et kunnskapsbasert Norge" by (Reve and Sasson, 2012) determined aquaculture to be one of Norway's three industries with the greatest potential to succeed in the international market. The two others are the offshore industry and the maritime sector. The past year, with the recession in the oil market, the aquaculture industry has been discussed in the media as one of the future leading technologies in Norway. A five-fold increase in salmon production from 2010 to 2050 is expected to be possible (Olafsen et al., 2012). If the industry is to grow as much as predicted, the farming sites have to move from protected locations close to the shore to more exposed areas offshore.

SalMar has already developed an offshore fish farm. It is a semi-submersible steel construction that is designed for the offshore environment outside the coast of Norway. However, the cage has not yet been approved by the authorities to be set in production.

1.3 Objective and Scope

The purpose of this master thesis is to develop a model of the sinker ring in a fish farm and investigate the effect of VIV. Questions that will be answered in this thesis are:

- *For which current velocities will VIV be significant?*
- *How will the axial forces in the ring influence the eigenfrequencies and the occurrence of VIV?*
- *How does the local model of the sinker ring perform?*

This thesis involves modeling the sinker ring with the ropes connecting it to the net pen in RIFLEX. To model the boundary conditions, analyses of a global fish cage model in AquaSim have to be performed for a variety of current velocities. The displacements of the nodes will then be implemented as boundary conditions in RIFLEX. The axial forces in both models can be used to verify the boundary conditions. VIV analyses in VIVANA with the local model for different current velocities is the last step. In consultation with Aqualine (Søreide, 2015, pers. comm.), current velocities in the range 0.1-1.5 m/s will be analyzed.

1.4 Outline of the report

Vortex induced vibrations are presented in detail in *Chapter2*. In *Chapter 3*, the software used in this thesis is introduced. Some background theory for the analysis procedure for VIVANA and AquaSim is included. The process of modeling the sinker ring in RIFLEX is described in *Chapter 4*. The analysis set-up for the VIVANA analysis is also explained. Some simple hand calculations for prediction of VIV on the sinker ring are included in *Chapter 5*. The results and discussion related to the findings are found in *Chapter 6*. Conclusions are made in *Chapter 7*. Recommendations for further work can be found in *Chapter 8*. The results for all the different velocities analyzed are collected in the *Appendix*.

2 Vortex Induced Vibrations (VIV)

The information in this chapter is mainly retrieved from (Larsen, 2011), unless stated otherwise.

2.1 Introduction

Slender marine structures like anchor lines, risers and free spanning pipelines exposed to ocean current may experience oscillating motions, or vibrations. These vibrations are caused by forces from vortices that are shed from both sides of the structure. This phenomenon is called vortex induced vibrations (VIV).

For VIV to occur, the vortex shedding frequency has to be close to the structure's eigenfrequency. The vortex shedding period is defined by the time it takes for two vortices to be shed from the same side of the cylinder. This is illustrated in Figure 2-1.

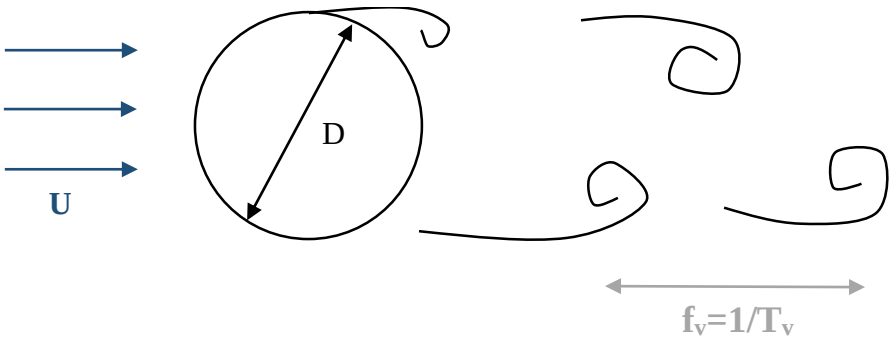

Figure 2-1 Vortex shedding frequency

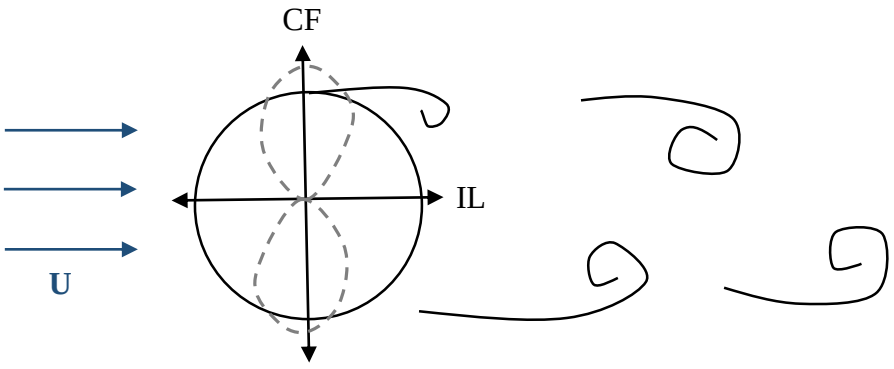

Figure 2-2 CF and IL motions

When vortices are shed from the cylinder, the pressure distribution on the cross section changes, and lift and drag forces act on the cylinder in cross flow and in-line directions respectively. The alternating lift force creates cross flow vibrations, while the drag force creates in-line vibrations.

If in-line vibrations and cross-flow vibrations are present at the same time, which they usually are, the cylinder will oscillate in a figure eight pattern. This is illustrated in Figure 2-2. The in-line vibrations have a frequency that is twice the cross flow frequency. This means that for low reduced velocities where there will be no cross-flow vibrations, in-line vibrations could still be present. In Figure 2-3, it is seen that cross flow vibrations will be present for reduced velocities larger than 2.5. However, the cross-flow vibrations are usually of interest since they have larger amplitudes than the in-line vibrations. The in-line vibrations are still important when considering the fatigue life of the structure.

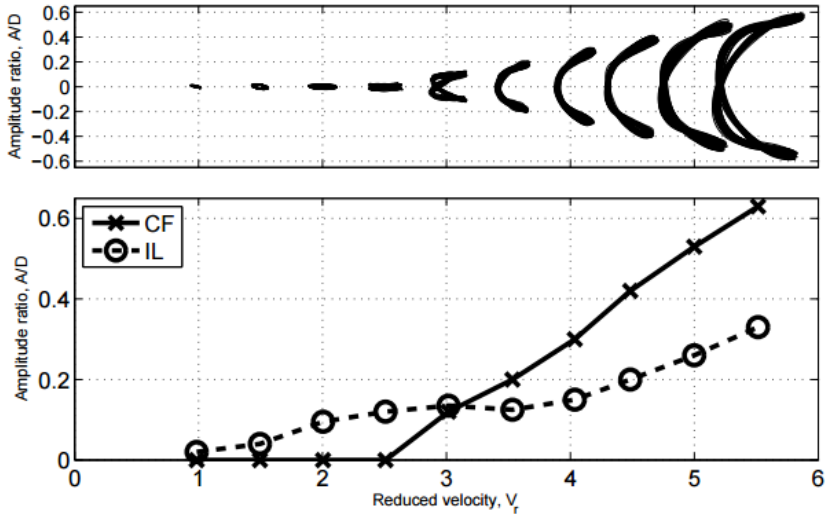

Figure 2-3 Response amplitudes in IL and CF and trajectories for vibrations at the midpoint of a flexible beam (Aronsen, 2007)

Vortex shedding will induce resonant vibrations when the shedding frequency coincides with the natural frequency of the structure. When this happens, the vortex shedding frequency tends to "lock" into the eigenfrequency. A small increase of the current velocity will not change a vortex shedding frequency that is locked into the eigenfrequency. Hence, the resonant region will be increased. This phenomenon is called *lock-in*. Large vibration amplitudes are usually observed when lock-in occurs.

2.2 Non-dimensional Parameters

Relevant parameters when considering flow around cylindrical structures are defined in this subchapter. Four non-dimensional numbers are often used when discussing hydrodynamics. These are Reynolds number, Strouhal number, reduced velocity and non-dimensional frequency.

Reynolds number:

$$Re = \frac{U \cdot D}{\nu} \tag{1}$$

where U is the current velocity, D is the cylinder diameter and ν is the kinematic viscosity. In water, ν is on the order of 10^{-6} m^2/s.

The flow pattern behind a cylinder in uniform current can be described by the Reynolds number. In Figure 2-4, a classification of different flow regimes for different Reynolds numbers is presented.

Strouhal number:

$$St = \frac{f_v \cdot D}{U} \tag{2}$$

where f_v is the vortex shedding frequency, D is the cylinder diameter and U is the current velocity.

The Strouhal number is nearly constant and equal to 0.2 for a large range of Reynolds numbers. See Figure 2-5.

Reduced velocity:

$$U_r = \frac{U}{D \cdot f_0} \tag{3}$$

where f_0 is the still water eigenfrequency.

The reduced velocity is a non-dimensional velocity, which makes it easier to compare results for cylinders with different properties.

Non-dimensional frequency:

$$\hat{f} = \frac{f_{osc} \cdot D}{U} \tag{4}$$

where f_{osc} is the oscillation frequency.

The non-dimensional frequency is often used to determine whether the frequency lies within the range that can excite VIV or not. The still water eigenfrequency f_0 and the oscillation frequency f_{osc}, are defined in Equations (5) and (7), respectively.

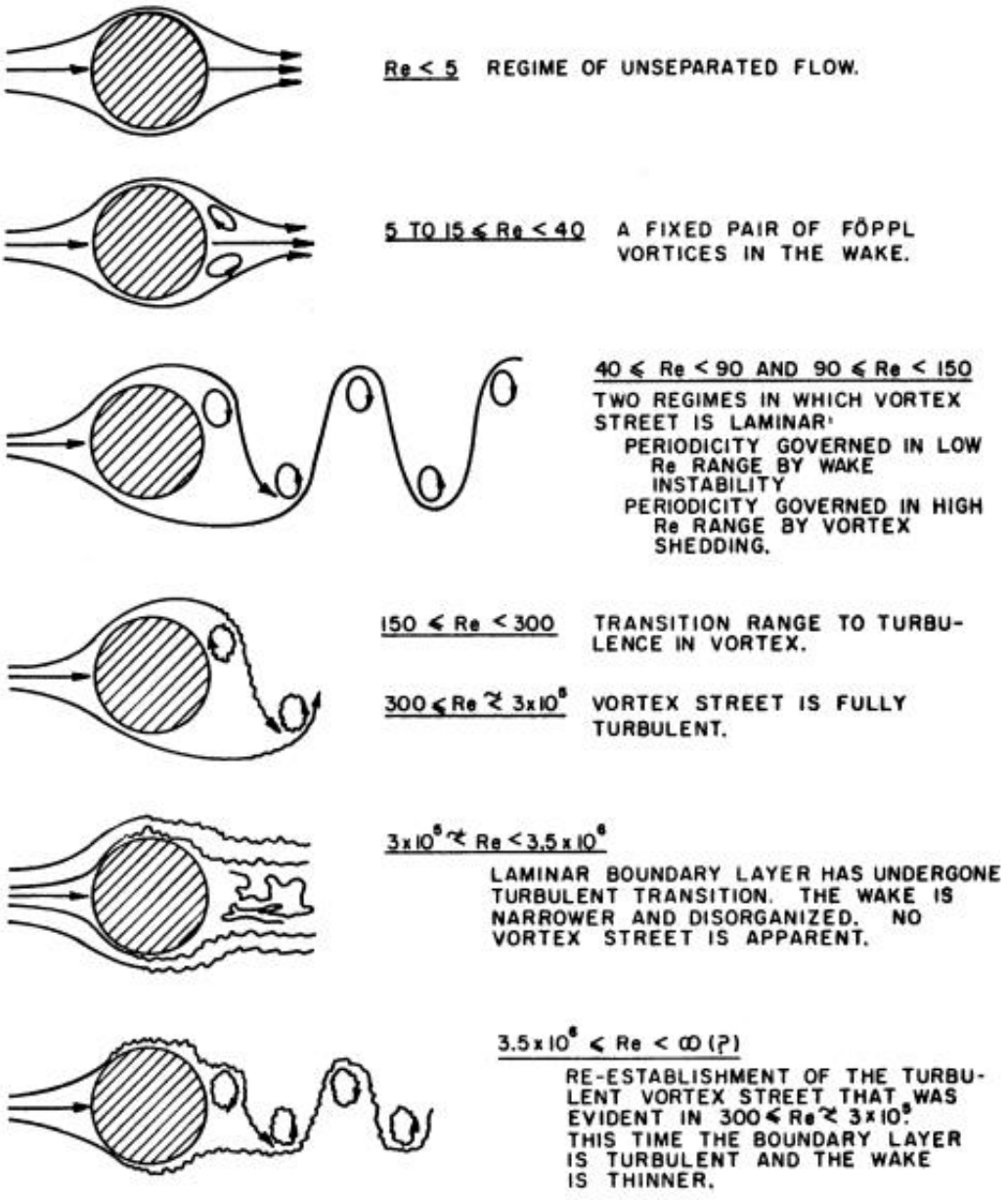

Figure 2-4 Regimes of fluid flow across smooth cylinders (Lienhard, 1966).

From Figure 2-4 it is seen that there will be vortex shedding when Re > 40. Notice the flow regime for Reynolds numbers in the range $3 \cdot 10^5 < Re < 3.5 \cdot 10^6$. This is called the critical regime. Here, no vortex street is visible. This phenomenon is also reflected in Figure 2-5, where an increase of the Strouhal number happens for Reynolds numbers in the critical flow regime. The Strouhal number is strongly dependent on surface roughness as seen from the figure.

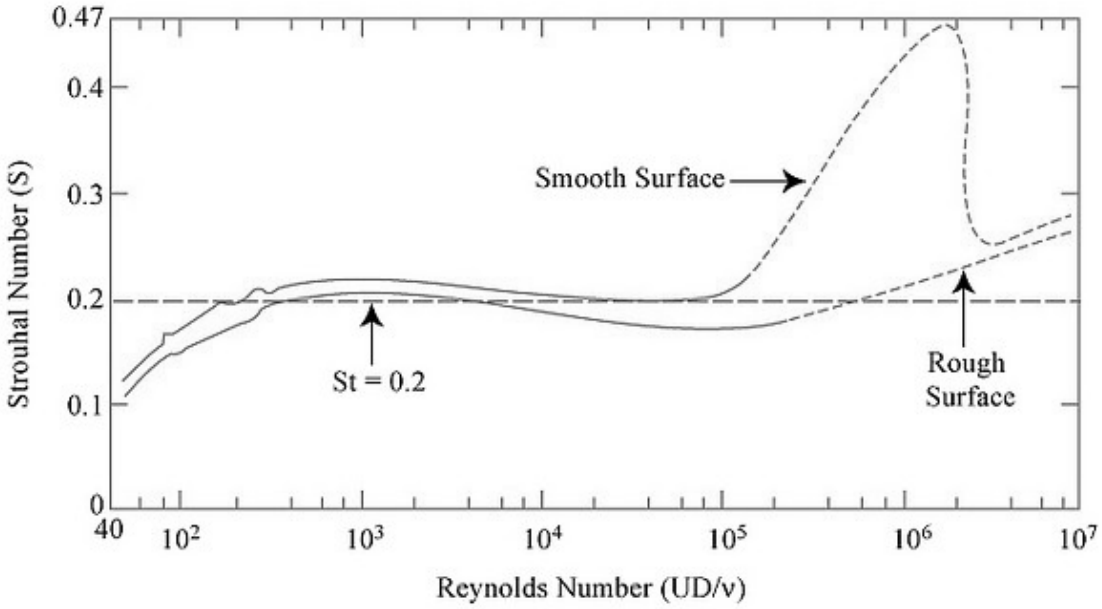

Figure 2-5 Relationship between Reynolds number and Strouhal number (Blevins, 1994).

2.3 Suppression of VIV

Figure 2-6 Helical strikes (VIV Solutions, 2013)

The best way to avoid VIV is to operate in current velocities less than those needed for VIV to occur, i.e. $U < 5Df_0$ for St=0.2. For higher velocities, the probability of hitting an eigenfrequency corresponding to a higher mode is large. However, if it is not possible to operate at velocities less than the critical current velocity, several ways to suppress VIV have been developed. An example of helical strikes can be seen in Figure 2-6. The advantage of using helical strikes is that they are equally efficient for current in every direction. The drawback of these types of suppression devices is increased cost due to extra materials, as well as the extra weight these materials have on the structure.

2.4 Free Oscillation Test

The free oscillation test is a classical experiment to illustrate VIV. It is performed with an elastically supported rigid cylinder in constant current (Figure 2-7).

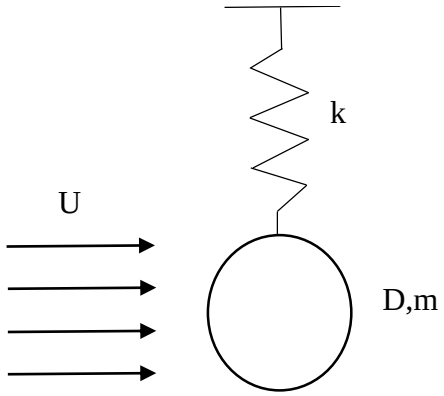

Figure 2-7 Free oscillation test set-up, adapted from (Larsen, 2011)

Three important parameters from this test are:

Still water eigenfrequency:

$$f_0 = \frac{1}{2\pi}\sqrt{\frac{k}{m + m_{a0}}} \tag{5}$$

where m_{a0} is the added mass in still water, k is the spring stiffness and m is the mass of the cylinder.

The vortex shedding frequency is given by:

$$f_v = \frac{St \cdot U}{D} \tag{6}$$

The oscillating frequency is given by:

$$f_{osc} = \frac{1}{2\pi}\sqrt{\frac{k}{m + m_a}} \tag{7}$$

Where m_a is the frequency dependent added mass.

Because the added mass varies, the oscillation frequency will not equal the still water eigenfrequency for resonance condition (lock-in) or to the vortex shedding frequency. The oscillation frequency in this case, will become a compromise between the vortex shedding

frequency and the still water eigenfrequency. This is illustrated in Figure 2-8. Because the effect of added mass on the eigenfrequency will depend on the dry mass of the cylinder, a light and a heavy cylinder will respond differently to the incoming current. The light cylinder's eigenfrequency will be influenced by added mass to a larger extent than the heavy cylinder's. Therefore, the oscillation frequency of a light cylinder will follow the vortex shedding frequency over a wider range of reduced velocities than that of a heavy pipe with the same dimensions. This is demonstrated in Figure 2-9.

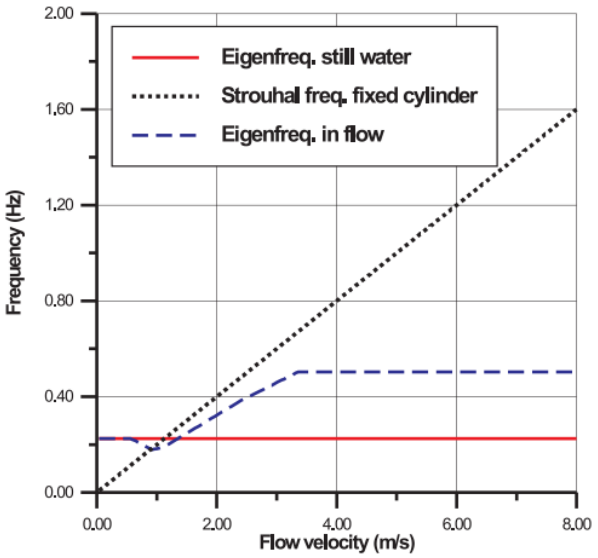

Figure 2-8 Strouhal frequency, eigenfrequency and oscillation frequency (Larsen, 2011)

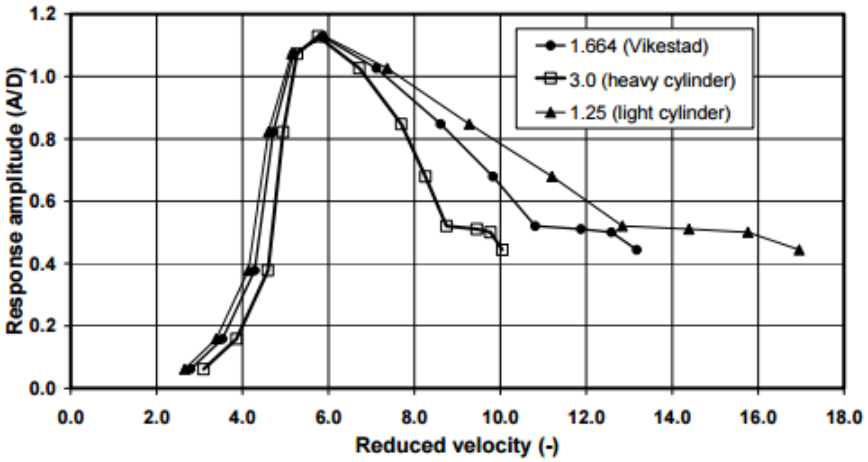

Figure 2-9 Response amplitudes for three cylinders with different weight (Larsen, 2011)

From a free oscillation test, these parameters are found:

- *Cross-flow amplitudes and frequencies*
- *In-line amplitudes and frequencies*
- *Drag coefficient for an oscillating cylinder*

The cross flow and in-line excitation forces cannot be found from free oscillation tests. This is because the mean forces are zero. In order to find these forces, forced oscillation tests need to be performed for the cylinder.

2.5 Forced Oscillation Test

A cylinder in a stationary uniform current is given a prescribed oscillation pattern. The pattern can be harmonic motion in CF or IL, or a combination of these:

$$x = x_0 \sin(4\pi f_{osc} t + \theta) \tag{8}$$

$$y = y_0 \sin(2\pi f_{osc} t) \tag{9}$$

where x and y are displacements in IL and CF directions respectively. The oscillation pattern for various phase angles θ, are shown in Figure 2-10.

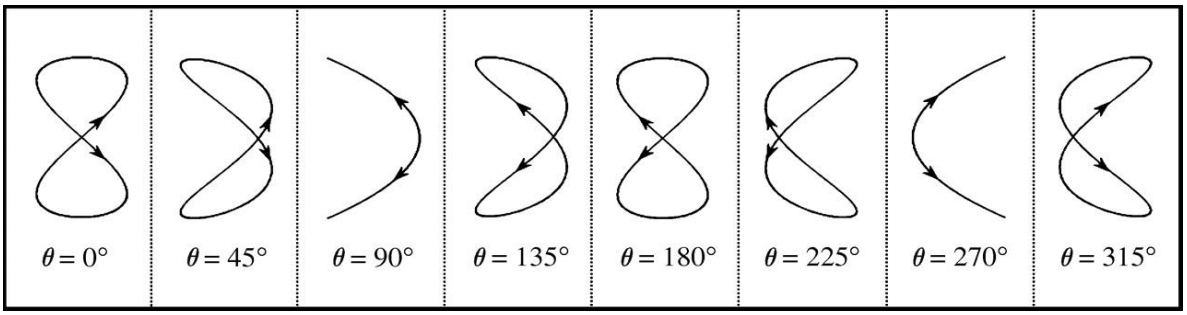

Figure 2-10 Trajectories of a cylinder oscillating cross-flow and in-line as a function of phase angle θ (Leong and Wei, 2008)

From the forced oscillation test, it is possible to find the added mass, lift, drag and dynamic force coefficients. The results are presented as contour plots for the coefficients in a non-dimensional amplitude/frequency plane.

Figure 2-11 shows the CF excitation coefficient found by tests performed by Gopalkrishnan (Gopalkrishnan, 1993). The eigenfrequencies that give a non-dimensional frequency that lies within the range 0.125-0.3 are considered as response frequency candidates. VIVANA uses these empirical coefficients for determining response frequency candidates (Passano et al., 2014).

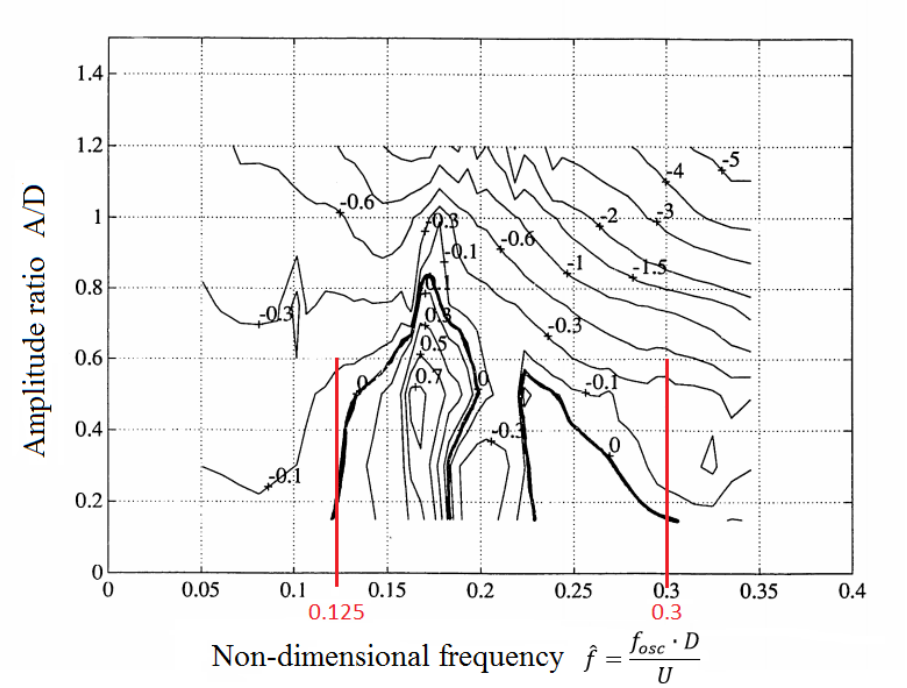

Figure 2-11 Contours of the lift coefficient in phase with velocity (Gopalkrishnan, 1993)

2.6 Time and Space Sharing

For a long slender marine structure in sheared current, there will be several competing mode shapes and frequencies to excite VIV. A common method to define the working areas for these frequencies is to define excitation zones for every actual frequency and calculate the response (see Figure 2-12). Two different approaches are used for this purpose, time sharing and space sharing.

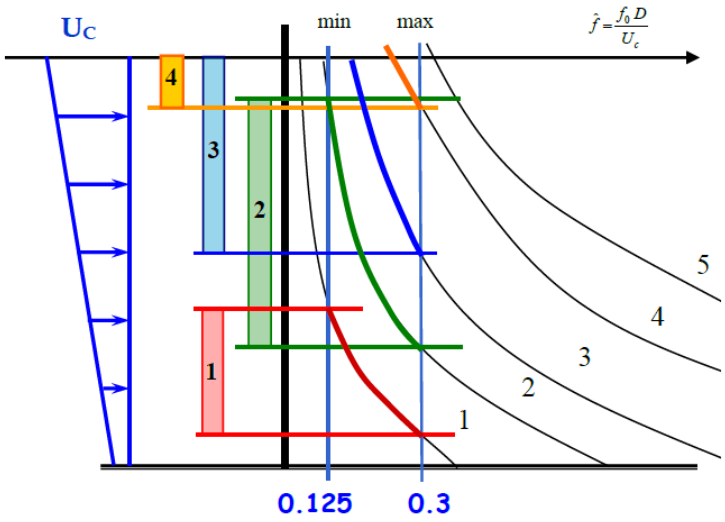

Figure 2-12 Overlapping excitation zones (Passano et al., 2014)

Time sharing

The competing frequencies will dominate in a period of time. The analysis must find the duration for each competing frequency.

The response takes place at a selected set of eigenfrequencies, but only one frequency will be active in a specific time period (see Figure 2-13). The excitation zones are allowed to overlap, but the frequencies compete to capture time windows.

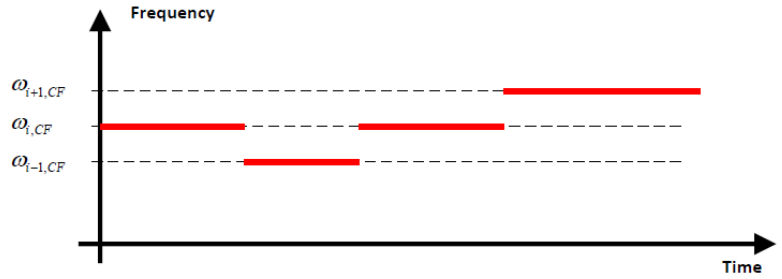

Figure 2-13 Time sharing (Passano et al., 2014)

Space sharing

All the competing frequencies are active at the same time. Vortex shedding can only excite one of these frequencies at a specific point on the structure. This means that the excitation zones cannot overlap. Hence, the space (length) has to be divided between the competing frequencies (see Figure 2-14).

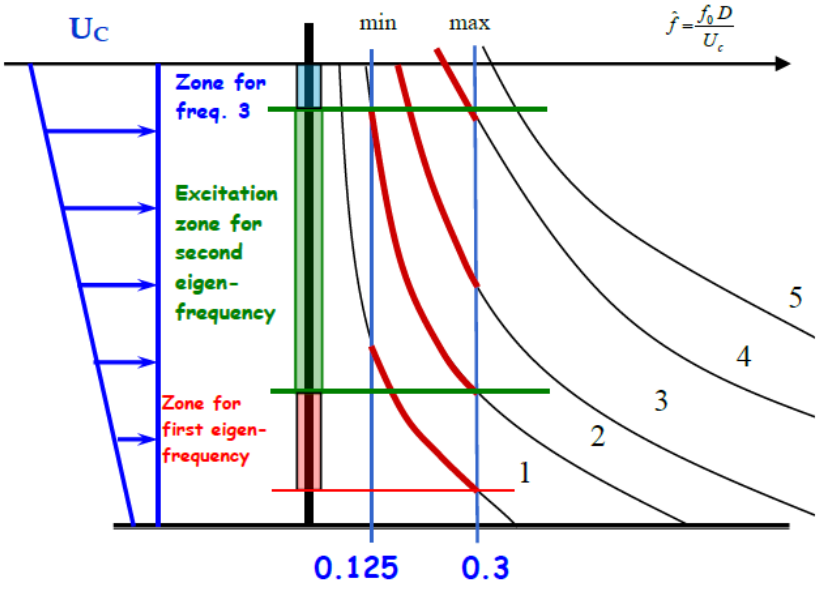

Figure 2-14 Space sharing (Passano et al., 2014)

2.7 Excitation Forces

The forces that drive the vibrations are called lift and drag. The lift force creates cross-flow oscillations, and is also called the cross-flow excitation force. The drag force excites in-line vibrations, and is hence also called the in-line excitation force.

The cross-flow excitation force is given by:

$$F_{e,CF} = \frac{1}{2}\rho C_{e,CF} D U^2 dl \tag{10}$$

Where $C_{e,CF}$ is the cross-flow excitation force coefficient, often just called the lift coefficient. The CF excitation force is defined as the component of the hydrodynamic force that is in phase with the cross-flow velocity of the cylinder. If $C_{e,CF}$ is positive, the CF force will add energy to the vibrating structure, while a negative value of the CF coefficient will lead to damping (see Figure 2-15).

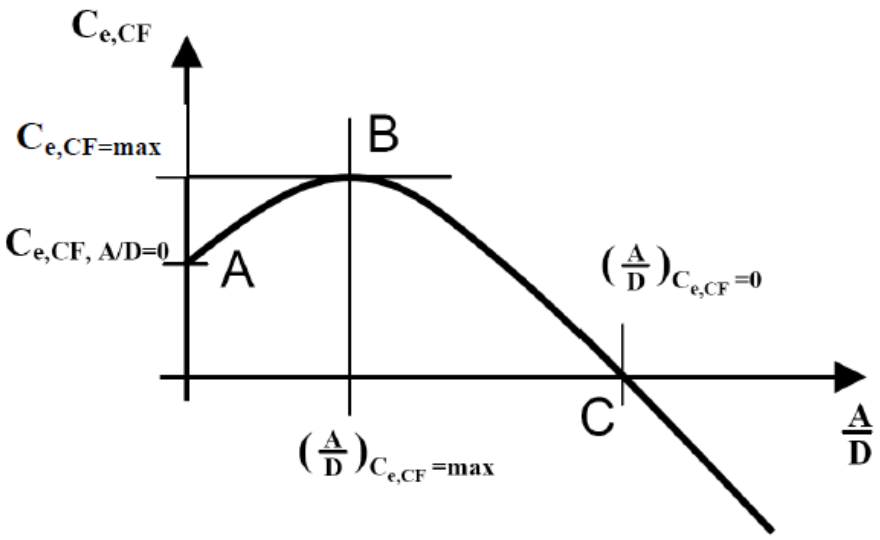

Figure 2-15 Cross-flow excitation force coefficient curve (Passano et al., 2014)

From the figure, it is seen that the coefficient becomes negative for a certain amplitude, which means that VIV is *self-limiting*. If the amplitude exceeds a certain level, the vortex shedding process will no longer transfer energy from the fluid to the structure, but will reverse the energy transfer process. The structure will transfer energy to the fluid, which means that the oscillations, or vibrations, will be damped. The response amplitude for a circular cylinder will be limited to:

$$\frac{A}{D} < 1.2$$

This is valid for circular cross sections only. Non-circular cross sections may not have a self-limiting vortex shedding process, and may hence experience *galloping*.

3 Software

This chapter presents the software used in this thesis and introduces the theory the software is based on. Both VIVANA and AquaSim will be briefly presented. In addition, MATLAB has been used for post-processing of results. MATLAB will not be further discussed. Some problems with VIVANA were experienced. Those are further described in Appendix C.

3.1 VIVANA

The information in this chapter is mainly retrieved from the VIVANA User's Manual (Yttervik et al., 2009) and the VIVANA Theory Manual (Passano et al., 2014), unless stated otherwise.

"VIVANA is a semi-empirical program for prediction of vortex-induced vibrations (VIV) for slender marine structures subjected to ocean current." (Passano et al., 2014)

VIVANA is developed by MARINTEK and NTNU. The latest versions are implemented in the SIMA software. VIVANA is linked to the RIFLEX module in SIMA. RIFLEX includes modeling features for analysis of slender marine structures like risers, anchor lines, tethers and pipelines.

The connection between RIFLEX and VIVANA is illustrated in Figure 3-1. The model input file (inpmod) is generated in RIFLEX. VIVANA also needs the stamod file from the static analysis in RIFLEX to run. VIVANA gives a result output file and matrix plots for the most relevant results.

The full analysis procedure can be described from the following steps:

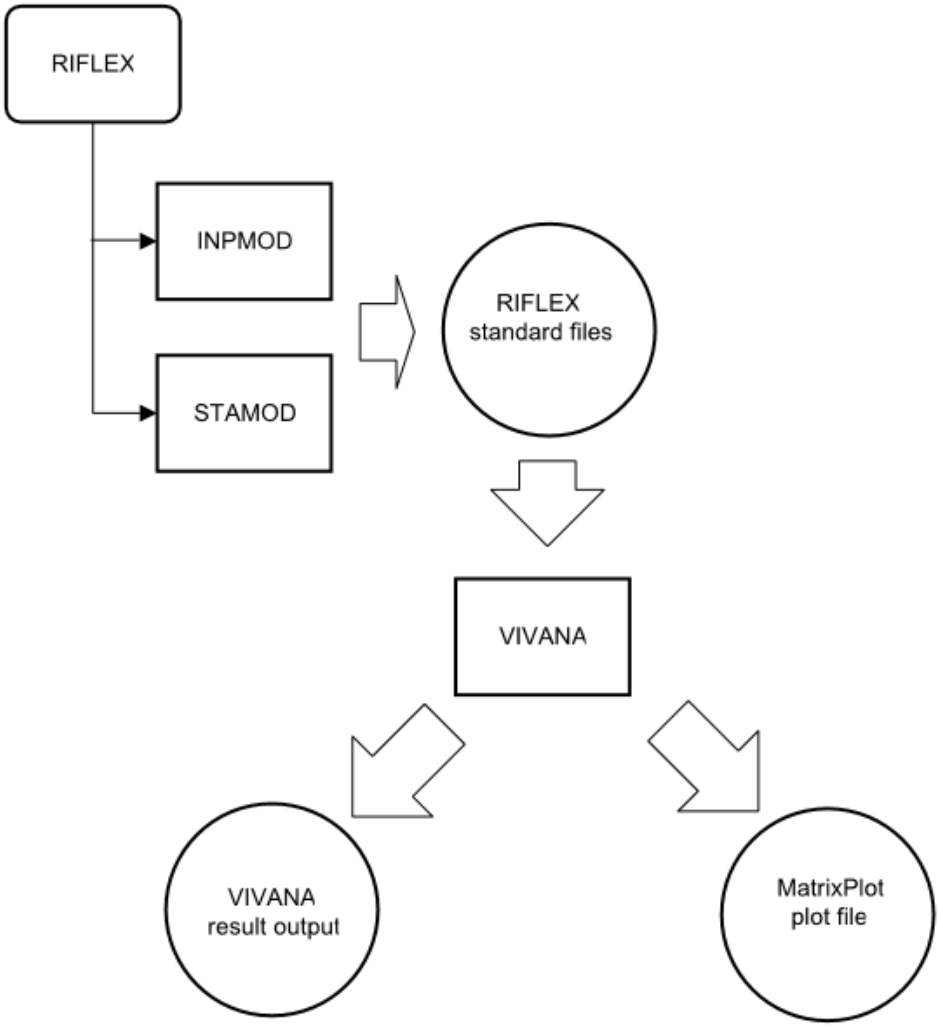

Figure 3-1 The VIVANA program system (Yttervik et al., 2009)

Step 1: Static analysis

The structure has to be analyzed to find the static shape. This analysis is performed by the RIFLEX module in SIMA.

Step 2: Eigenvalue analysis

The eigenfrequencies and mode shapes of the structure are identified. To find all the active frequencies that can induce vortex-induced vibrations, a sufficient number of eigenfrequencies need to be given as input.

The eigenvalue problem:

All the solutions of the eigenvectors have to satisfy the equation:

$$(\boldsymbol{K} - \omega_i^2 \boldsymbol{M})\phi_i = 0 \tag{11}$$

Where M and K are the mass and stiffness matrices, respectively. The eigenfrequencies ω_i and the eigenvectors ϕ_i are computed in the global coordinate system and are not used directly in

the dynamic analysis, but will function as initial values in iterations for response frequencies and mode shapes.

Step 3: Identification of possible and dominating excitation frequencies

When all the eigenfrequencies for the structure in still water are identified, all the possible active eigenfrequencies are also determined. Added mass for VIV conditions will be different from the still water case, and to identify the eigenfrequencies corrected for different added mass distribution, iterations must be performed. The iteration has converged when there is consistency between the modified eigenfrequency and the modified added mass distribution.

Step 4: Analysis of the response at the dominating frequency

The response at the frequencies found in step 3 is calculated from the frequency response method.

The dynamic equilibrium equation:

$$\boldsymbol{M\ddot{r} + C\dot{r} + Kr = R} \tag{12}$$

Where:

$$\boldsymbol{R = Xe^{i\omega t}}$$

$$\boldsymbol{r = xe^{i\omega t}}$$

$$\boldsymbol{\dot{r} = i\omega xe^{i\omega t}}$$

$$\boldsymbol{\ddot{r} = -\omega xe^{i\omega t}}$$

Substituting:

$$-\omega^2(\boldsymbol{M_S + M_H})\boldsymbol{x} + i\omega(\boldsymbol{C_s + C_H})\boldsymbol{x} + \boldsymbol{Kx} = \boldsymbol{X_L} \tag{13}$$

$\mathbf{M_S}$ - Structural mass matrix

$\mathbf{M_H}$ - Hydrodynamic mass matrix

$\mathbf{C_S}$ - Structural damping matrix

$\mathbf{C_H}$ - Hydrodynamic damping matrix

K - Stiffness matrix

$\mathbf{X_L}$ - Excitation force vector

The solution of Eq. (13) can be written as:

$$\boldsymbol{x} = [-\omega^2(\boldsymbol{M_S + M_H}) + i\omega(\boldsymbol{C_s + C_H}) + \boldsymbol{K}]^{-1} \cdot \boldsymbol{X_L} \tag{14}$$

Or:

$$\boldsymbol{x} = \boldsymbol{H(\omega)X_L} \tag{15}$$

Where H(ω) is the complex frequency response function.

Step 5a: Response analysis for other frequencies than the dominating frequency – concurrent response frequencies (space sharing)

The excitation zone for the dominating frequency may not cover the whole length of the structure. This means that excitation may take place at other frequencies in zones outside the identified excitation zone. New response analyses should be carried out for the other frequencies. The excitation zones for the new active frequencies will be reduced by the excitation zone of the dominating frequency.

Excitation force:

$$F_{e,CF/IL} = \frac{1}{2}\rho C_{e,CF/IL} D_H U_N^2 \Delta L \tag{16}$$

Where the excitation coefficient $C_{e,CF/IL}$ is a function of the non-dimensional amplitude $A_{CF/IL}/D_H$ and the corrected non-dimensional frequency $\hat{f}_{c,CF/IL}$. The excitation coefficient is normally found from contour plots, which are a result of Gopalkrishnan's forced oscillation tests (Gopalkrishnan, 1993). Note that the excitation force is the component of the hydrodynamic force that is in phase with the response velocity.

Step 5b: Response analysis for other frequencies than the dominating frequency – consecutive response frequencies (time sharing)

Same as for step 5a, but the excitation frequency candidates may have overlapping excitation zones (full length), but only one frequency can be excited at a time. The excitation frequency will hence vary with time.

Step 6: Post-processing of results

Includes fatigue analysis and drag amplification analysis.

Fatigue analysis based on time sharing for combined IL and CF response:

For this case, two frequencies will act simultaneously (f_{CF} and $f_{IL}=2f_{CF}$). The Miner-Palmgren summation is used in the fatigue damage calculation:

$$D = \sum_{i=1}^{N} \frac{n_i}{N_i} \tag{17}$$

where n_i is the number of cycles and N_i is the number of cycles until failure.

The fatigue damage from all the response frequency pairs can be found by:

$$D_{tot} = \frac{\sum_{i=1}^{n} \mu_i D_i}{\sum_{i=1}^{n} \mu_i} \tag{18}$$

Here, D_{tot} is the total damage accumulated during a time period. D_i is the fatigue damage due to the response frequency pair i, and μ_i is the ranking parameter.

3.2 AquaSim

AquaSim is an analysis and simulation tool developed by Aquastructures. The program is based on the finite element method. It can calculate response for slender marine structures and coupled systems when they are exposed to dynamic environment loads like waves, current, wind, impulse loads and periodic excitation forces (Aquastructures.no).

AquaSim can handle both rigid and flexible structures, and a combination of these. The software uses the time domain to estimate response from non-linear effects. Local and global forces, as well as stress, deformations, accelerations and eigenfrequencies, -can be estimated locally and globally (Aquastructures.no).

The program includes four different element types:

- *Beam elements*
- *Bar elements*
- *Membrane elements*
- *Shell elements*

In addition, buoys, anchors, springs, bottom springs and hinges are accounted for.

The program can execute static and dynamic time domain simulations of structures. Structures exposed to environmental conditions like waves, wind and current can be analyzed, as well as structures exposed to operational conditions like lifting the net or ships hitting the floater rings.

The information on the analysis method is based on (Halse, 1997), (Langen and Sigbjörnsson, 1979) and (Aquastructures, 2006).

Nonlinear static analysis

To find the equilibrium point at a given displacement x, the tangential stiffness matrix K_T is used. This is an approximation that may lead to significant deviations between internal and external forces (see Figure 3-2). Therefore, incremental solutions by applying a fraction of the load and using the tangential stiffness matrix for each step give a more accurate solution.

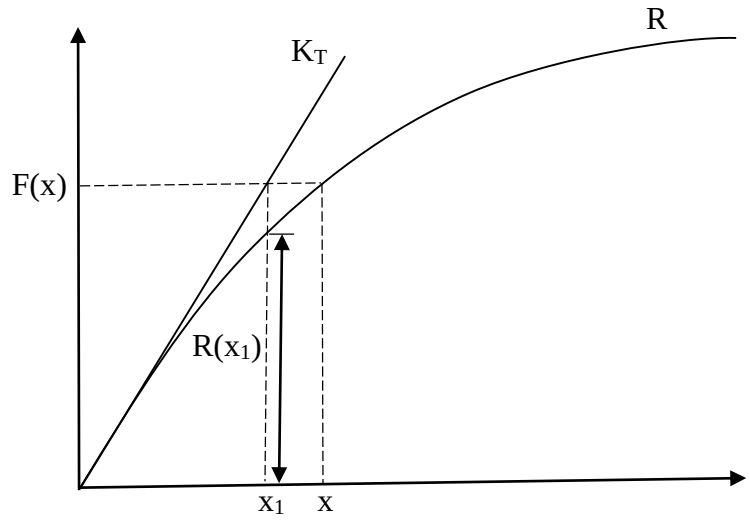

Figure 3-2 The incremental tangential matrix approximation of a nonlinear problem. This figure is adapted from (Halse, 1997).

Static equilibrium means that there is a balance between the external and internal forces on the structure.

$$f(x_n) = R_{ext}(x_n) - R_{int}(x_n) = 0 \tag{19}$$

R_{ext} is the external static forces acting on the structure, while R_{int} is the internal forces.

The internal forces can be written as:

$$R_{int}(x_n) = R_{int}(x_{n-1}) - \Delta R_{int,n} \tag{20}$$

where $\Delta R_{int,n}$ is the increment in internal forces corresponding to the increment in element displacements. This increment can be approximated as:

$$\Delta R_{int,n} \approx K_{T,n-1}\Delta x_n \tag{21}$$

where Δx_n is a vector of incremental nodal displacements.

Then the equilibrium formula can be written as:

$$R_{ext}(x_n) - R_{int}(x_{n-1}) = K_{T,n-1}\Delta x_n \tag{22}$$

By solving for Δx_n, the approximation of displacements for the next load increment can be found:

$$x_n = x_{n-1} + \Delta x_n$$

By increasing the number of increments, the solution becomes more accurate.

The nonlinear dynamic analysis procedure is not presented here because it is not relevant for the analysis performed in this thesis. Information about the method can be found from (Aquastructures, 2006).

4 Modeling

4.1 Model and Data

The fish cage studied in this thesis is a traditional cage with circular plastic floating collars and a sinker ring used to stretch and distend the net. Figure 4-1 below shows the global cage model in AquaSim. The model is the property of Aqualine.

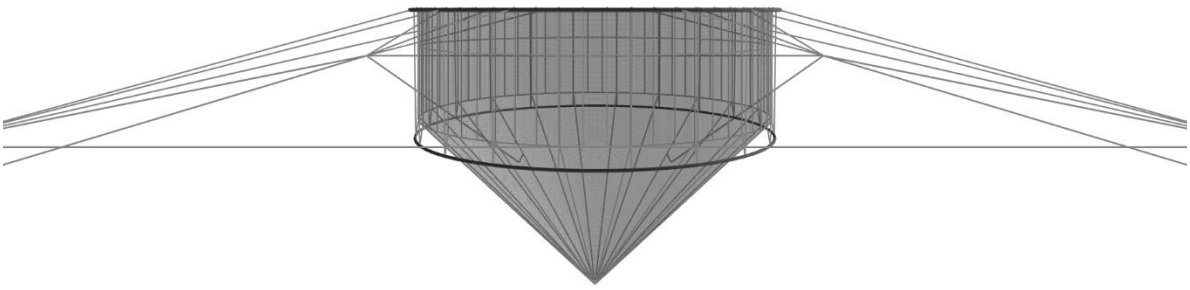

Figure 4-1 Model of a fish cage with floating collar, net pen, sinker ring and a mooring system

The scope of this thesis is to make a local model of the sinker ring and the ropes connecting the sinker ring with the net pen in RIFLEX. Then VIVANA will be used for prediction of vortex induced motions.

A good location for fish farming includes good current conditions. Current velocities in the range 0.1-1.5 m/s are in a typical fish farm site (Søreide, 2015, pers. comm.). Ocean current ensures a good throughput of water and good environmental conditions for the fish. The sinker ring has a circular cross-section. Because the fish cages are intentionally placed in locations with currents, VIV is very likely to occur and to contribute to fatigue damage on the sinker ring.

Data for the sinker ring and the connection ropes are are found in Table 4-1 and Table 4-2. The sinker ring has a circumference of 160 meters. There are 20 ropes connecting the sinker ring to the net pen.

Table 4-1 Data for sinker ring provided by Aqualine

Main data	
Circumference	160 m
Material	PE-80 (Polyethylene)
Pipe diameter	400 mm
Material properties	
E-modulus	1E9 N/m^2
G-modulus	3.85E8 N/m^2
Cross-sectional properties	
Outer diameter	400 mm
Inner diameter	327 mm
Wall thickness	SDR11 (36.36 mm)
Area	0.041167 m^2
Iy	6.8848E-4 m^4
Iz	6.8848E-4 m^4
Ix	1.377E-3 m^4
Weight and volume per meter length	
Volume	0.01 m^3
Mass density	3255.034372 kg/m^3
Weight in air	134.0 kg/m
Weight in water	80.0 kg/m

The sinker ring is filled with water and contains a steel wire to obtain the desired weight. The weight in air excludes the water. The total weight in air including water is around 210 kg/m. Only then can a weight in water of 80 kg/m be obtained.

Table 4-2 Data for connection ropes provided by Aqualine

Main data	
Material	Three-strand twisted fiber rope
Diameter	22 mm
Length	2.5 m
Material properties	
E-modulus	1.87E9 N/m^2
Cross-sectional properties	
Diameter	22 mm
Area	3.8E-4 m^2
Weight and volume per meter length	
Volume	3.8E-4 m^3
Mass density	990.0 kg/m^3
Weight in air	0.3762 kg/m
Weight in water	0.101937 kg/m

4.2 Modeling in RIFLEX

A local model of the sinker ring and the connection ropes has been modeled in RIFLEX. A detail illustration of how the connection ropes connect the sinker ring and the net pen is shown in Figure 4-2.

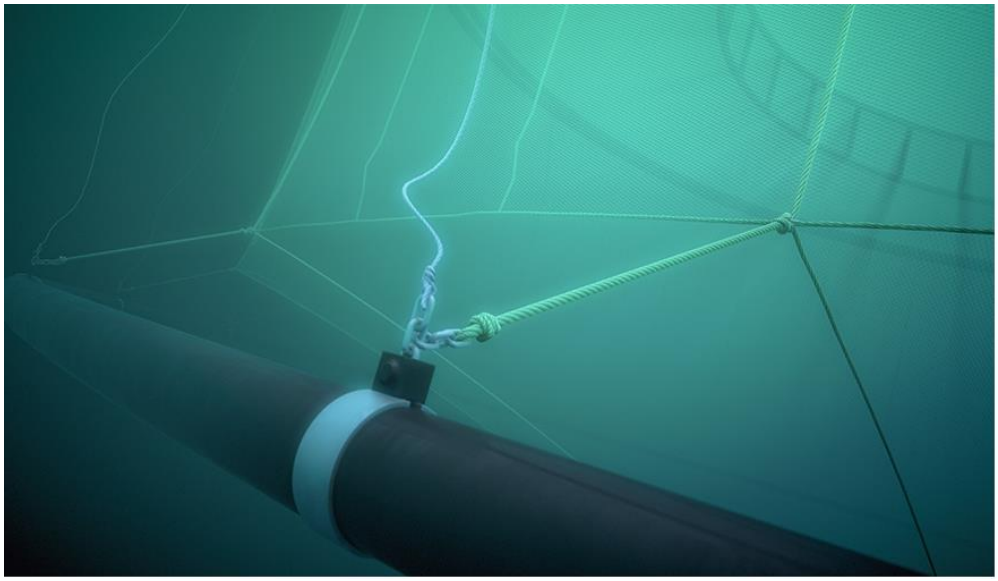

Figure 4-2 Detail of the connection point between sinker tube and net pen (aqualine.no)

Step I

The sinker ring is formed of 20 supernodes with straight line segments in between. This means that the ring is not actually circular. Every supernode, has a straight line representing the connection rope. The angle between the ropes and the horizontal plane is approximately 80 degrees pointing towards the center of the ring. The RIFLEX model at this stage is shown in Figure 4-3.

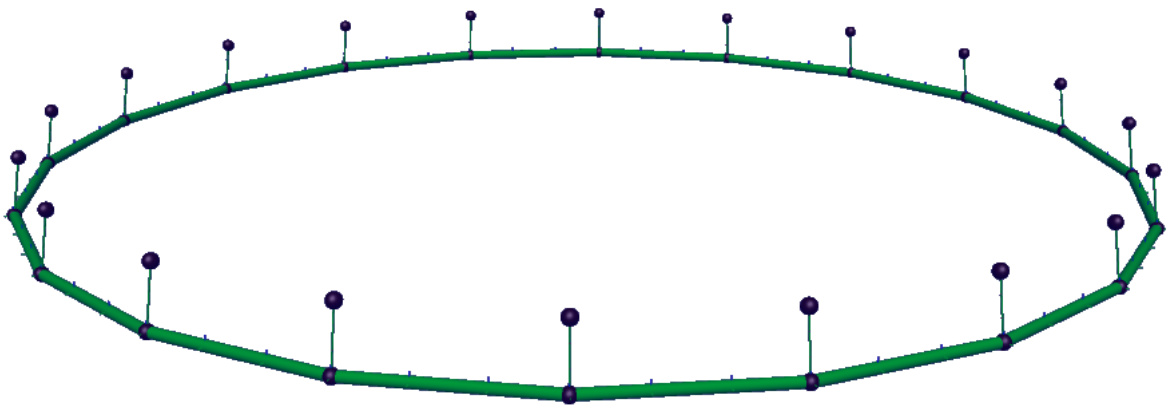

Figure 4-3 Simple RIFLEX model (Step I)

Every line segment is divided into three elements. To use three elements per segment was chosen on the basis that the AquaSim model also used three elements per segment. When comparing for example axial forces in RIFLEX and AquaSim, the accuracy will be the same.

The 20 nodes forming the sinker ring are set as free for translations and rotations in x, y and z-direction. The 20 nodes that represent the connection points on the net pen are set as fixed for all translations, but are free to rotate.

The line segments are given properties equivalent to the data given for the sinker ring and connection ropes in Table 4-1 and Table 4-2.

Some simplifications in the modeling were made:

- *The ropes are modeled as beams where the bending stiffness is set to a very small value.*
- *The steel wire placed inside the ring for extra weight is not possible to model in RIFLEX. Instead, the plastic material was given higher mass to obtain the correct weight.*
- *The sinker ring is placed at z=-17 m. It is assumed to be undisturbed from surface waves. Hence, only current forces have been studied.*
- *The sinker ring segments are given an internal fluid with the density of 1025 kg/m^3. This becomes incorrect because a part of the volume inside the ring is in reality occupied by the steel wire. This will give the sinker ring a slightly higher weight.*

Step II

At this point, when current forces are applied for the static analyses in RIFLEX, the structure will not move in the current direction because the connection nodes are fixed. To improve the boundary conditions and make the model more realistic, static analyses in AquaSim with current velocities ranging from 0.1-1.5 m/s are performed with the full cage model. The displacements of the connection nodes are found, and given to RIFLEX as prescribed displacements.

The deformed shape is illustrated in Figure 4-5. The blue line shows the initial position before any forces are applied. The red line shows the displacements and the deformed shape after current forces are applied. The green line places the deformed shape back to the initial position. The coordinates of the green line were implemented in RIFLEX as prescribed displacements for the connection points. This example shows the displacements of the connection nodes with a current with velocity 1.0 m/s coming from the negative x-direction. The prescribed displacement pattern for the connection nodes can be seen in Figure 4-4.

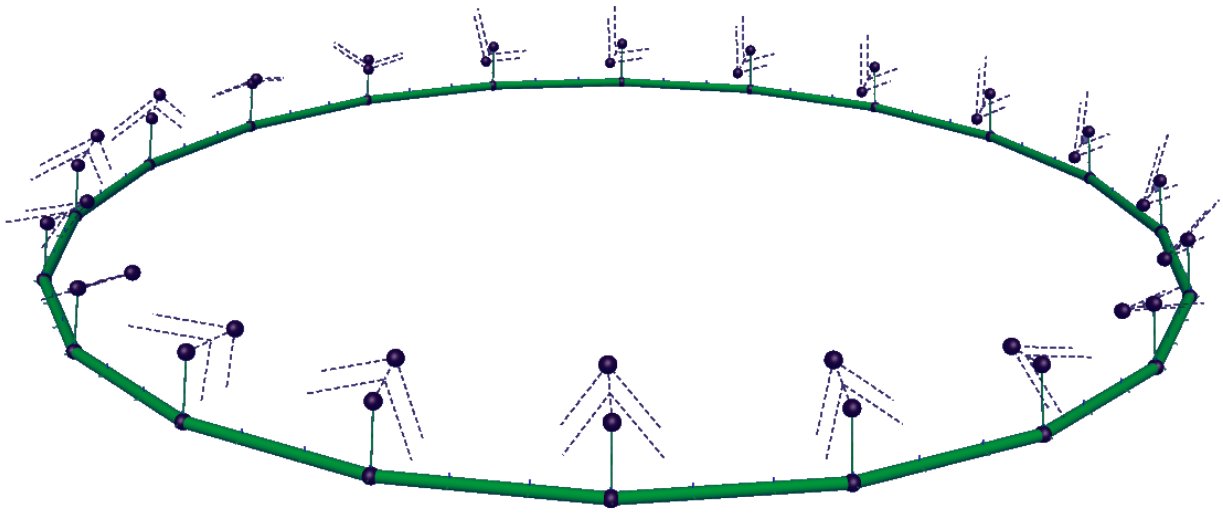

Figure 4-4 RIFLEX model with prescribed displacements (Step II)

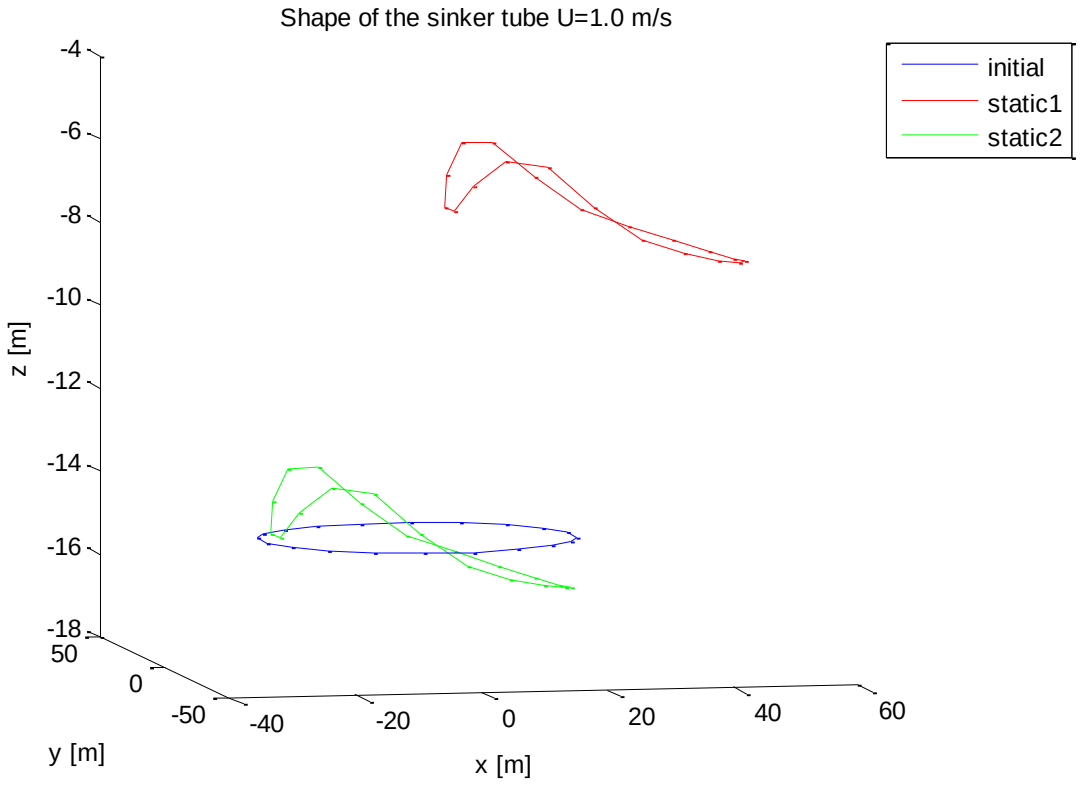

Figure 4-5 Displacement and deformation of the ring (connection points) in current

Step III

To improve the model further, another static analysis in AquaSim was performed, this time without any external forces. The aim was to find the stiffness from the net pen. The weight of the sinker ring will stretch the net. The vertical displacement of the ring was found, and the stiffness was calculated from:

$$F = k\Delta z \tag{23}$$

where k is the stiffness, F is the gravitation force of the ring (weight in water is used), and Δz is the initial z-position minus the static z-position. The boundary conditions that the connection nodes will have when the stiffness of the net pen is included are shown in Figure 4-6. However, the springs were not possible to model correctly in RIFLEX. The boundary conditions the connection nodes ended up of having are illustrated in Figure 4-7.

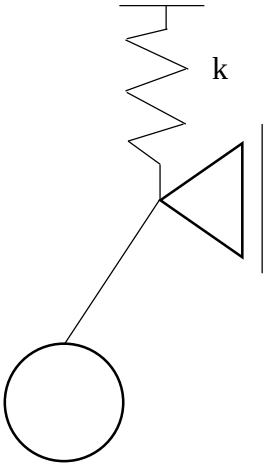

Figure 4-6 Boundary condition for connection nodes

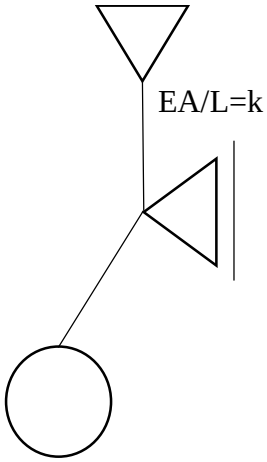

Figure 4-7 Boundary conditions applied in RIFLEX

The springs were modeled as lines with an axial stiffness EA/L=k. The connection nodes are free to move in the z-direction. The RIFLEX model with prescribed displacements and "springs" for modeling the stiffness of the net pen is shown in Figure 4-8. This is the model used for further analyses in VIVANA. Further details of the RIFLEX model are found in the inpmod-file in Appendix A.

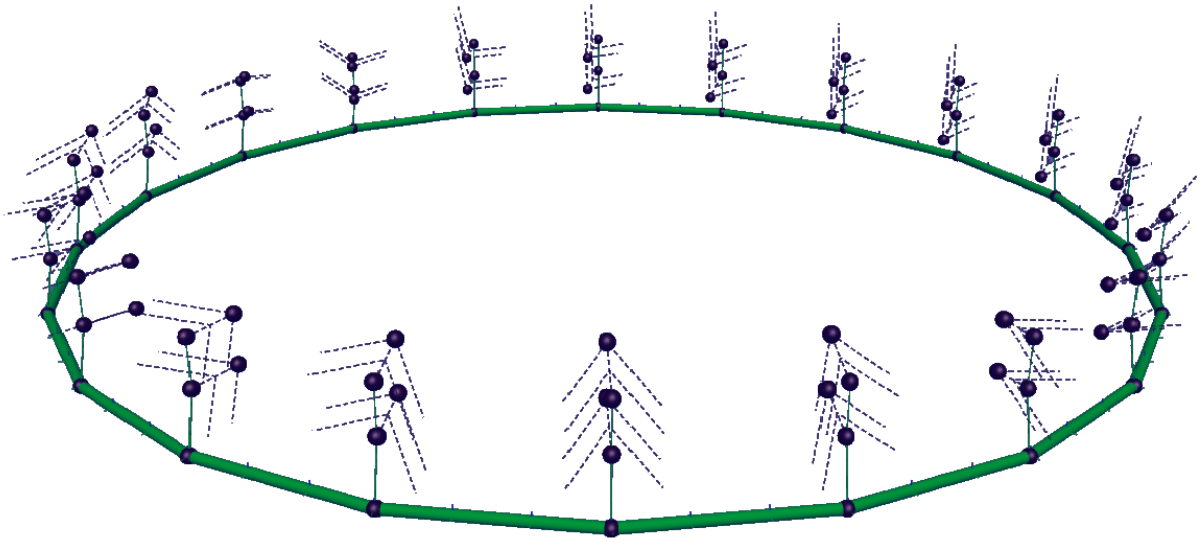

Figure 4-8 RIFLEX model with prescribed displacements and "springs" representing the stiffness of the net pen (Step III)

4.3 VIVANA Analysis

In VIVANA, analyses of combined CF and IL vibrations are performed. The time sharing analysis method has been used. That means that if the excitation frequency candidates have overlapping excitation zones, only one frequency can be excited at a time. The excitation frequency will hence vary with time.

Added mass coefficient for both CF added mass, and IL added mass is set constant to 1.0 (Larsen, 2015, pers. comm.-b). This is done to reduce the computation time. Nevertheless, since the eigenfrequencies in CF and IL direction are not the same, VIVANA only uses the constant added mass for the CF analysis. Iterations are made to find the IL response.

The eigenfrequencies in CF direction are not dependent on the curvature of the ring. Therefore, the ring can be treated like a beam. In IL direction, the curvature of the ring will have an influence on the eigenfrequencies.

It is of interest to look at VIV on the sinker ring only. To exclude the connection ropes and the springs from the VIV analysis, the Strouhal number is set to 0.0001. Then vortex induced motions of these segments are avoided.

For the fatigue analysis, Aqualine did not provide proper SN curve data for the plastic material in the sinker ring. Instead, an SN curve from a paper on fatigue of PE pipes (Pinter et al., 2005) was used. This document has also been used by Aqualine for fatigue references. The reference SN curve is shown in Figure 4-9.

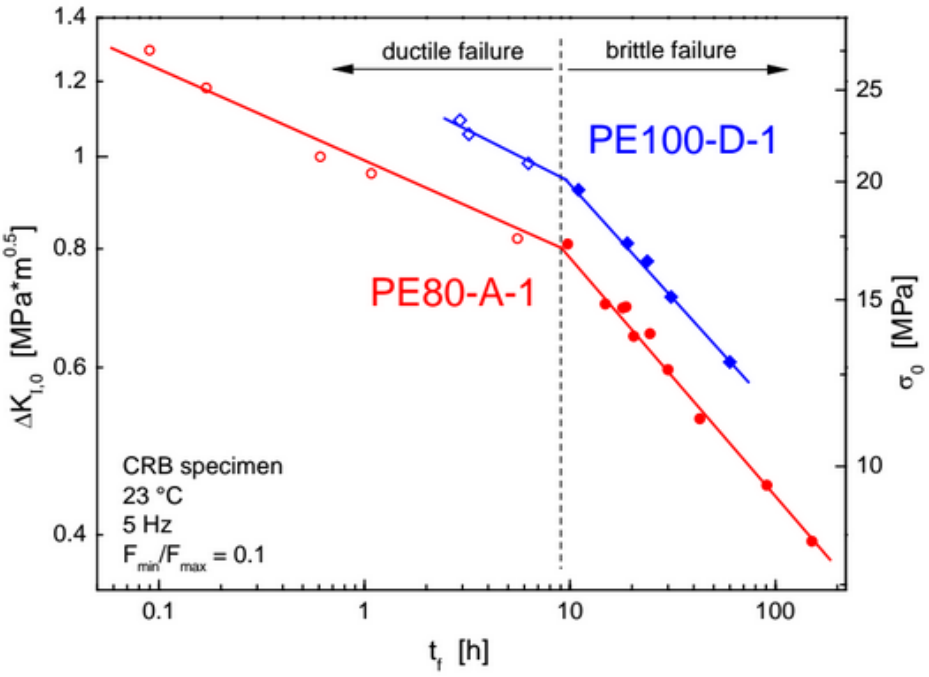

Figure 4-9 SN curve for PE-80 (Pinter et al., 2005)

The SN curve used in the VIVANA analysis is shown in Figure 4-10. The x-axis has been transformed from hours to cycles to failure. Only the part of the curve showing ductile failure has been used.

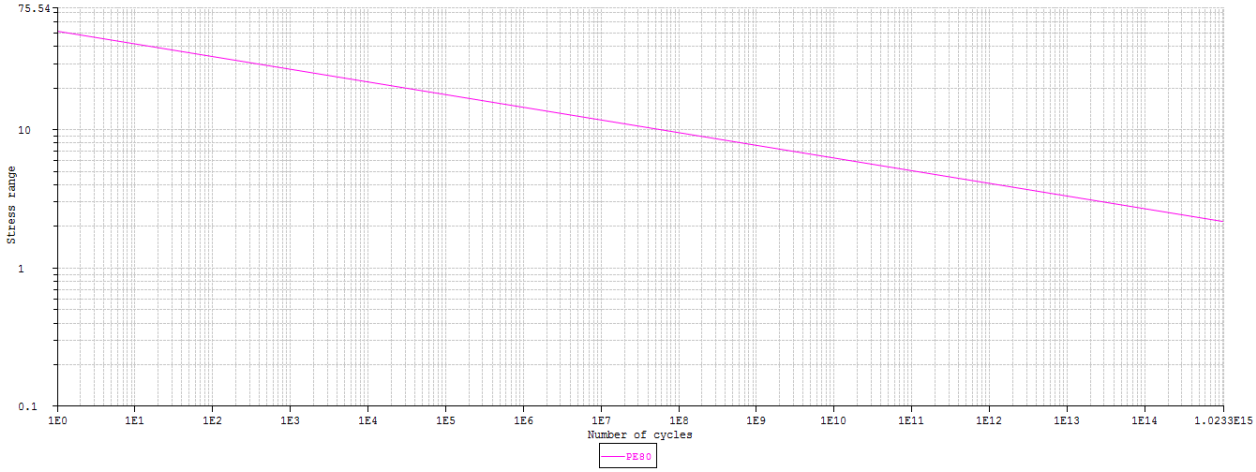

Figure 4-10 SN curve for PE-80

5 A Simple Estimation of VIV

In this chapter, simple hand calculations for the prediction of VIV are performed. Often it is necessary to perform simple hand calculations for engineering problems. This is useful to see if the results given by the analysis program are reasonable. In this case, simple formulas will be used to see if and when VIV will occur in this case. These findings will later be compared to the results obtained from the VIVANA analyses.

5.1 Vortex Shedding Frequency

A range of current velocities from 0.1-1.5 m/s has been used in the calculations. The applied current is constant. Because of the shape of the structure, the velocity has to be decomposed find the component normal to the ring. The velocity will vary from 0 m/s at the edges, to maximum velocity upstream and downstream.

The maximum vortex shedding frequency that can occur for every velocity is presented in Table 5-1. The frequencies are calculated from this formula:

$$f_v = \frac{St \cdot U}{D} \tag{24}$$

where St is the Strouhal number and is assumed constant (=0.2). D is the diameter of the cross-section (=0.4 m), and U is the current velocity.

Table 5-1 Current velocity vs. vortex shedding frequency

Current Velocity [m/s]	**Vortex Shedding Frequency [Hz]**
0.1	0.05
0.2	0.1
0.3	0.15
0.4	0.2
0.5	0.25
0.6	0.3
0.7	0.35
0.8	0.4
0.9	0.45
1.0	0.5
1.1	0.55
1.2	0.6
1.3	0.65
1.4	0.7
1.5	0.75

5.2 Eigenfrequencies

The eigenfrequencies are listed in Table 5-2. These are obtained from the eigenfrequency solution of a simply supported beam. CF vibrations are vibrations out of the plane. Hence, the curvature of the beam is not significant. The eigenfrequencies in in-line direction will depend on the curvature.

The applied equation is:

$$\omega_n = \frac{n^2\pi^2}{l^2}\sqrt{\frac{EI}{m}} \tag{25}$$

where m is the mass per length including added mass. The added mass is assumed to be constant, and equal to the mass of the structure.

The modeshapes can be described as:

$$\Phi_n = a_n \sin\frac{n\pi x}{L} \tag{26}$$

where n is the mode number and a_n is the mode amplitude.

Table 5-2 Eigenfrequencies

Mode shape n	Eigenfrequency [Hz]
2	0.0099
4	0.0397
6	0.0894
8	0.1590
10	0.2484
12	0.3577
14	0.4869
16	0.6360
18	0.8049
20	0.9937

The eigenfrequencies for mode shapes 2-16 lie within the Strouhal frequency range. It is known that if the eigenfrequency coincides with the Strouhal frequency, the natural frequency will lock into the vortex shedding frequency, and VIV will occur.

The eigenfrequencies of the ring will be influenced by two factors:

1. *Larger axial forces will give decreased stiffness to the system. Decreased stiffness leads to lower eigenfrequencies. (When a member buckles, the eigenfrequency is zero because there is no longer any stiffness in the member).*
2. *The radial forces from the angle of the connection ropes provide the system with additional horizontal stiffness. This will give higher eigenfrequencies.*

5.3 Possible Excited Frequencies

Table 5-3 Non-dimensional frequencies for the eigenfrequencies and associated mode shapes

Mode		2	4	6	8	10	12	14	16	18	20
Eigenfreq.		0,01	0,04	0,09	0,15	0,25	0,36	0,49	0,64	0,80	0,99
U [m/s]	**fv [1/s]**	**f [-]**	**f [-]**	**f [-]**	**f [-]**	**f [-]**	**f [-]**	**f [-]**	**f [-]**	**f [-]**	**f [-]**
0,1	0,05	0,040	0,160	0,360	0,600	1,000	1,440	1,960	2,560	3,200	3,960
0,2	0,1	0,020	0,080	0,180	0,300	0,500	0,720	0,980	1,280	1,600	1,980
0,3	0,15	0,013	0,053	0,120	0,200	0,333	0,480	0,653	0,853	1,067	1,320
0,4	0,2	0,010	0,040	0,090	0,150	0,250	0,360	0,490	0,640	0,800	0,990
0,5	0,25	0,008	0,032	0,072	0,120	0,200	0,288	0,392	0,512	0,640	0,792
0,6	0,3	0,007	0,027	0,060	0,100	0,167	0,240	0,327	0,427	0,533	0,660
0,7	0,35	0,006	0,023	0,051	0,086	0,143	0,206	0,280	0,366	0,457	0,566
0,8	0,4	0,005	0,020	0,045	0,075	0,125	0,180	0,245	0,320	0,400	0,495
0,9	0,45	0,004	0,018	0,040	0,067	0,111	0,160	0,218	0,284	0,356	0,440
1	0,5	0,004	0,016	0,036	0,060	0,100	0,144	0,196	0,256	0,320	0,396
1,1	0,55	0,004	0,015	0,033	0,055	0,091	0,131	0,178	0,233	0,291	0,360
1,2	0,6	0,003	0,013	0,030	0,050	0,083	0,120	0,163	0,213	0,267	0,330
1,3	0,65	0,003	0,012	0,028	0,046	0,077	0,111	0,151	0,197	0,246	0,305
1,4	0,7	0,003	0,011	0,026	0,043	0,071	0,103	0,140	0,183	0,229	0,283
1,5	0,75	0,003	0,011	0,024	0,040	0,067	0,096	0,131	0,171	0,213	0,264

It was established in Chapter 2.5 that excitation frequency candidates usually are selected on the basis that the non-dimensional frequency is in the range 0.125-0.3. In Table 5-3, an overview of the non-dimensional frequencies for every eigenfrequency vs. the maximum current velocity is presented. The possible excitation frequency candidates are marked in red. Mode 2 and 4 are not going to be excited. It looks like there can be vortex induced motions for velocities larger than 0.2 m/s.

Due to the geometry, the normal component of the current velocity varies from 0 m/s to the maximum value in Table 5-3. This can induce a multimode response, i.e. response at more than one frequency.

However, as discussed before, due to compression forces the real eigenfrequencies are expected to be lower. Hence, this could require larger current velocities before VIV can be observed.

5.4 Axial Forces

Due to the compression of the ring, its eigenfrequencies will change. Compressive axial forces will decrease the stiffness of the structure, and the eigenfrequencies will become lower. This means that higher mode VIV is more likely to occur.

There will be tension in the connection ropes due to the weight of the ring. An illustration of the forces acting in the ring is shown in Figure 5-1. The radial force H is found by decomposing the force T in the connection rope as shown in Figure 5-2. The axial forces found here only account for the weight of the ring. The axial forces will also be influenced by the current condition. The magnitude of the compression forces depends on the angle α of the ropes, and also the length of the ropes. This is illustrated in Figure 5-2. The angle α between the horizontal plane and the ropes will be determined by the elasticity of the cage net. It is seen that the smaller the angle between the rope and the horizontal force is, the greater will the compression force become.

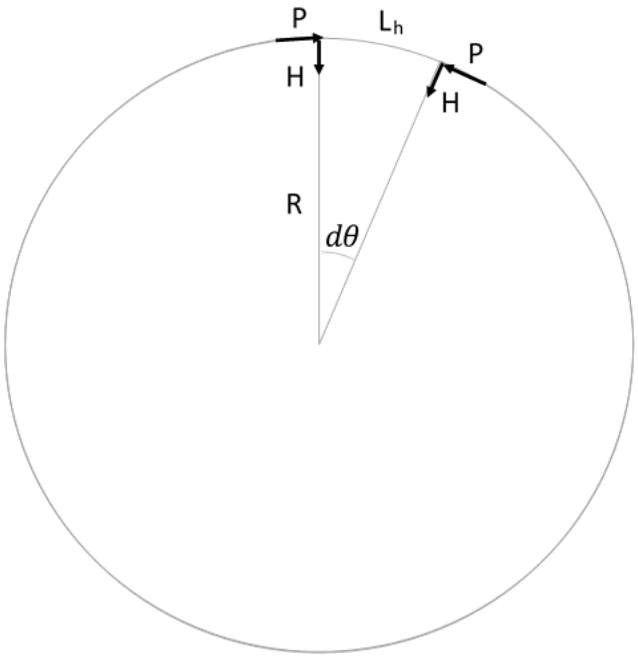

Figure 5-1 Forces in the ring

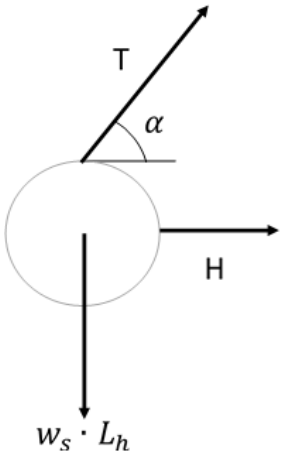

Figure 5-2 Decomposition of forces

Assume small angles:

$$d\theta \approx \sin d\theta \tag{27}$$

So that:

$$d\theta = \frac{L_h}{R} \tag{28}$$

Then the radial force H can be written as:

$$H = P \cdot d\theta \qquad (29)$$
$$H \cong P \cdot \frac{L_h}{R}$$

Then the axial force in the ring can be expressed as:

$$P = \frac{H \cdot R}{L_h} \qquad (30)$$

The radial force H can be determined from decomposition of the connection rope force T:

$$T \sin\alpha = w_s L_h \qquad (31)$$
$$T = \frac{w_s L_h}{\sin\alpha}$$

$$H = T \cos\alpha \qquad (32)$$

The gravity force acting on one rope is:

$$w_s \cdot L_h = 80\frac{kg}{m} \cdot 8m \cdot 9.81\frac{m}{s^2} = 6280\ N$$

The rope force:

$$T = \frac{6280\ N}{\sin 80°} = 6377\ N$$

The radial force:

$$H = 6377\ N \cdot \cos 80° = 1107\ N$$

The axial force:

$$P = \frac{1107\ N \cdot 25.5\ m}{8\ m} = 3530\ N$$

The axial force is defined as a compressive force. The calculations above show that there will be a compressive axial force in the ring of approximately 3.5 kN due to its own weight.

The eigenfrequencies of the ring will be influenced by this. The compression in the ring leads to lower eigenfrequencies, and this will increase the probability of VIV. Large axial compression forces can also cause buckling of the ring.

5.5 Buckling

In this subchapter it is investigated whether the ring could buckle under the compressive axial forces.

The critical Euler buckling load for a beam-column is:

$$P_E = \frac{\pi^2 EI}{L_e^2} \tag{33}$$

Where EI is the bending stiffness and L_e the buckling length. In this case the a simply supported beam is analyzed, and L_e=L.

From Euler's buckling load formula, an axial force of approximately 100 kN is needed for the ring to buckle. This force is too large for buckling to be likely to occur.

$$P_E \approx 106\ kN$$

From a conversation with Professor Svein Sævik (Sævik, 2015, pers. comm.), this formula for the buckling load was derived for a curved beam segment.

$$Q_{cr} = \pi^2 EI \frac{\left[\frac{1}{l^4} - \frac{1}{R^2\pi^2}\frac{1}{l^2}\right]}{\left[\frac{1}{l^2} - \frac{1}{R^2\pi^2}\right]} = \frac{\pi^2 EI\left[\frac{1}{l^2} - \frac{1}{R^2\pi^2}\right]}{\left[1 - \frac{l^2}{R^2\pi^2}\right]} \tag{34}$$

where R is the radius and l is the length of the curved segment.

This equation gives the same result as Euler's buckling load formula.

$$Q_{cr} \approx 106\ kN$$

With a safety factor of 2, the requirement of the axial force, P, in the ring will be:

$$P \leq 53\ kN$$

6 Results and Discussion

In this chapter, the results together with a discussion of every plot will be presented.

Analysis for current velocities in the range 0.1-1.5 m/s have been carried out. For velocities from 0.1-0.7 m/s, VIV did not occur. Therefore, only results from velocities larger than 0.7 m/s will be presented.

- *Case 1: U=0.8 m/s*
- *Case 2: U=0.9 m/s*
- *Case 3: U=1.0 m/s*
- *Case 4: U=1.1 m/s*
- *Case 5: U=1.2 m/s*
- *Case 6: U=1.3 m/s*
- *Case 7: U=1.4 m/s*

The case U=1.5 m/s was excluded from the analysis because there were a few problems with the VIVANA analysis for this model. Probably because the model has different properties in the cross-flow and in-line directions, VIVANA could not calculate the response for this velocity. Cross-flow and in-line analysis could have been performed separately, but there is no reason to think that this case would not follow the pattern of the previous cases.

In the following subchapters, results for velocity distribution and vortex shedding frequency around the ring, displacement and deformation from the AquaSim analysis and axial forces in the ring are presented. Results from VIVANA have been presented for the velocities U=1.0 m/s and U=1.3 m/s. This includes information about excited frequencies, excitation zones and coefficients, response amplitudes in both CF and IL directions, stress amplitudes and accumulated fatigue damage. The same results for the other velocities can be found in Appendix B. The appendices are organized according to the cases defined above.

A comparison of the VIVANA results for all velocities is made at the end of this chapter.

In the following, the part of the ring located upstream will be referred to as Region I or (I) and the part of the ring located downstream will be referred to as Region II or (II). The part in between these two regions is called the middle region. An illustration of the ring seen from above is in Figure 6-1. The current comes from the negative x-direction. The actual regions are marked in the figure. The definition of length is shown in Figure 6-2.

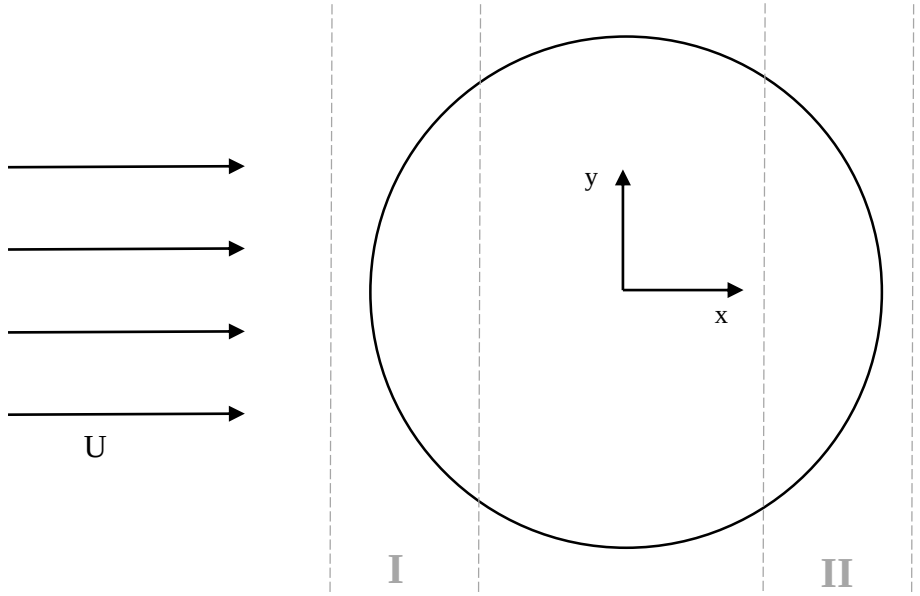

Figure 6-1 Region I and II of the ring

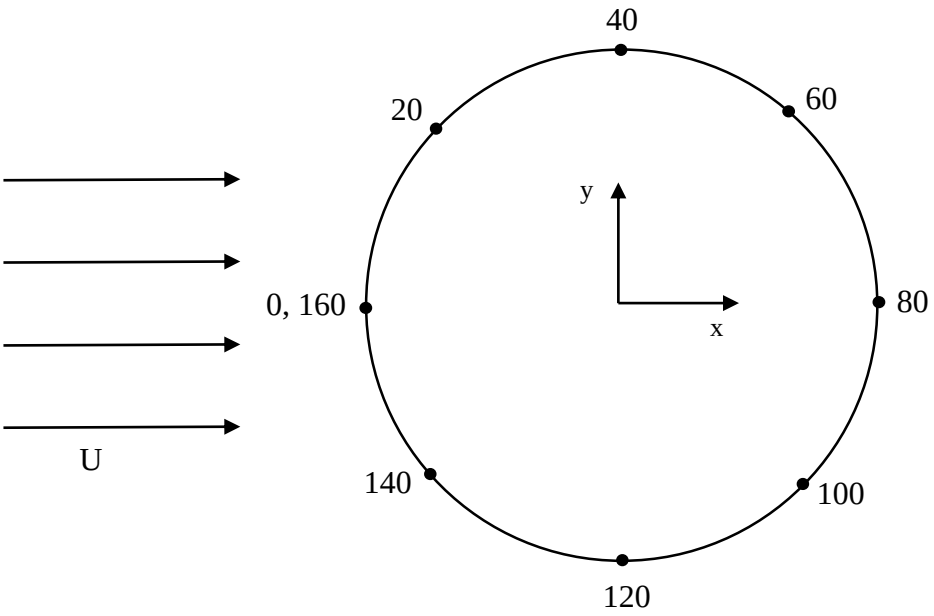

Figure 6-2 Definition of length. All numbers are given in [m].

6.1 Current Velocity and Vortex Shedding Frequency

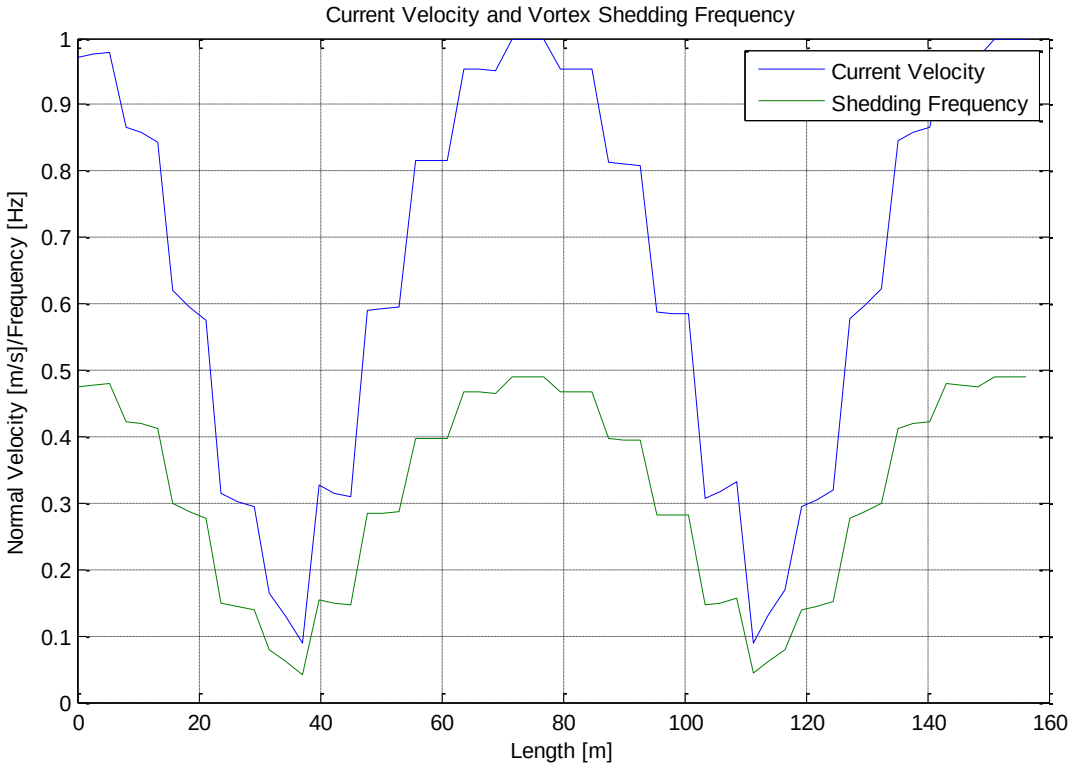

Figure 6-3 Current velocity distribution and vortex shedding frequency over the length of the structure. Initial current velocity is U=1.0 m/s.

Figure 6-3 shows the current velocity distribution over the length of the ring as well as the vortex shedding frequency. The component of the velocity normal to the cross-section of the structure is of interest. The initial current velocity is 1.0 m/s and the current enters from the negative x-direction. According to the model, the segments at 0, 80 and 160 meters will be normal to the incoming flow. Hence, the largest velocity will be experienced for these segments. Ideally, the current velocity normal to the ring should be equal to zero at the sides at 40 and 120 meters. Since the shape of the ring is not circular but consists of 20 straight-line segments, the distribution is uneven and not equal to zero at the sides. The vortex shedding frequency is proportional to the current velocity, and will therefore follow the same pattern. When the eigenfrequency of the ring is close to the vortex shedding frequency, vibrations due to the vortex shedding can occur.

When the current is sheared as in this case, it is likely that several frequencies can be excited. If the lowest eigenfrequency that can be excited is larger than the vortex shedding frequency, VIV can be avoided.

The initial current velocity will be varied from 0.1-1.5 m/s in the simulations. The component of the velocity normal to the line segments and the vortex shedding frequency will follow the same pattern for all velocities as in Figure 6-3.

6.2 Deformation of Ring

In this subchapter, the displacements and the deformations of the sinker ring from the AquaSim analyses are presented. Three velocities, 0.5, 1.0 and 1.5 m/s, are shown to illustrate how increasing current forces will influence the displacements and deformations. The static shape of the ring is of significance when considering the axial forces in the ring. The coordinates of the deformed static shape are used to give the local RIFLEX model prescribed displacements. This has been a part of the process of giving the model correct boundary conditions.

In Figure 6-4, a three-dimensional plot of the ring at U=1.0 m/s is shown. The blue line indicates the initial position of the ring. The red line is the static position from AquaSim after current forces are applied. The green line places the ring on the same origin as for the initial position, but the deformed shape is maintained.

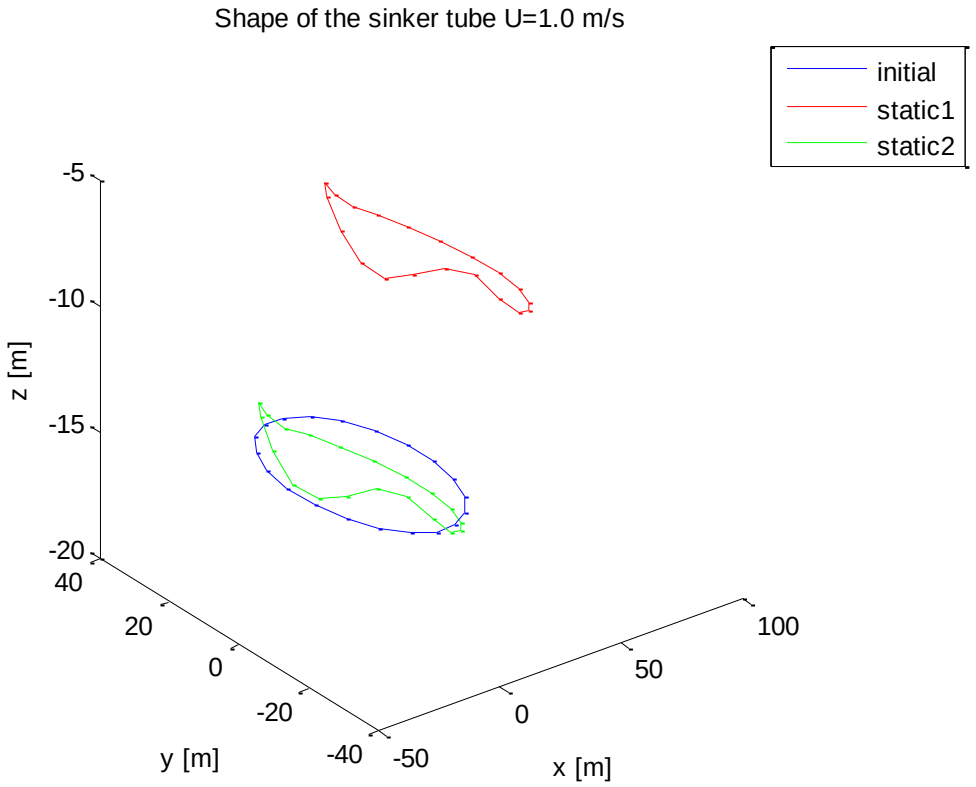

Figure 6-4 3D plot of the position and deformation of the sinker tube with U=1.0 m/s.

In Figure 6-5 - Figure 6-7, the displacements of the ring at current velocity U=0.5 m/s are illustrated in the xy, xz and yz -planes respectively. The same are shown for current velocity U=1.0 m/s in Figure 6-8 - Figure 6-10, and for U=1.5 m/s in Figure 6-11 - Figure 6-13. The colors in the plots have the same meaning as in Figure 6-4.

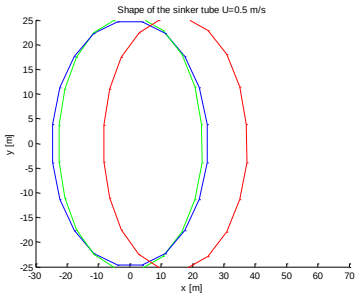

Figure 6-5 Displacement of ring in the xy-plane after current forces are applied with a velocity U=0.5 m/s

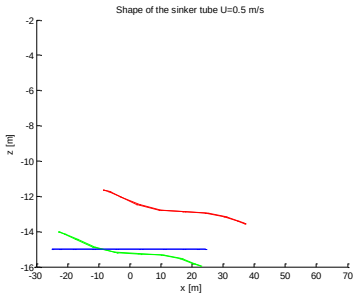

Figure 6-6 Displacement in the xz-plane

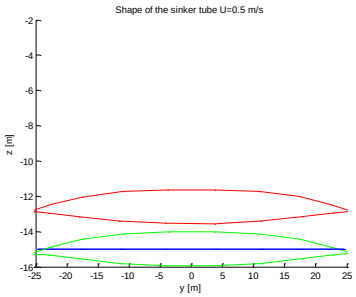

Figure 6-7 Displacement in the yz-plane

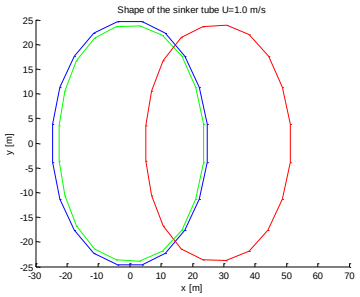

Figure 6-8 Displacement of ring in the xy-plane after current forces are applied with a velocity U=1.0 m/s

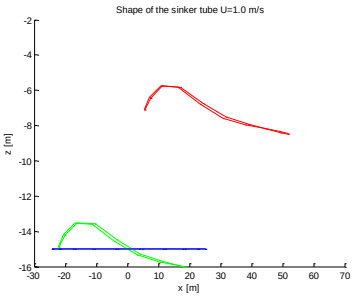

Figure 6-9 Displacement in the xz-plane

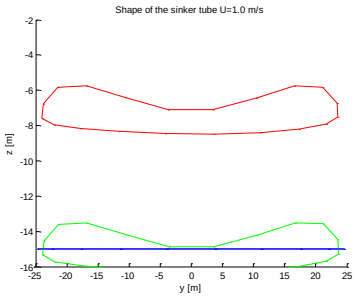

Figure 6-10 Displacement in the yz-plane

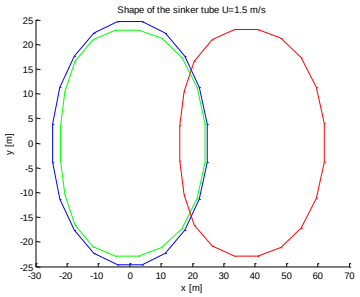

Figure 6-11 Displacement of ring in the xy-plane after current forces are applied with a velocity U=1.5 m/s

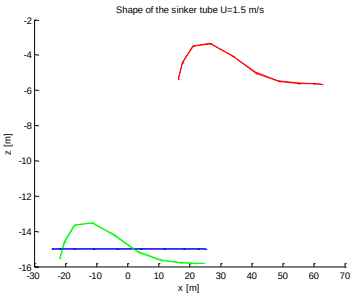

Figure 6-12 Displacement in the xz-plane

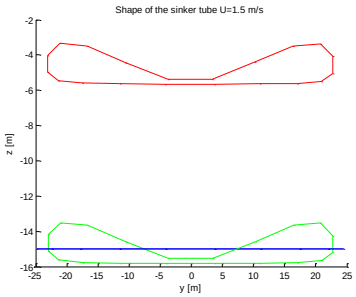

Figure 6-13 Displacement in the yz-plane

It is seen that the structure is very flexible and will move large distances in the current direction. It is implicit that the displacements become larger with increasing current velocity. The ring also experiences larger deformations with increasing velocity.

6.3 Axial Forces

The axial forces in the ring are expected to be compressive due to the tension in the connection ropes.

6.3.1 Buckling

In Chapter 5.5, the critical buckling load was determined. The axial compressive force cannot exceed 100 kN. Given a safety factor of 2, the axial forces cannot exceed 50 kN. This is a very conservative limit. For current velocity U=1.5 m/s, the maximum compressive axial force is less than 30 kN (see Figure 6-14 and Figure 6-15). This means that the ring will not buckle. When the ring buckles, there is no longer stiffness in the structure. This means that the eigenfrequency is zero. Increased compressive axial forces will hence reduce the stiffness, which again will reduce the eigenfrequencies:

$$\omega = \sqrt{\frac{k}{m}} \tag{35}$$

where ω is the eigenfrequency, k is the stiffness and m is the mass of the structure.

6.3.2 Comparison of Axial Forces from SIMA and AquaSim

The axial forces of the model in SIMA have been compared to the axial forces from the static analysis in AquaSim. The AquaSim-model includes a complete cage, and therefore takes into account the deformation of the net pen. This will influence the position and angle of the connection rope, and will have a significant influence on the axial forces and thus also the eigenfrequencies. When the angle of the ropes becomes smaller, the compressive force in the ring will become greater. This is also discussed in Chapter 5.4.

It is seen from Figure 6-14 that regardless of current velocity, the axial force distribution in the ring varies considerably. There are compressive forces over the whole length. However, it is seen that the forces in Region II are less than the forces in Region I. Negative forces are compressive. In this case, -25 kN is considered as a greater force than -5 kN, having larger magnitude.

The varying forces for (I) and (II) have to be understood in conjunction with the deformation of the ring discussed in the previous subchapter.

In this paragraph, the green line in the plots on page 43 is considered. This line shows the deformed ring in the same origin as the initial ring. It is seen that (I) will be "pushed" up and in and (II) "dragged" down and out. There are 20 connection ropes connecting the sinker ring to the net pen. These have an angle pointing diagonally into the ring. The forces in the ropes will give an axial compressive force in the ring. When (I) is pushed upwards, the angle of the ropes will become smaller, and the compressive force will become larger. For (II), there will be an elongation of the actual segments, i.e. tensional forces, and the compressive force in the ring are expected to be less than for (I). The effect of this becomes larger with increasing velocity.

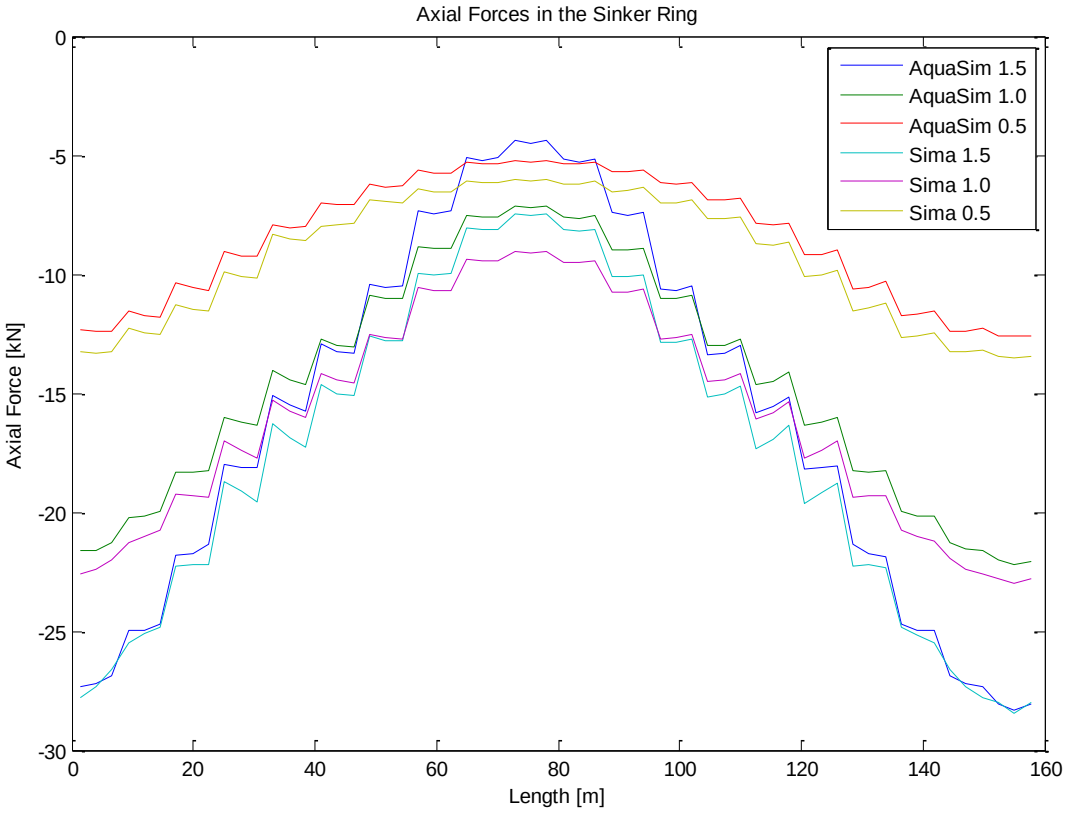

Figure 6-14 Comparison of axial forces from AquaSim and SIMA

Figure 6-14 shows axial forces in the sinker ring from both AquaSim and SIMA for three different velocities; 0.5 m/s, 1.0 m/s and 1.5 m/s. SIMA gives larger compression forces than AquaSim, but the forces for the two models follow the same trend. For higher velocities, SIMA and AquaSim predict the axial forces in (I) that are almost equal, while for higher velocities an increasing gap between the axial forces in (II) is observed.

AquaSim is expected to predict the forces more precisely, as the whole cage model is included. The local model in SIMA could be further improved to enhance the accuracy of the axial forces. Overall, this comparison shows that SIMA gives acceptable results.

6.3.3 Comparison of Axial Forces for Different Velocities

The effect of different current velocities is illustrated in Figure 6-15. When the velocity increases, the axial compressive forces become larger. It is also seen that the larger the velocity is, the larger the difference between the axial forces in (I) and (II) becomes.

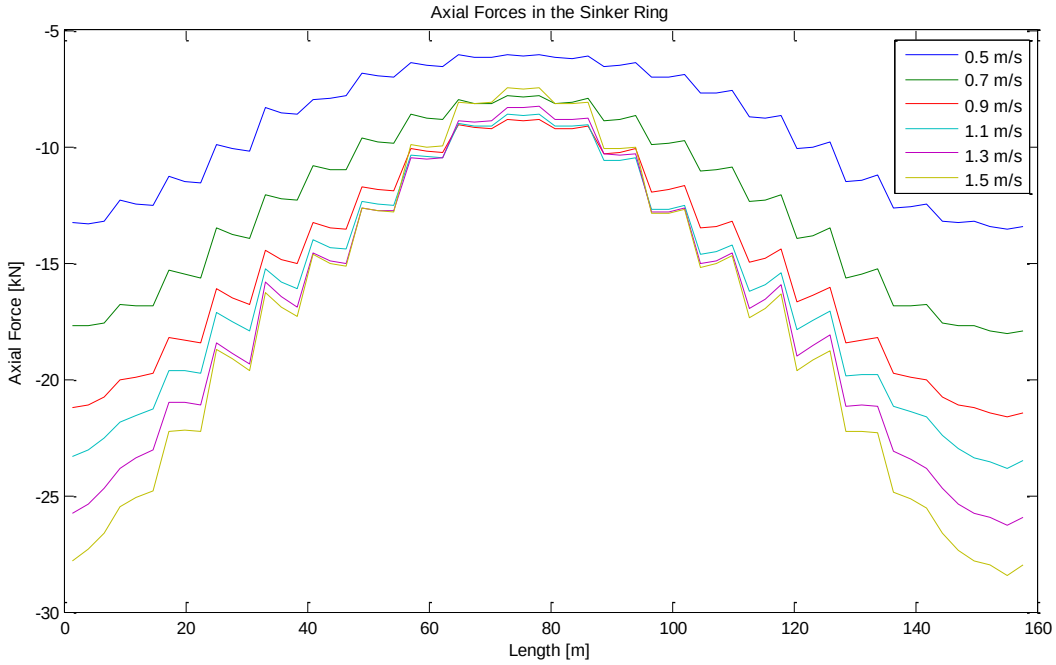

Figure 6-15 Effect of current velocity on the axial forces from SIMA

6.4 Case 3: U=1.0 m/s

The following figures shows the excited frequencies with excitation zones and duration, lift coefficients, CF and IL response amplitudes, stress amplitudes and accumulated fatigue damage for the case where the current velocity U=1.0 m/s.

6.4.1 Excitation Frequencies and Excitation Zones

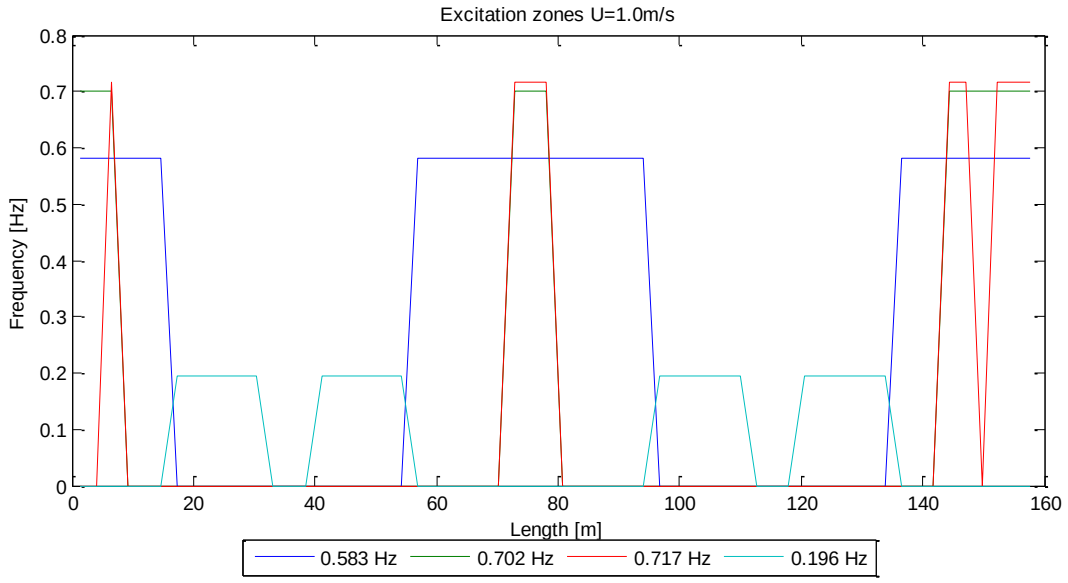

Figure 6-16 Excitation zones for U=1.0 m/s, time sharing

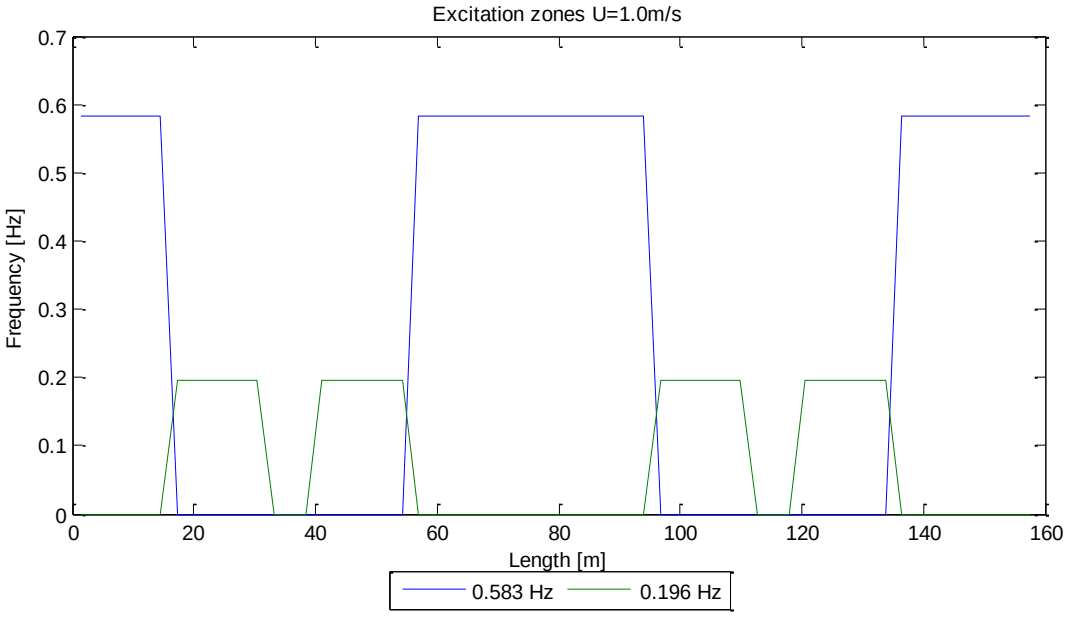

Figure 6-17 Excitation zones for U=1.0 m/s, space sharing

Figure 6-16 shows which frequencies that will excite VIV and the part of the ring that will be excited for each frequency. The dominant frequency is 0.583 Hz and Regions I and II will be excited. These areas are also where the velocity is at its maximum (see Figure 6-3). According to the same figure, the vortex shedding frequency here is 0.5 Hz. The excitation and response frequency is slightly higher than the vortex shedding frequency. However, this difference is small, and this result is considered reasonable. There is also a lower frequency being excited in the middle region. At these positions, the vortex shedding frequencies are around 0.15-0.25 Hz and they match the excited frequency, 0.196 Hz. From Figure 6-16 it is also seen that there will be two other excited frequencies, 0.702 Hz and 0.717 Hz, at a small area where the velocity is at its maximum. Generally VIV will not occur if the eigenfrequencies are higher than the vortex shedding frequency.

From Table 6-1 it is seen that these frequencies will be excited 10-20% of the time. Figure 6-17 shows which frequencies can be excited with the space sharing analysis method. For space sharing, the frequencies act simultaneously. This means that if two excitation frequency candidates have overlapping excitation zones, only the dominant frequency will be excited. For this analysis method, the high frequencies will not occur because f=0.583 will dominate that area.

Table 6-1 Excitation frequencies for U=1.0 m/s

Frequency number	**Frequency [Hz]**	**Duration [%]**
2	0.583	59.2
3	0.702	18.4
4	0.717	12.9
1	0.196	9.5

It is however, a possibility that these frequencies excite vortex induced response. For lower reduced velocities, the structure can oscillate with a frequency higher than the vortex shedding frequency. This is illustrated in Figure 2-8.

6.4.2 Lift Coefficients

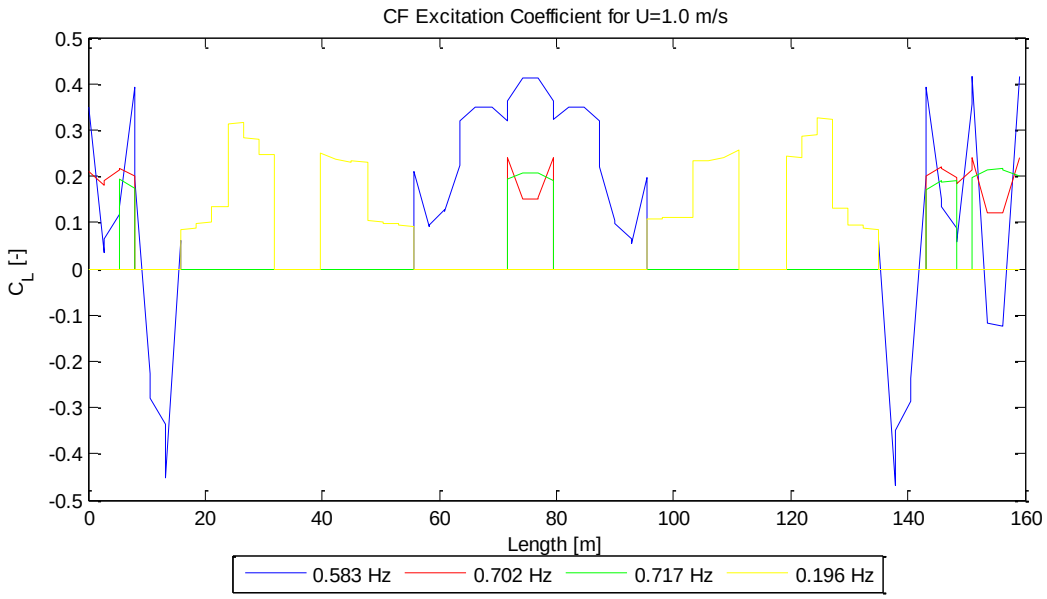

Figure 6-18 Lift coefficients

Figure 6-18 has to be viewed in context with Figure 6-19. Here, the response in (II) will be smaller than for (I). This is despite the excitation coefficients for (II) being higher. This can be explained by the curve showing the relation between the lift coefficient and the amplitude ratio (Figure 2-15). As discussed before, VIV is self-limiting. When the amplitude ratio increases, C_L will increase until it reaches a maximum, then it will decrease and for a certain amplitude ratio (normally A/D=1.2) it will become negative. The excitation coefficients for the lengths around 15 and 140 meters are negative. In these areas, the amplitudes will start to decrease. However, for (II), the lift coefficient probably is close to its maximum, hence the amplitude will be lower.

6.4.3 CF and IL Response Amplitudes

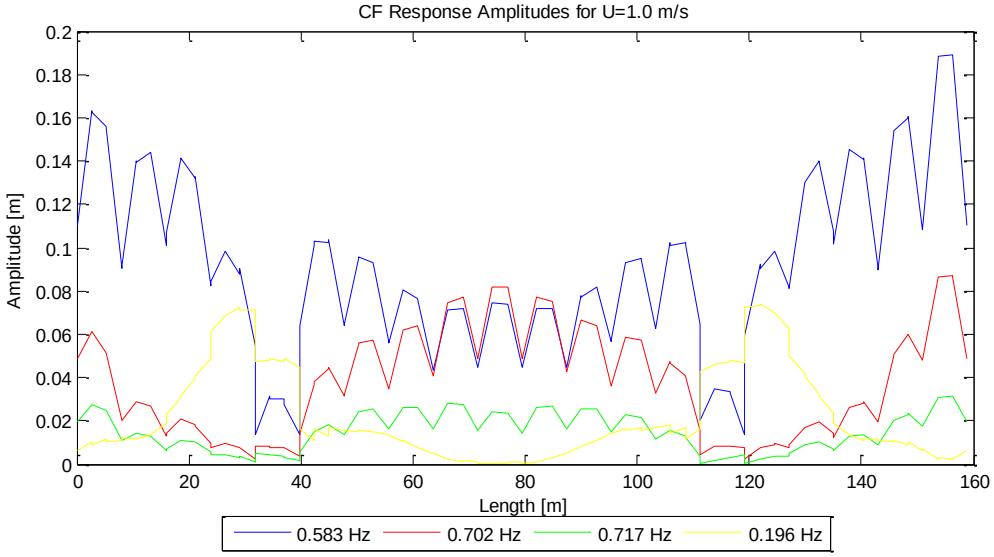

Figure 6-19 CF response amplitudes

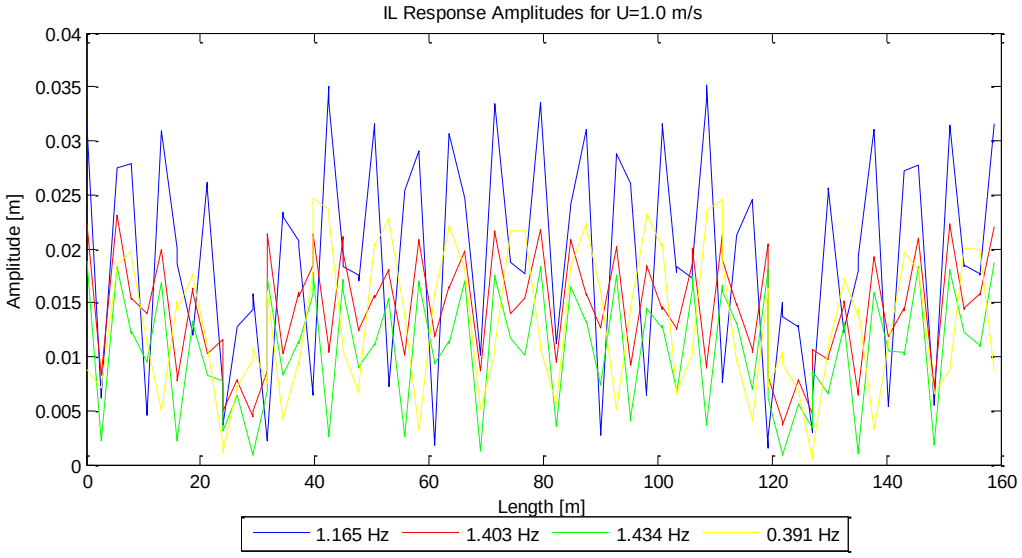

Figure 6-20 IL response amplitudes

The dominant frequency is seen to give the largest response. The dominant frequency is also the frequency closest to the maximum vortex shedding frequency and the resonance area. When comparing Figure 6-19 and Figure 6-20, the IL response amplitudes are smaller than the CF amplitudes. This is according to the expectations and the literature. The IL response occurs at a frequency that is twice the CF frequency.

The CF and IL response shows that different modes are excited in CF and IL directions. This is because the eigenfrequencies in CF and IL directions are not equal. The IL eigenfrequency will be influenced by the curvature of the ring, while the CF eigenfrequencies will not. Hence, an IL eigenfrequency corresponding to twice the CF frequency may excite a different mode than for CF.

6.4.4 Stress Amplitudes

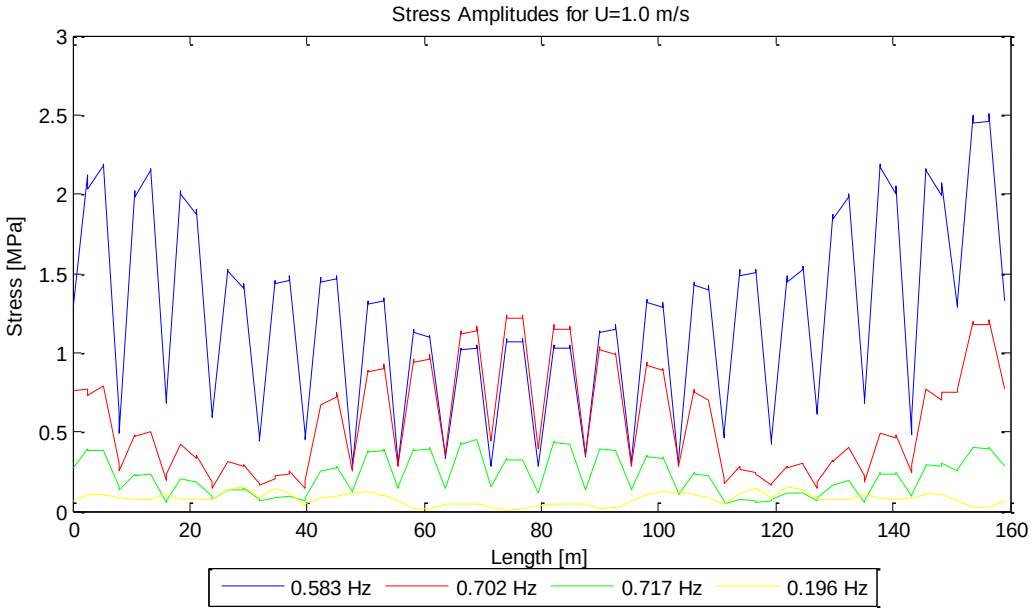

Figure 6-21 Stress amplitudes for CF vibrations

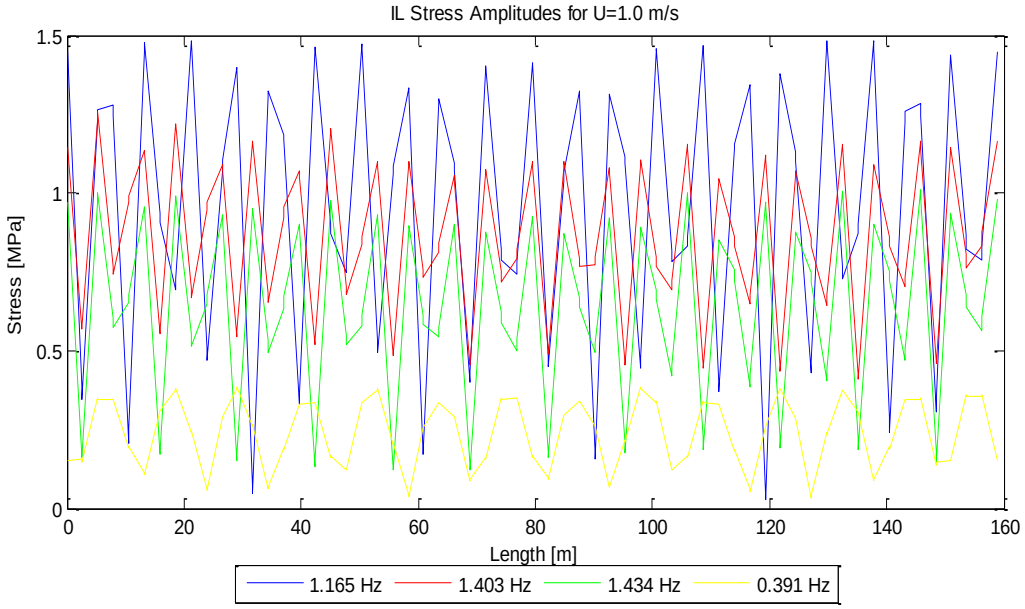

Figure 6-22 Stress amplitudes for IL vibrations

Figure 6-21 and Figure 6-22 show the stress amplitudes for the CF and IL vibrations respectively. These follow the same pattern as the response amplitudes. The dominant frequency f=0.583 Hz gives the largest response and stress amplitudes. These results are as expected because the response frequency is close to the vortex shedding frequency, and resonant vibrations can occur.

6.5 Case 6: U=1.3 m/s

An example of Case 6 with current velocity U=1.3 m/s is also included. For the higher velocities, the frequencies around 0.7 Hz are more active. This leads to higher response amplitudes and more accumulated fatigue damage.

For high current velocities, a large number of frequencies can be excited. It is very unlikely that all of them are excited in reality, so in the following figures and plots, the five most dominating frequencies are presented.

6.5.1 Excitation Frequencies and Excitation Zones

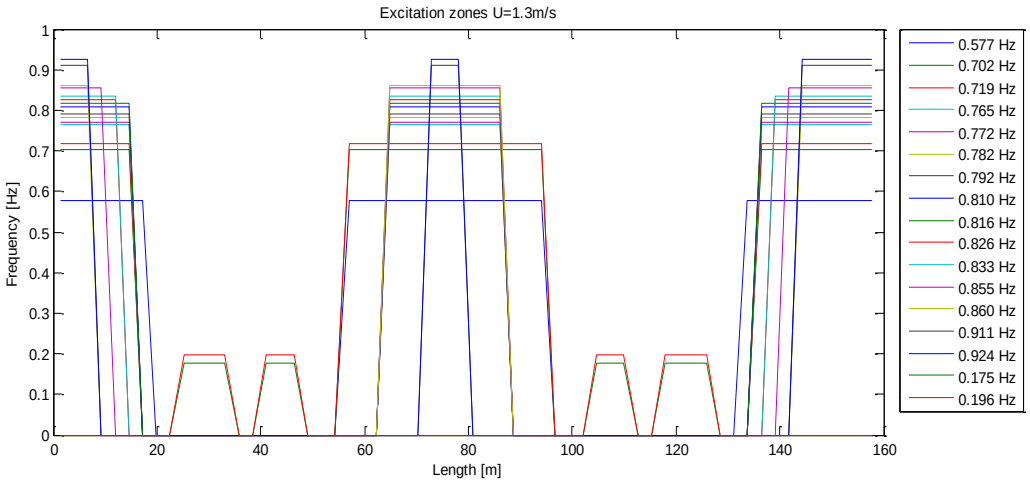

Figure 6-23 Excited frequency and zones for U=1.3 m/s

In total 17 frequencies will be excited for U=1.3 m/s. All possible excited frequencies and duration in the percentage of the time are listed in Table 6-2. An overview of the length and location of the excitation zones is shown in Figure 6-23.

Table 6-2 Excitation frequencies for U=1.3 m/s

Frequency number	Frequency [Hz]	Duration [%]
3	0.577	14.3
4	0.702	9.6
5	0.719	9.1
6	0.765	7.4
7	0.772	7.2
8	0.782	7.0
9	0.792	6.8
10	0.810	6.3
11	0.816	6.2
12	0.826	5.7
13	0.833	5.6
14	0.855	4.9
15	0.860	4.5
16	0.911	2.7
17	0.924	2.5
1	0.176	0.2
2	0.196	0.2

For U=1.3 m/s, the maximum vortex shedding frequency is 0.65 Hz. From Table 6-2 it is seen that a frequency close to 0.58 Hz still is the most dominant frequency. For this case, it is also seen that the second most dominating frequencies have a larger share of the time compared to the most dominating frequency than before. This is because the frequencies around 0.7 Hz is closer to the vortex shedding frequency and hence will have a larger impact.

6.5.2 Lift Coefficients

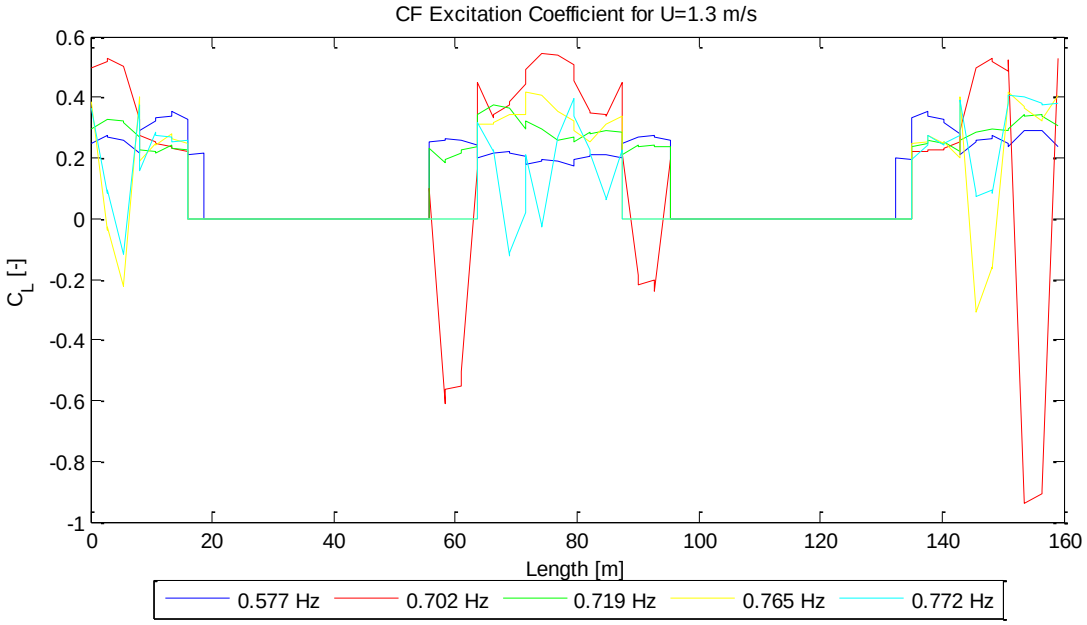

Figure 6-24 Excitation coefficients for U=1.3 m/s

The lift coefficients in Figure 6-24 show that the lift coefficient for f=0.702 Hz becomes negative several places. Then the response amplitudes can be expected to be close to their maximum value here.

6.5.3 CF and IL Response Amplitudes

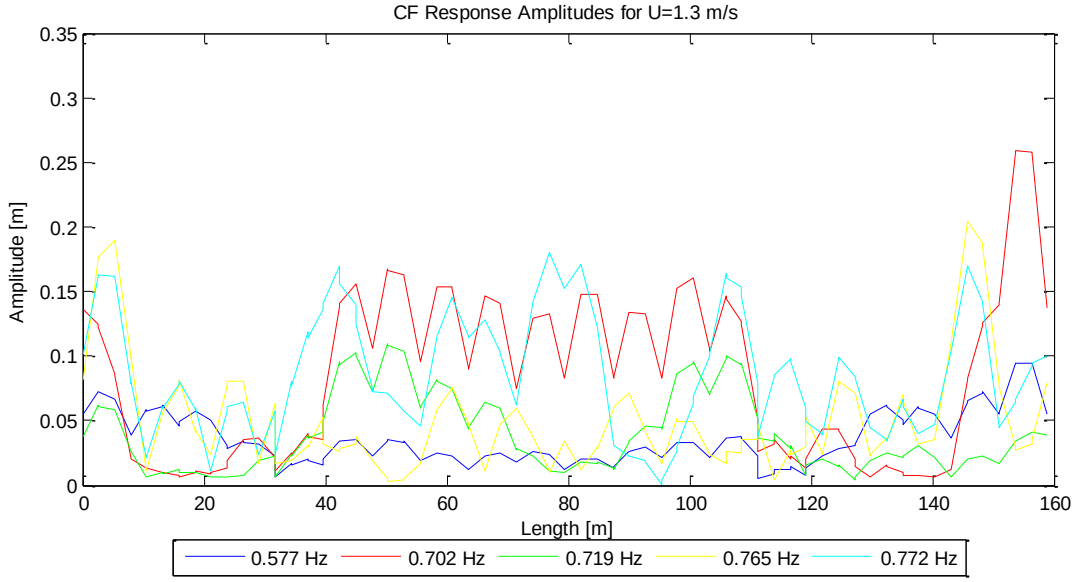

Figure 6-25 CF response amplitudes for U=1.3 m/s

As for the previous case, the maximum response amplitudes are found for (I). Figure 6-25 shows that f=0.702 Hz gives the largest amplitudes, as expected based on the lift coefficients. This is because it is the frequency closest to the maximum vortex shedding frequency, and hence close to the resonance region. The dominant frequency f=0.577 Hz gives smaller amplitudes than the frequencies above 0.7 Hz. However, the dominant frequency gives the largest IL response amplitudes (see Figure 6-26).

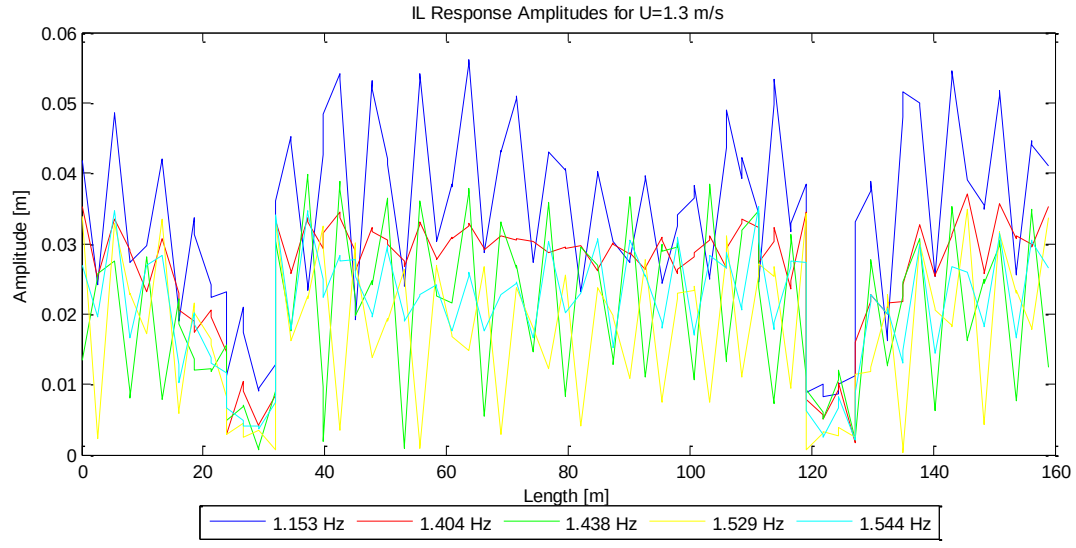

Figure 6-26 IL response amplitudes for U=1.3 m/s

6.5.4 Stress Amplitudes

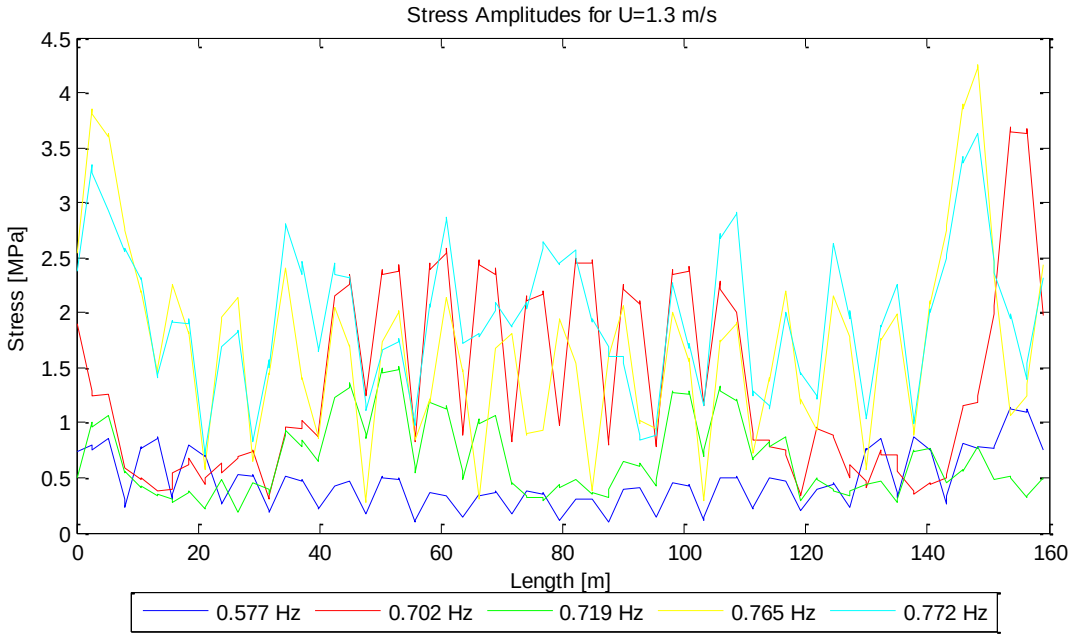

Figure 6-27 Stress amplitudes for CF vibrations for U=1.3 m/s

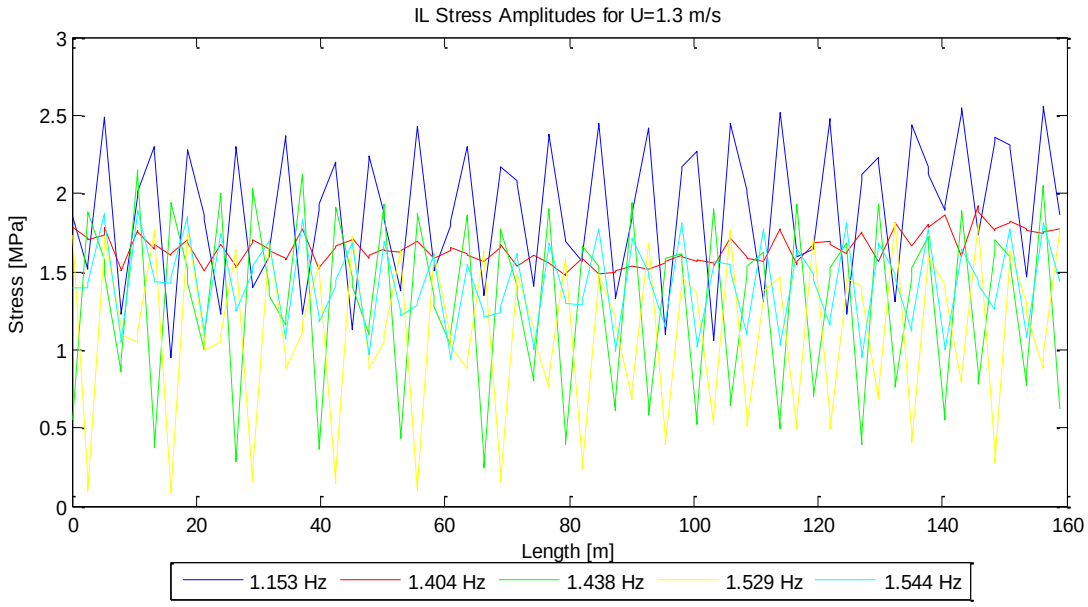

Figure 6-28 IL stress amplitudes for U=1.3 m/s

The higher frequencies give higher stress amplitudes. This corresponds to the findings in Figure 6-25. Larger response amplitude gives larger stress amplitude as seen in Figure 6-27. For IL response, the IL frequency that corresponds to twice the most dominating CF frequency (f=0.577 Hz) give the highest response and stress amplitudes. This can be seen from Figure 6-20 and Figure 6-22.

6.6 Comparison of Response Amplitudes

6.6.1 Cross-flow

In Figure 6-29, the maximum CF response amplitudes for every velocity are presented. The maximum amplitude occurs at U=1.3 m/s. The overall trend is that the response amplitude increases with increasing velocity. There are two exceptions, at U=1.1 m/s and U=1.4 m/s.

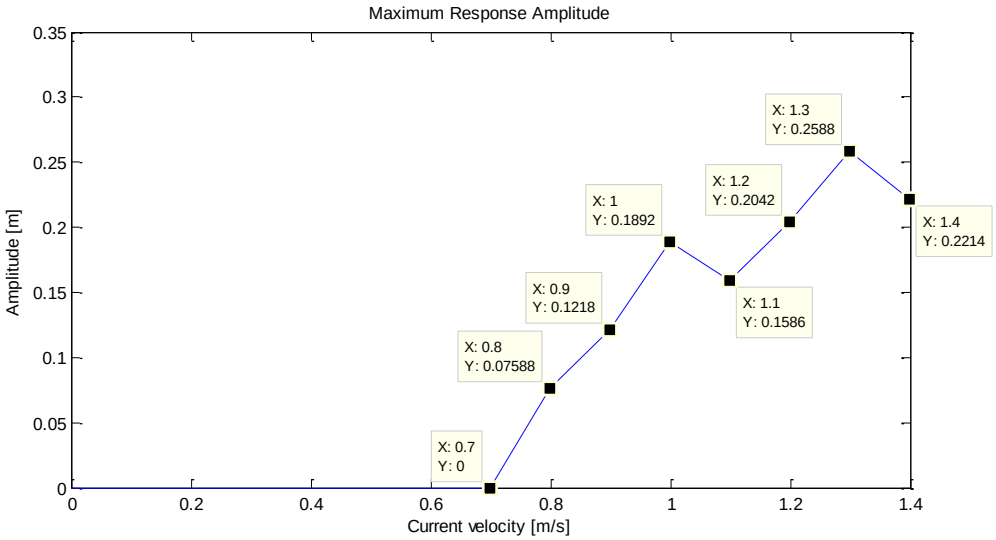

Figure 6-29 Maximum response amplitudes for velocities 0.7-1.4 m/s

In Figure 6-30, the maximum response amplitudes for the five most dominating frequencies for every velocity are plotted. It is seen that for both U=1.1 m/s and U=1.4 m/s the frequency changes. That means that there is a change of mode, then the response amplitude often decreases as seen in Figure 6-29.

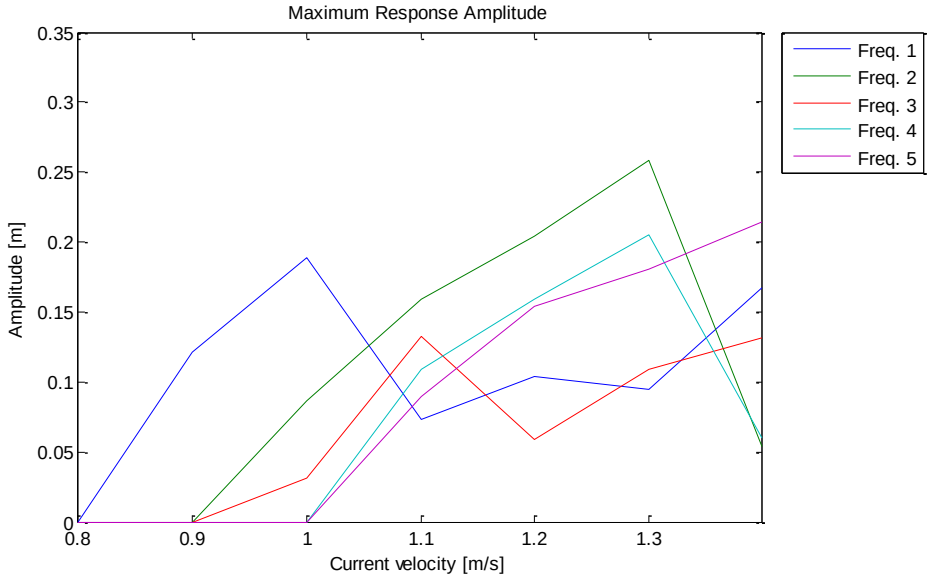

Figure 6-30 Maximum response amplitudes for the five most dominating frequencies for every velocity

6.6.2 In-line

Figure 6-31 shows the maximum response amplitudes for IL vibrations for the five most dominating frequencies. These are, as expected less than the CF response amplitudes. Here it is also seen that the dominant frequency gives the largest response, regardless of current velocity. The trend is as for CF response, the response increases for increasing current velocity.

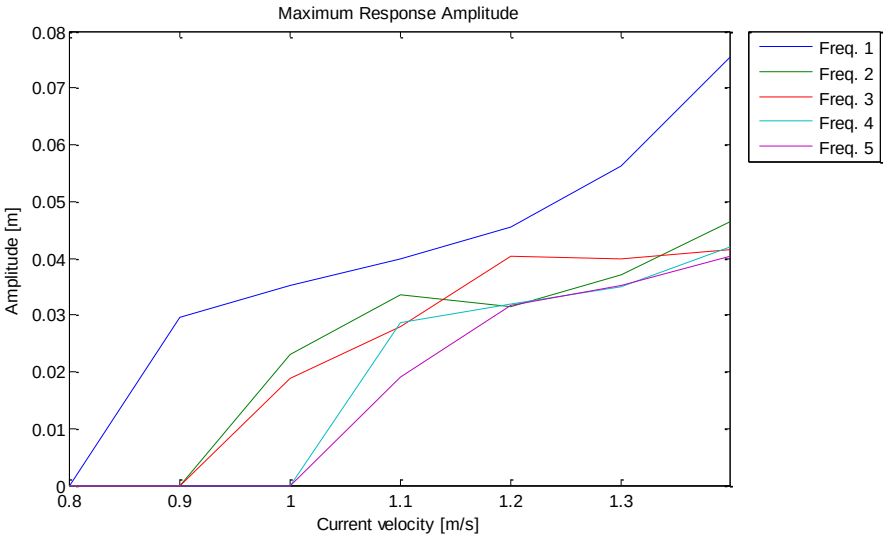

Figure 6-31 Maximum IL response amplitudes for the five most dominating frequencies for every velocity

6.7 Fatigue

The SN curve shown in Figure 4-9 is taken from an article provided by Aqualine. It is the SN curve for polyethylene (PE) pipes, that are commonly used as materials in both the floating collar and the sinker ring. The SN curve used for the fatigue analysis is shown in Figure 4-10.

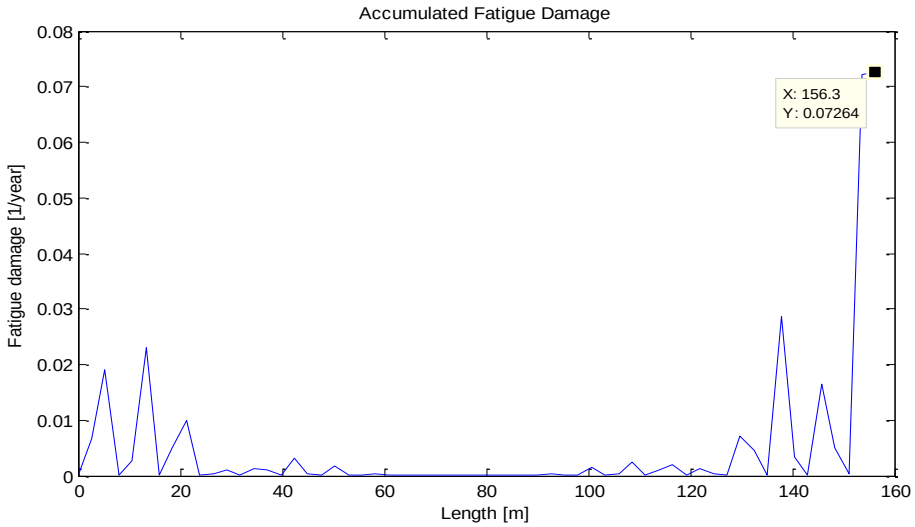

Figure 6-32 Total accumulated fatigue damage for U=1.0 m/s

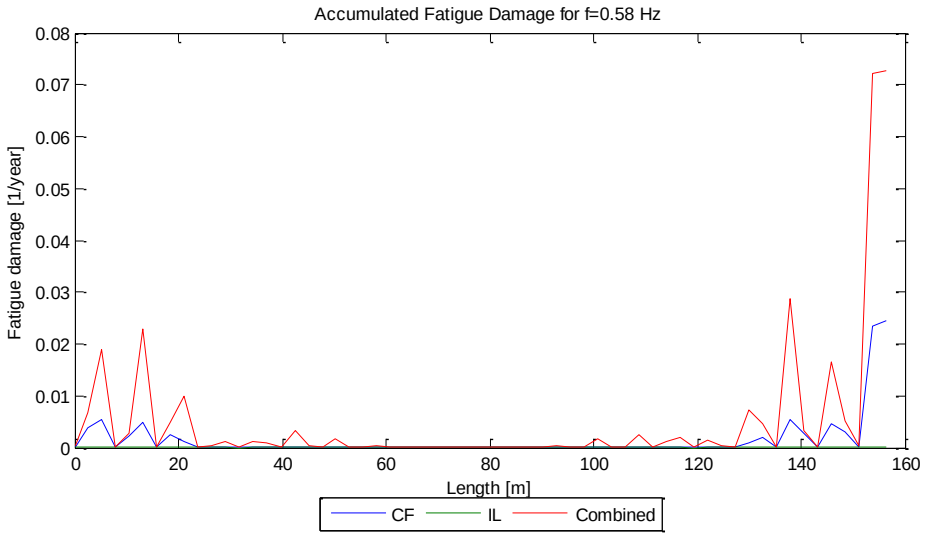

Figure 6-33 Accumulated fatigue damage for f=0.58 Hz

Figure 6-32 and Figure 6-33 above shows the total accumulated fatigue damage and accumulated fatigue damage for the dominant frequency respectively for U=1.0 m/s. For this velocity, the dominant frequency (f=0.85 Hz) will be active approximately 60 percent of the time. It is seen that the response for this frequency will account for most of the fatigue damage alone. Figure 6-33 shows fatigue damage for the IL and CF vibrations, as well as for the combined loading.

It is seen that for the combined loading, the fatigue damage increases drastically. The reason for this is unknown, but could be caused by some effects due to the geometry of the structure. Pure CF and IL fatigue damage is usually calculated for two points on the cross-section as shown in Figure 6-34 and Figure 6-35. Due to the structure geometry, IL vibrations could also have a component in CF direction and vice versa. This will cause fatigue damage also at other points at the cross-section. When combined CF and IL loading is applied, the total fatigue damage will account for the coupled IL and CF effects. Hence, the combined CF and IL fatigue damage could become significantly greater than if fatigue damage contributions of pure IL and CF loading were added together (Larsen, 2015, pers. comm.-a).

CF

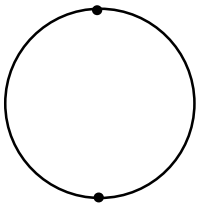

Figure 6-34 Fatigue calculation points for CF loads

IL

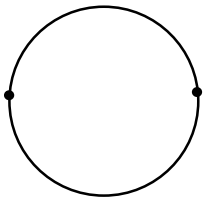

Figure 6-35 Fatigue calculation points for IL loads

Combined CF and IL

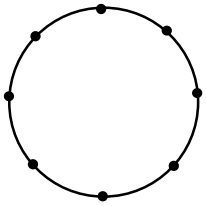

Figure 6-36 Fatigue calculation points for combined CF and IL loads

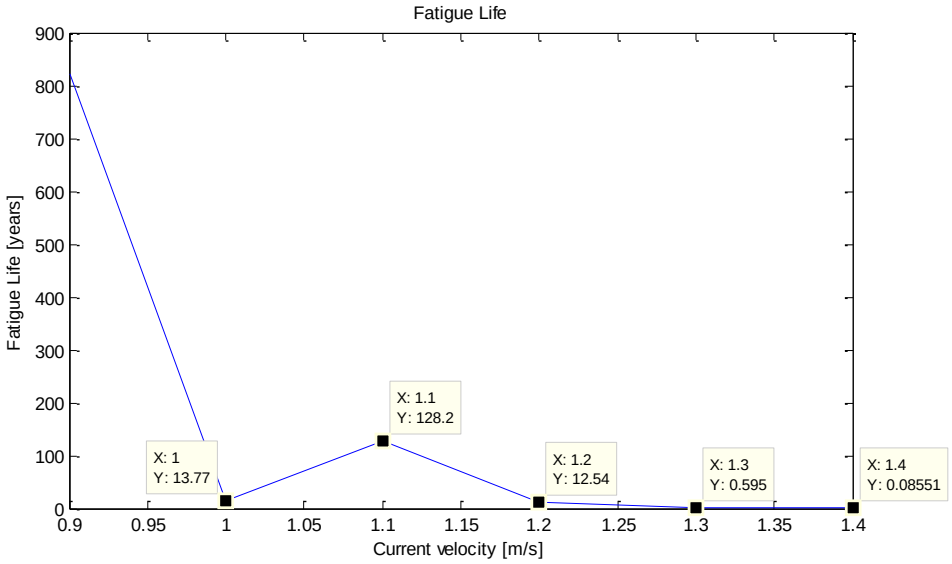

Figure 6-37 Fatigue life for velocities 0.9-1.4 m/s

Figure 6-37 shows the fatigue life of the structure for combined IL and CF loading for current velocities from 0.9-1.4 m/s. The fatigue life decreases tremendously for velocities higher than 1 m/s.

One would expect that the fatigue life of the structure would decrease with incoming current velocity. The reason for the little peak at U=1.1 m/s can be explained by the decreased response amplitude due to the shift of mode that occurs for this velocity.

6.8 Comparison between VIVANA and Expectations Prior to the Analyses

In Chapter 5.3 an overview of possible excited frequencies for a simply supported beam with eigenfrequencies as in Table 5-2, is shown. These eigenfrequencies are assumed valid for the ring's eigenfrequencies in the CF direction. However, as discussed before, the real eigenfrequencies of the ring are expected to be somewhat lower due to the compression forces in the ring. The eigenfrequencies obtained from VIVANA are listed in Table 6-3. When comparing the two sets of eigenfrequencies, the beam frequencies are lower than the VIVANA frequencies for the modes 2-8. For higher modes, the VIVANA frequencies become lower than the beam frequencies.

This is according to the expectations. For the ring, the radial compression forces due to the connection ropes provide the system with additional stiffness. For higher modes, the compressive axial forces cause a decrease of the stiffness. Hence, the eigenfrequencies will become lower.

Table 6-3 Eigenfrequencies for U=1.0 m/s (from VIVANA)

Frequency number	**Frequency Hz**	**CF mode**
1	0.1582	
2	0.1646	
3	0.1750	
4	0.1771	
5	0.1825	
6	0.1832	
7	0.1952	
8	0.1954	1
9	0.2209	
10	0.2399	
11	0.2407	
12	0.3386	
13	0.3390	
14	0.4682	
15	0.4701	
16	0.5826	2
17	0.6257	
18	0.6261	
19	0.7016	3
20	0.7170	4

In the VIVANA analyses, VIV only occur for current velocities higher than U=0.7 m/s. From Table 5-3, it is seen that VIV is expected to occur earlier. The first eigenfrequency that lies in the interval for possible excited frequencies is found at U=0.2 m/s. It is very likely to believe that VIV would occur for velocities lower than 0.7 m/s.

The reason why VIVANA does not give VIV for lower velocities is unknown, but there could be an error in the identification of active frequencies. There is a possibility that the problem occurs due to the ring structure, and may not be a problem for structures traditionally analyzed in VIVANA. This should be investigated further. There is no basis for saying that VIV will not occur at velocities lower than 0.7 m/s.

7 Conclusions

In this thesis, a local model of the sinker ring with connection ropes was established in RIFLEX. Some adjustments and improvements on the basis of analyses done with a full cage model in AquaSim were implemented in the model boundary conditions. Then, VIV analyses for current velocities from 0.1-1.4 m/s were performed. VIV is known to give significant contributions to fatigue damage on slender marine structures. A collapse of the sinker ring could damage the net pen and cause fish escapes.

Evaluation of model

- *The local model defined in RIFLEX shows good coherence with the global cage model analyzed in AquaSim.*
- *When axial forces are compared for the two models, they follow the same trend. However, RIFLEX slightly over predicts the forces.*
- *The model's eigenfrequencies are dependent on the axial forces in the ring. Because the ring experiences compression forces, the eigenfrequencies become lower. Increased current velocity gives increased compression forces.*
- *The eigenfrequencies in CF correspond well to the eigenfrequencies predicted prior to the analyses. The deviations can be explained by increased stiffness due to the radial compression forces for the first modes, and the reduced stiffness due to compressive axial forces for the higher modes.*
- *The model might not be suitable for analyses in VIVANA.*

Evaluation of results

- *According to VIVANA, VIV will not occur for velocities lower than 0.7 m/s. This is not according to the predictions made prior to the analyses. VIV is very likely to occur at lower velocities.*
- *The maximum CF amplitudes observed at U=1.3 m/s, and were in the magnitude 0.6D.*
- *The maximum response amplitudes and fatigue damage will occur at the part of the ring located upstream (Region I).*
- *The fatigue calculations are considered unreliable due to missing data.*

The results obtained from this study shows that VIV will become a problem for high current velocities, i.e. U > 0.7 m/s. It is surprising that no vortex induced motions are generated at lower velocities. There might be a problem with the identification of active frequencies in VIVANA for this structure. According to theory and simple calculations, VIV is expected to occur also at lower velocities. Therefore, final conclusions regarding the survivability of the sinker ring should not be made only out of this study. Recommendations further work are listed in Chapter 8.

8 Further Work

The simple model provides good information compared to the full global cage model in AquaSim. However, the model can be improved. There could be better ways of modeling the existing boundary conditions, or applying boundary conditions not discussed in this thesis. Another way to increase the accuracy of the calculations is to increase the number of elements and/or segments.

Further investigation of which velocities that will induce VIV should be prioritized.

The effect of pure IL response has not been studied in this thesis. Pure IL vibrations occur at lower reduced velocities than CF vibrations, and can be a significant contributor to fatigue. Looking into this is recommended.

The SN curve model for fatigue calculations used in the VIVANA analysis is considered untrustworthy. Correct SN data for the sinker ring material should be found and used. In addition, statistical analysis of the current conditions at a typical location is recommended. To decide the fatigue life of the sinker ring, the directions and velocities of the currents as well as duration of every current state should be determined.

The influence of surface waves has been disregarded. The model has only been exposed to current forces. It is seen from the displacements of the sinker ring from the AquaSim analysis that the structure will move from 17 meters below the surface up to 7 meters below the surface for U=1.0 m/s. This means that waves are likely to affect the structure. Vortex shedding can also be caused by the horizontal velocity the water particles have in waves. This phenomenon has not been mentioned in this thesis, but could still be relevant for this structure. Of course, dynamic loads from waves can have additional effects, and can also influence the fatigue life of the structure.

It would also be very interesting to perform model tests or CFD analyses to validate the results obtained.

9 References

AQUALINE.NO. Available: http://www.aqualine.no/ [Accessed April 8 2015].

AQUASTRUCTURES 2006. "The AQUAstructureSIMulator. Theoretical Formulation of Structure and Load Modeling" Report No. 2006-FO06

AQUASTRUCTURES.NO. *AquaSim* [Online]. Available: http://aquastructures.no/aquasim/ [Accessed April 23 2015].

ARONSEN, K. H. 2007. *An experimental investigation of in-line and combined in-line and cross-flow vortex induced vibrations*, Trondheim, Norges teknisk-naturvitenskapelige universitet.

BLEVINS, R. D. 1994. *Flow-induced vibration*, Malabar, Fla., Krieger.

DN.NO. 2015. *Børs & Marked* [Online]. Dagens Næringsliv. Available: http://www.dn.no/finans/#/energi [Accessed June 8 2015].

GOPALKRISHNAN, R. 1993. Vortex-induced forces on oscillating bluff cylinders. DTIC Document.

HALSE, K. H. 1997. *On vortex shedding and prediction of vortex-induced vibrations of circular cylinders*, Trondheim, NTH.

LAKSEFAKTA.NO. 2014. *Havbruk og Miljø* [Online]. Available: http://www.laksefakta.no/Milj%C3%B8-og-b%C3%A6rekraft/Havbruksn%C3%A6ringens-milj%C3%B8fokus/Les-mer-om/Havbruk-og-milj%C3%B8 [Accessed June 7 2015].

LANGEN, I. & SIGBJÖRNSSON, R. 1979. *Dynamisk analyse av konstruksjoner*, [Trondheim], Tapir.

LARSEN, C. M. 2011. Vortex Induced Vibrations - A short and incomplete introduction to fundamental concepts. Trondhem, Norway: Norwegian University of Science and Technology.

LARSEN, C. M. June 9 2015, pers. comm.-a. *RE: Combined CF and IL fatigue damage.* Type to WERGELAND, T.

LARSEN, C. M. 2015, pers. comm.-b. *RE: Constant added mass coefficient in SIMA.* Type to WERGELAND, T.

LEONG, C. M. & WEI, T. 2008. *Two-degree-of-freedom vortex-induced vibration of a pivoted cylinder below critical mass ratio*.

LIENHARD, J. H. 1966. *Synopsis of Lift, Drag, and Vortex Frequency Data for Rigid Circular Cylinders*, Technical Extension Service, Washington State University.

NOAA FISHERIES. *What is Aquaculture?* [Online]. Available: http://www.nmfs.noaa.gov/aquaculture/what_is_aquaculture.html [Accessed June 7 2015].

NÆRINGS- OG FISKERIDEPARTEMENTET 2015. Meld. St. 16 (2014-2015) Forutsigbar og miljømessig bærekraftig vekst i norsk lakse- og ørretoppdrett. *In:* NÆRINGS- OG FISKERIDEPARTEMENTET (ed.).

OLAFSEN, T., WINTHER, U., OLSEN, Y. & SKJERMO, J. 2012. Verdiskapning basert på produktive hav i 2050. Det Kongelige Videnskabers Selskab (DKNVS) and Norges Tekniske Vitenskapsakademi (NTVA).

PASSANO, E., LARSEN, C. M., LIE, H. & WU, J. 2014. Vivana Theory Manual. Release 4.2. MARINTEK, Trondheim.

PINTER, G., HAAGER, M., BALIKA, W. & LANG, R. W. 2005. Fatigue crack growth in PE-HD pipe grades. *Plastics, Rubber and Composites,* 34**,** 25-33.

QVALE, P. 2014. *OLJEPRISEN: Derfor er oljeprisen i fritt fall* [Online]. Teknisk Ukeblad. Available: http://www.tu.no/petroleum/2014/10/10/derfor-er-oljeprisen-i-fritt-fall [Accessed June 8 2015].

REVE, T. & SASSON, A. 2012. *Et kunnskapsbasert Norge,* Oslo, Universitetsforl.

ROSTEN, T. W., ULGENES, Y., HENRIKSEN, K., TERJESEN, B. F., BIERING, E. & WINTHER, U. 2011. Oppdrett av laks og ørret i lukkede anlegg - forprosjekt. SINTEF Fiskeri og Havbruk.

SSB.NO. 2014. *Akvakultur, 2013, endelige tall* [Online]. Available: http://www.ssb.no/jord-skog-jakt-og-fiskeri/statistikker/fiskeoppdrett/aar/2014-10-30 [Accessed April 22 2015].

STANDARD NORGE 2009. NS 9415:2009 Marine fish farms. Requirements for site survey, risk analysis, design, dimensioning, production, installation and operation.

SÆVIK, S. 2015, pers. comm. *RE: Buckling load for a curved beam* Type to WERGELAND, T.

SØREIDE, M. May 11 2015, pers. comm.

UNITED NATIONS: DEPARTMENT OF ECONOMIC AND SOCIAL AFFAIRS. 2012. *World Population Prospects: The 2012 Revision* [Online]. Available: http://esa.un.org/unpd/wpp/unpp/panel_population.htm [Accessed April 29 2015].

VIV SOLUTIONS. 2013. *Helical Strikes* [Online]. Available: http://www.vivsolutions.com/products/helical-strakes/ [Accessed June 9 2015].

YTTERVIK, R., PASSANO, E., KROKSTAD, J., LARSEN, C. M. & BAARHOLM, G. S. 2009. VIVANA - User's Manual. Version 3.7. MARINTEK, Trondheim.

Appendix

A inpmod.res

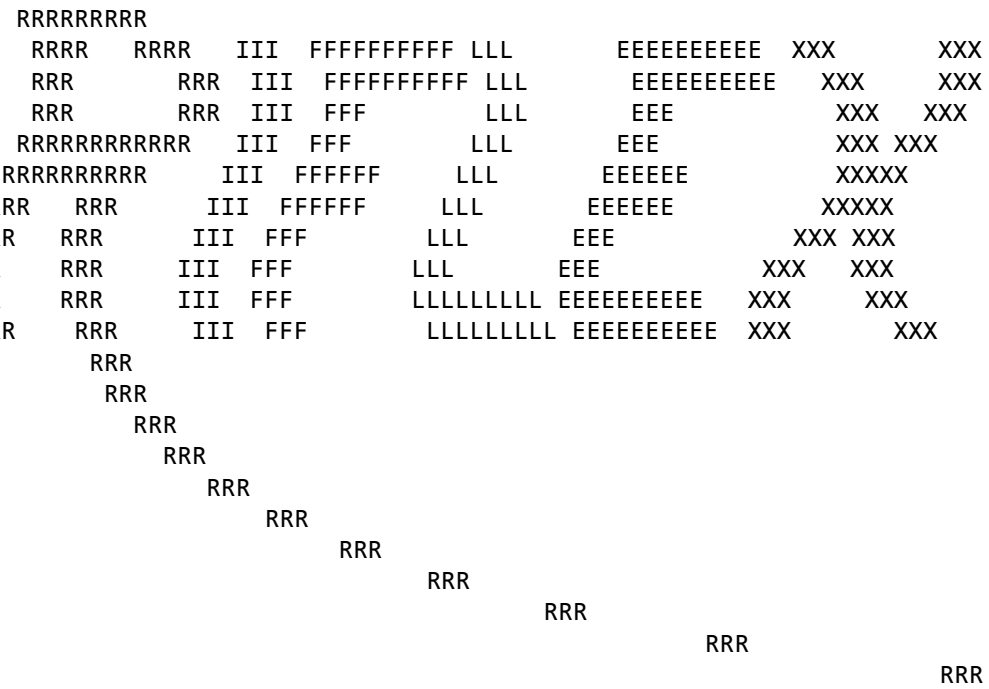

```
   CYGWIN_NT-6.1-WOW64  version linked 2015-02-24 22:11:33

** RIFLEX_INPMOD FLEXlm license checked out **
   Licensed to NTNU, Trondheim
   License expires 31-oct-2015

  *                                          *
  *     WARNING: non-commercial license      *
  *                                          *

   Execution date and time 2015-06-08 11:55:13

    INPUT FILE VERSION ................: 4.4.1

    FILES USED IN THIS RUN
    ----------------------

    INPUT. . . . . : sima_inpmod.inp
    OUTPUT . . . . : sima_inpmod.res
    INPFIL . . . . : sima_ifninp.sam

    MAXIMUM NUMBER OF SOME PARAMETERS SET IN INPMOD
    -----------------------------------------------

    NUMBER LINE TYPES . . . . . . . . . . . . . . : 200
    NUMBER OF PIPE-IN-PIPE PAIRS. . . . . . . . . : 400
    NUMBER COMPONENT TYPES. . . . . . . . . . . . : 200
    NUMBER ENVIRONMENTAL DESCRIPTIONS . . . . . . :  50
    NUMBER TRANSFER FUNCTIONS . . . . . . . . . . :  50
    NUMBER VESSELS. . . . . . . . . . . . . . . . :  10

    +-----------------------------------------------------------+
    !     CONSISTENT UNITS USED THROUGHOUT THE ANALYSES         !
    !-----------------------------------------------------------!
    !     NAME FOR TIME   :  T = s                              !
    !     NAME FOR LENGTH :  L = m                              !
    !     NAME FOR MASS   :  M = Mg                             !
    !     NAME FOR FORCE  :  F = kN                             !
    !                                                           !
    !     GRAVITATIONAL CONSTANT :                              !
    !     G     =   9.810     L/T**2                            !
    !     CONSISTENCY ACCELERATION PARAMETER :                  !
    !     GCONS =  1.0000     (F/M)/(L/T**2)                    !
    +-----------------------------------------------------------+

    NEW SINGLE RISER
    ----------------

    RISER TYPE AND IDENTIFIER :

    SINGLE RISER TYPE . . .: AR
    RISER IDENTIFIER  . . .: ARSYS

    ARBITRARY SYSTEM AR
    -------------------
```

```
Number of supernodes . . . . . :   60
Number of lines. . . . . :   60
Number of fixed supernodes . . . . . :   40
Number of vessels. . . . . :    0
Number of rigid supernode connections:    0 NO RIGID CONNECTIONS PRESENT
Number of springs  . . . . . :    0 NO SPRINGS
Number of kill & choke lines . . . . :    0 NO KILL & CHOKE LINES
Bottom tangent option. . . . . :    0 NO SEAFLOOR CONTACT
Z-coordinate of seafloor (L) . . . . : -100.00     *** DUMMY INPUT ***
3-D bottom option. . . . . :    0 *** DUMMY INPUT ***

Supernode identification :
Line id, Line type, supernode at end 1 and 2 :
```

Lin-id	Lin-type-ref	Isnod1-ref	Isnod2-ref
line1	line90	node1	node2
line2	line90	node2	node3
line3	line90	node3	node4
line4	line90	node4	node5
line5	line90	node5	node6
line6	line90	node6	node7
line7	line90	node7	node8
line8	line90	node8	node9
line9	line90	node9	node10
line10	line90	node10	node11
line11	line90	node11	node12
line12	line90	node12	node13
line13	line90	node13	node14
line14	line90	node14	node15
line15	line90	node15	node16
line16	line90	node16	node17
line17	line90	node17	node18
line18	line90	node18	node19
line19	line90	node19	node20
line20	line90	node20	node1
line21	line91	node1	node21
line22	line91	node2	node22
line23	line91	node3	node23
line24	line91	node4	node24
line25	line91	node5	node25
line26	line91	node6	node26
line27	line91	node7	node27
line28	line91	node8	node28
line29	line91	node9	node29
line30	line91	node10	node30
line31	line91	node11	node31
line32	line91	node12	node32
line33	line91	node13	node33
line34	line91	node14	node34
line35	line91	node15	node35
line36	line91	node16	node36
line37	line91	node17	node37
line38	line91	node18	node38
line39	line91	node19	node39

```
line40       line91      node20      node40
line41       line92      node21      node41
line42       line92      node22      node42
line43       line92      node23      node43
line44       line92      node24      node44
line45       line92      node25      node45
line46       line92      node26      node46
line47       line92      node27      node47
line48       line92      node28      node48
line49       line92      node29      node49
line50       line92      node30      node50
line51       line92      node31      node51
line52       line92      node32      node52
line53       line92      node33      node53
line54       line92      node34      node54
line55       line92      node35      node55
line56       line92      node36      node56
line57       line92      node37      node57
line58       line92      node38      node58
line59       line92      node39      node59
line60       line92      node40      node60

Boundary conditions for fixed or prescribed supernodes:

IPOS = 0 :  No connection to support vessel
IPOS > 0 :  Connection to support vessel nr ipos
IX   = 0 :  X-dof is free
IX   = 1 :  X-dof is fixed or prescribed

SNOD-ID IPOS  IX  IY  IZ  IRX  IRY  IRZ   CHREF  CHUPRO
node21     0   1   1   0   0    0    0    GLOBAL   NO
node22     0   1   1   0   0    0    0    GLOBAL   NO
node23     0   1   1   0   0    0    0    GLOBAL   NO
node24     0   1   1   0   0    0    0    GLOBAL   NO
node25     0   1   1   0   0    0    0    GLOBAL   NO
node26     0   1   1   0   0    0    0    GLOBAL   NO
node27     0   1   1   0   0    0    0    GLOBAL   NO
node28     0   1   1   0   0    0    0    GLOBAL   NO
node29     0   1   1   0   0    0    0    GLOBAL   NO
node30     0   1   1   0   0    0    0    GLOBAL   NO
node31     0   1   1   0   0    0    0    GLOBAL   NO
node32     0   1   1   0   0    0    0    GLOBAL   NO
node33     0   1   1   0   0    0    0    GLOBAL   NO
node34     0   1   1   0   0    0    0    GLOBAL   NO
node35     0   1   1   0   0    0    0    GLOBAL   NO
node36     0   1   1   0   0    0    0    GLOBAL   NO
node37     0   1   1   0   0    0    0    GLOBAL   NO
node38     0   1   1   0   0    0    0    GLOBAL   NO
node39     0   1   1   0   0    0    0    GLOBAL   NO
node40     0   1   1   0   0    0    0    GLOBAL   NO
node41     0   1   1   1   0    0    0    GLOBAL   NO
node42     0   1   1   1   0    0    0    GLOBAL   NO
node43     0   1   1   1   0    0    0    GLOBAL   NO
node44     0   1   1   1   0    0    0    GLOBAL   NO
node45     0   1   1   1   0    0    0    GLOBAL   NO
```

node46	0	1	1	1	0	0	0	GLOBAL NO
node47	0	1	1	1	0	0	0	GLOBAL NO
node48	0	1	1	1	0	0	0	GLOBAL NO
node49	0	1	1	1	0	0	0	GLOBAL NO
node50	0	1	1	1	0	0	0	GLOBAL NO
node51	0	1	1	1	0	0	0	GLOBAL NO
node52	0	1	1	1	0	0	0	GLOBAL NO
node53	0	1	1	1	0	0	0	GLOBAL NO
node54	0	1	1	1	0	0	0	GLOBAL NO
node55	0	1	1	1	0	0	0	GLOBAL NO
node56	0	1	1	1	0	0	0	GLOBAL NO
node57	0	1	1	1	0	0	0	GLOBAL NO
node58	0	1	1	1	0	0	0	GLOBAL NO
node59	0	1	1	1	0	0	0	GLOBAL NO
node60	0	1	1	1	0	0	0	GLOBAL NO

Stressfree configuration :

ISNOD	X0 (L)	Y0 (L)	Z0 (L)
node21	-24.68	3.910	-15.00
node22	-22.26	11.34	-15.00
node23	-17.67	17.67	-15.00
node24	-11.34	22.26	-15.00
node25	-3.910	24.68	-15.00
node26	3.910	24.68	-15.00
node27	11.34	22.26	-15.00
node28	17.67	17.67	-15.00
node29	22.26	11.34	-15.00
node30	24.68	3.910	-15.00
node31	24.68	-3.910	-15.00
node32	22.26	-11.34	-15.00
node33	17.67	-17.67	-15.00
node34	11.34	-22.26	-15.00
node35	3.910	-24.68	-15.00
node36	-3.910	-24.68	-15.00
node37	-11.34	-22.26	-15.00
node38	-17.67	-17.67	-15.00
node39	-22.26	-11.34	-15.00
node40	-24.68	-3.910	-15.00
node41	-24.68	3.910	-13.00
node42	-22.26	11.34	-13.00
node43	-17.67	17.67	-13.00
node44	-11.34	22.26	-13.00
node45	-3.910	24.68	-13.00
node46	3.910	24.68	-13.00
node47	11.34	22.26	-13.00
node48	17.67	17.67	-13.00
node49	22.26	11.34	-13.00
node50	24.68	3.910	-13.00
node51	24.68	-3.910	-13.00
node52	22.26	-11.34	-13.00
node53	17.67	-17.67	-13.00
node54	11.34	-22.26	-13.00
node55	3.910	-24.68	-13.00
node56	-3.910	-24.68	-13.00
node57	-11.34	-22.26	-13.00

node58	-17.67	-17.67	-13.00
node59	-22.26	-11.34	-13.00
node60	-24.68	-3.910	-13.00

Static equilibrium configuration :

ISNOD	X1 (L)	Y1 (L)	Z1 (L)	Rot (deg)	Dir (deg)
node21	-22.57	3.630	-14.87	0.000	0.000
node22	-20.76	10.60	-14.22	0.000	0.000
node23	-17.00	16.77	-13.52	0.000	0.000
node24	-11.27	21.33	-13.58	0.000	0.000
node25	-4.260	23.63	-14.48	0.000	0.000
node26	3.240	23.83	-15.29	0.000	0.000
node27	10.43	21.92	-15.68	0.000	0.000
node28	16.56	17.56	-15.98	0.000	0.000
node29	21.10	11.27	-16.18	0.000	0.000
node30	23.54	3.860	-16.27	0.000	0.000
node31	23.59	-3.930	-16.21	0.000	0.000
node32	21.14	-11.35	-16.11	0.000	0.000
node33	16.55	-17.58	-15.95	0.000	0.000
node34	10.36	-21.85	-15.73	0.000	0.000
node35	3.170	-23.85	-15.34	0.000	0.000
node36	-4.310	-23.68	-14.53	0.000	0.000
node37	-11.31	-21.37	-13.60	0.000	0.000
node38	-17.02	-16.79	-13.51	0.000	0.000
node39	-20.77	-10.61	-14.19	0.000	0.000
node40	-22.57	-3.630	-14.86	0.000	0.000
node41	-22.57	3.630	-12.87	0.000	0.000
node42	-20.76	10.60	-12.22	0.000	0.000
node43	-17.00	16.77	-11.52	0.000	0.000
node44	-11.27	21.33	-11.58	0.000	0.000
node45	-4.260	23.63	-12.48	0.000	0.000
node46	3.240	23.83	-13.29	0.000	0.000
node47	10.43	21.92	-13.68	0.000	0.000
node48	16.56	17.56	-13.98	0.000	0.000
node49	21.20	11.27	-14.18	0.000	0.000
node50	23.54	3.860	-14.27	0.000	0.000
node51	23.59	-3.930	-14.21	0.000	0.000
node52	21.14	-11.35	-14.11	0.000	0.000
node53	16.55	-17.58	-13.95	0.000	0.000
node54	10.36	-21.85	-13.73	0.000	0.000
node55	3.170	-23.85	-13.34	0.000	0.000
node56	-4.310	-23.68	-12.53	0.000	0.000
node57	-11.31	-21.37	-11.60	0.000	0.000
node58	-17.02	-16.79	-11.51	0.000	0.000
node59	-20.77	-10.61	-12.19	0.000	0.000
node60	-22.57	-3.630	-12.86	0.000	0.000

BOUNDARY CONDITIONS FOR FREE SUPERNODES:

Stressfree configuration :

ISNOD	X0 (L)	Y0 (L)	Z0 (L)
node1	-25.10	3.980	-17.50

```
        node2      -22.64       11.54      -17.50
        node3      -17.97       17.97      -17.50
        node4      -11.54       22.64      -17.50
        node5      -3.980       25.10      -17.50
        node6       3.980       25.10      -17.50
        node7       11.54       22.64      -17.50
        node8       17.97       17.97      -17.50
        node9       22.64       11.54      -17.50
        node10      25.10       3.980      -17.50
        node11      25.10      -3.980      -17.50
        node12      22.64      -11.54      -17.50
        node13      17.97      -17.97      -17.50
        node14      11.54      -22.64      -17.50
        node15      3.980      -25.10      -17.50
        node16     -3.980      -25.10      -17.50
        node17     -11.54      -22.64      -17.50
        node18     -17.97      -17.97      -17.50
        node19     -22.65      -11.54      -17.50
        node20     -25.10      -3.980      -17.50

      NEW LINE TYPE
      -------------

      LINE TYPE DATA :
        Line type identifier . . . . . :  line90
        Number of segments . . . . . :  1
        Component type id,(BODY or CONB type)
        Body or connector at end 2 of segment NSEG :  0
        Component type id of internal fluid
        flow . . . . . :  Water
        Additional twist specification?  . . . . . : NO
        Additional pre-bend specification? . . . . : NO

      SEGMENT SPECIFICATION :
        ISEG   - Segment number
        ICMPTY - Component type id
        ICN1TY - Component type id, body or connector at end 1
        IEXWTY - Component type id, external wrapping
        NELSEG - Number of elements for fem analysis
        SLGTH  - Segment length (L)
        SLGTH0 - Stressfree length of segment (L)
        NSTRPS - Number of subelements per element (STATIC ANALYSIS)
        NSTRPD - Number of subelements per element (DYNAMIC ANALYSIS)
        ISOIL  - Soil id to be used in seafloor contact

        ISEG ICMPTY ICN1TY IEXWTY     NELSEG    SLGTH   SLGTH0  NSTRPS NSTRPD  ISOIL
           1 cRS1    0       0             3     7.95     7.95       3             5
NONE

      NEW LINE TYPE
      -------------

      LINE TYPE DATA :
        Line type identifier . . . . . :  line91
        Number of segments . . . . . :  1
```

```
       Component type id,(BODY or CONB type)
       Body or connector at end 2 of segment NSEG :  0
       Component type id of internal fluid
       flow . . . . . . . . . . . . . . . . . . . :  0
       Additional twist specification?  . . . . . : NO
       Additional pre-bend specification? . . . . : NO

     SEGMENT SPECIFICATION :
       ISEG   - Segment number
       ICMPTY - Component type id
       ICN1TY - Component type id, body or connector at end 1
       IEXWTY - Component type id, external wrapping
       NELSEG - Number of elements for fem analysis
       SLGTH  - Segment length (L)
       SLGTH0 - Stressfree length of segment (L)
       NSTRPS - Number of subelements per element (STATIC ANALYSIS)
       NSTRPD - Number of subelements per element (DYNAMIC ANALYSIS)
       ISOIL  - Soil id to be used in seafloor contact

       ISEG ICMPTY ICN1TY IEXWTY     NELSEG    SLGTH   SLGTH0  NSTRPS NSTRPD  ISOIL
          1 cRS2    0       0             3     2.54     2.54       3             5
NONE

     NEW LINE TYPE
     -------------

     LINE TYPE DATA :
       Line type identifier . . . . . . . . . . . :  line92
       Number of segments . . . . . . . . . . . . :  1
       Component type id,(BODY or CONB type)
       Body or connector at end 2 of segment NSEG :  0
       Component type id of internal fluid
       flow . . . . . . . . . . . . . . . . . . . :  0
       Additional twist specification?  . . . . . : NO
       Additional pre-bend specification? . . . . : NO

     SEGMENT SPECIFICATION :
       ISEG   - Segment number
       ICMPTY - Component type id
       ICN1TY - Component type id, body or connector at end 1
       IEXWTY - Component type id, external wrapping
       NELSEG - Number of elements for fem analysis
       SLGTH  - Segment length (L)
       SLGTH0 - Stressfree length of segment (L)
       NSTRPS - Number of subelements per element (STATIC ANALYSIS)
       NSTRPD - Number of subelements per element (DYNAMIC ANALYSIS)
       ISOIL  - Soil id to be used in seafloor contact

       ISEG ICMPTY ICN1TY IEXWTY     NELSEG    SLGTH   SLGTH0  NSTRPS NSTRPD  ISOIL
          1 cRS3    0       0             3     2.00     2.00       3             5
NONE



       NEW COMPONENT CRS1
```

```
------------------

COMPONENT TYPE ID  . . . . . .  :     cRS1
TEMPERATURE AT WHICH THE SPEC. APPLIES :   0.00
THERMAL EXPANSION COEFFICIENT . . . . .:    0.000E+00
PRESSURE EXPANSION COEFFICIENT (1/F/L2):    0.000E+00

MASS AND VOLUME :

MASS-UNIT LENGTH (M/L)  . . . . . .:  0.1340
EXTERNAL VOLUME/LENGTH (L2) . . . . . .:  0.1257
INTERNAL VOLUME/LENGTH (L2) . . . . . .:  0.8450E-01
RADIUS OF GYRATION ABOUT X-AXIS (L) . .:  0.1818
AREA FOR STRESS CALCULATIONS (L2) . . .:  0.4117E-01
SECTION MODULUS FOR STRESS CAL. (L3)  .:  0.3442E-02
OUTER DIAMETER FOR STRESS CAL. (L)  . .:  0.4000
THICKNESS FOR STRESS CAL. (L) . . . . .:  0.3600E-01
EXTERNAL RADIUS FOR CONTACT (L)  . .. .:   0.000
INTERNAL RADIUS FOR CONTACT (L)  . .. .:   0.000

STIFFNESS PROPERTIES CLASSIFICATION :

AXIAL STIFFNESS CODE  . . . . :   1  CONSTANT STIFFNESS
BENDING STIFFNESS CODE  . . . :   1  CONSTANT STIFFNESS
TORSION STIFFNESS CODE  . . . :   1  CONSTANT STIFFNESS
PRESSURE DEPENDENCY PARAMETER :   0  NO PRESSURE DEPENDENCY
HYSTERESIS OPTION CODE  . . . :   0  NO HYSTERESIS

AXIAL STIFFNESS :

AXIAL STIFFNESS . . (F) :  0.4154E+05

BENDING STIFFNESS :

BENDING STIFFNESS AROUND Y-AXIS  (FL2) :   688.5

SHEAR STIFFNESS (F) :  0.1599E+05

TORSION STIFFNESS :

CONSTANT STIFFNESS  (FL2/RAD):   265.1

NON-DIMENSIONAL HYDRODYNAMIC FORCE COEFFICIENTS :

DRAG FORCE COEFFICIENT; TANGENTIAL             :  0.3000E-01
                        NORMAL                 :  0.8000
ADDED MASS; TANGENTIAL                         :   0.000
            NORMAL                             :  1.0000

NO LINEAR DRAG COEFFICIENTS
COEFFICIENT INPUT CODE, ICODE                    :   2   NON-DIMENSIONAL COEFF.
HYDRODYNAMIC DIAMETER                      (L)   :  0.4000
FROUDE-KRILOFF SCALING FACTOR; NORMAL DIRECTION :  1.0000

CAPACITY PARAMETER :
```

```
TENSION    MAXIMUM
CAPACITY   OF CURVATURE
 (F)       (1/L)
0.1438E+05   0.4329

NEW COMPONENT CRS1
------------------

COMPONENT TYPE ID  . . . . . .  :     cRS2
TEMPERATURE AT WHICH THE SPEC. APPLIES :   0.00
THERMAL EXPANSION COEFFICIENT . . . . .:    0.000E+00
PRESSURE EXPANSION COEFFICIENT (1/F/L2):    0.000E+00

MASS AND VOLUME :

MASS-UNIT LENGTH (M/L)  . . . . . .:  0.3762E-03
EXTERNAL VOLUME/LENGTH (L2) . . . . .:  0.3801E-03
INTERNAL VOLUME/LENGTH (L2) . . . . .:   0.000
RADIUS OF GYRATION ABOUT X-AXIS (L) . .:  0.7000E-02
AREA FOR STRESS CALCULATIONS (L2) . . .:  0.3801E-03
SECTION MODULUS FOR STRESS CAL. (L3)  .:  0.1045E-05
OUTER DIAMETER FOR STRESS CAL. (L)  . .:  0.2200E-01
THICKNESS FOR STRESS CAL. (L) . . . . .:  0.1100E-01
EXTERNAL RADIUS FOR CONTACT (L)  . .. .:   0.000
INTERNAL RADIUS FOR CONTACT (L)  . .. .:   0.000

STIFFNESS PROPERTIES CLASSIFICATION :

AXIAL STIFFNESS CODE  . . . . :   1  CONSTANT STIFFNESS
BENDING STIFFNESS CODE  . . . :   1  CONSTANT STIFFNESS
TORSION STIFFNESS CODE  . . . :   1  CONSTANT STIFFNESS
PRESSURE DEPENDENCY PARAMETER :   0  NO PRESSURE DEPENDENCY
HYSTERESIS OPTION CODE  . . . :   0  NO HYSTERESIS

AXIAL STIFFNESS :

AXIAL STIFFNESS . . (F) :   710.6

BENDING STIFFNESS :

BENDING STIFFNESS AROUND Y-AXIS  (FL2) :  0.1000E-02

SHEAR STIFFNESS (F) :   NOT INCLUDED

TORSION STIFFNESS :

CONSTANT STIFFNESS  (FL2/RAD):  0.1000E+00


NON-DIMENSIONAL HYDRODYNAMIC FORCE COEFFICIENTS :

DRAG FORCE COEFFICIENT; TANGENTIAL            :  0.3000E-01
                        NORMAL                :  0.8000
ADDED MASS; TANGENTIAL                        :   0.000
```

```
           NORMAL                              :  1.0000

NO LINEAR DRAG COEFFICIENTS
COEFFICIENT INPUT CODE, ICODE                  :   2   NON-DIMENSIONAL COEFF.
HYDRODYNAMIC DIAMETER                    (L)   :  0.2200E-01
FROUDE-KRILOFF SCALING FACTOR; NORMAL DIRECTION :  1.0000

CAPACITY PARAMETER :

TENSION    MAXIMUM
CAPACITY   OF CURVATURE
 (F)       (1/L)
0.1438E+05   0.4329


NEW COMPONENT CRS1
------------------

COMPONENT TYPE ID  . . . . . .  :     cRS3
TEMPERATURE AT WHICH THE SPEC. APPLIES :   0.00
THERMAL EXPANSION COEFFICIENT . . . . .:    0.000E+00
PRESSURE EXPANSION COEFFICIENT (1/F/L2):    0.000E+00

MASS AND VOLUME :

MASS-UNIT LENGTH (M/L)  . . . . . .:  0.1000E-04
EXTERNAL VOLUME/LENGTH (L2) . . . . .:  0.1000E-04
INTERNAL VOLUME/LENGTH (L2) . . . . .:   0.000
RADIUS OF GYRATION ABOUT X-AXIS (L) . .:  0.1000E-02
AREA FOR STRESS CALCULATIONS (L2) . . .:  0.1000E-04
SECTION MODULUS FOR STRESS CAL. (L3)  .:  0.4460E-08
OUTER DIAMETER FOR STRESS CAL. (L)  . .:  0.3568E-02
THICKNESS FOR STRESS CAL. (L) . . . . .:  0.1784E-02
EXTERNAL RADIUS FOR CONTACT (L)  . .. .:   0.000
INTERNAL RADIUS FOR CONTACT (L)  . .. .:   0.000

STIFFNESS PROPERTIES CLASSIFICATION :

AXIAL STIFFNESS CODE  . . . . :   1  CONSTANT STIFFNESS
BENDING STIFFNESS CODE  . . . :   1  CONSTANT STIFFNESS
TORSION STIFFNESS CODE  . . . :   1  CONSTANT STIFFNESS
PRESSURE DEPENDENCY PARAMETER :   0  NO PRESSURE DEPENDENCY
HYSTERESIS OPTION CODE  . . . :   0  NO HYSTERESIS

AXIAL STIFFNESS :

AXIAL STIFFNESS . . (F) :   173.7

BENDING STIFFNESS :

BENDING STIFFNESS AROUND Y-AXIS  (FL2) :  0.1000E-02

SHEAR STIFFNESS (F) :   NOT INCLUDED

TORSION STIFFNESS :
```

```
CONSTANT STIFFNESS  (FL2/RAD):  0.1000E-02


NON-DIMENSIONAL HYDRODYNAMIC FORCE COEFFICIENTS :

DRAG FORCE COEFFICIENT; TANGENTIAL             :  0.3000E-01
                        NORMAL                 :  0.8000
ADDED MASS; TANGENTIAL                         :   0.000
            NORMAL                             :  1.0000

NO LINEAR DRAG COEFFICIENTS
COEFFICIENT INPUT CODE, ICODE                   :   2   NON-DIMENSIONAL COEFF.
HYDRODYNAMIC DIAMETER                     (L)   :  0.3568E-02
FROUDE-KRILOFF SCALING FACTOR; NORMAL DIRECTION :  1.0000

CAPACITY PARAMETER :

TENSION    MAXIMUM
CAPACITY   OF CURVATURE
 (F)       (1/L)
 0.000        0.000


NEW COMPONENT FLUID
-------------------

COMPONENT TYPE ID :

COMPONENT TYPE ID . . . . . :    Water

FLUID FLOW CHARACTERISTICS :

DENSITY (M/L3) . . . . . :   1.025
VOLUME VELOCITY (L2) . . . . . :   0.000
PRESSURE AT FLUID INLET END (F/L2) :   0.000
PRESSURE DROP (F/L3) . . . . . :   0.000
FLOW DIRECTION CODE  . . . . . :     1  INLET AT SUPERNODE 1


ENVIRONMENTAL IDENTIFICATION
----------------------------

DESCRIBING TEXT . . . .:


DATA SET IDENTIFIER . .: ENV1


WATERDEPTH AND WAVE TYPE CONTROL
--------------------------------

WATER DEPTH (L) . . . . . :  100.00
NUMBER OF IRREGULAR WAVE CASES . .:  0
NUMBER OF REGULAR WAVE CASES  . ..:  0
```

```
       NUMBER OF CURRENT STATES . . . . .:  1
       NUMBER OF WIND STATES  . . . . . .:  0

       ENVIRONMENTAL CONSTANTS
       -----------------------

       AIR DENSITY (M/L**3). . . . . . . . . :  0.1250E-02
       WATER DENSITY (M/L**3). . . . . . . . :   1.025
       KINEMATIC VISCOSITY OF WATER (L**2/T) :  0.1188E-05
       KINEMATIC VISCOSITY OF AIR   (L**2/T) :  0.1824E-04

       NEW CURRENT STATE
       -----------------

       CURRENT STATE NUMBER . . . . :  1

       NUMBER OF CURRENT LEVELS . . :  2

       LEVEL (L)       DIRECTION (DEG)  VELOCITY (L/T)

        0.000            0.000           1.0000
      -100.00            0.000           1.0000
1

       I N P M O D - S U M M A R Y
       ---------------------------

       THE FOLLOWING DATA HAVE BEEN CREATED:

       +-----------------------------------------------------------+
       ! IDENTIFICATION  !  TYPE   !  NO OF SUPERNODES             !
       +-----------------------------------------------------------+
       ! ARSYS           !  AR     !    60                         !
       +-----------------------------------------------------------+

       NUMBER OF LINES . . . . . . . . :   3

       +-----------------------------------------------------------+
       ! LINE TYPE ID    !  NO SEGMENTS                            !
       +-----------------------------------------------------------+
       ! line90          !       1                                 !
       ! line91          !       1                                 !
       ! line92          !       1                                 !
       +-----------------------------------------------------------+

       NUMBER OF COMPONENTS. . . . . . :   4

       +-----------------------------------------------------------+
       ! COMPONENT TYPE ID   !  TYPE                               !
       +-----------------------------------------------------------+
       ! cRS1               !  CRS1                               !
       ! cRS2               !  CRS1                               !
       ! cRS3               !  CRS1                               !
       ! Water              !  FLUID                              !
       +-----------------------------------------------------------+
```

NUMBER OF ENVIRONMENT CASES . . : 1

IDENTIFICATION	NO OF IRREGULAR SEASTATES	NO OF REGULAR SEASTATES	NO OF CURRENT STATES	NO OF WIND STATES
ENV1	0	0	1	0

NUMBER OF TRANSFER FUNCTION OF
THE SUPPORT VESSEL MOTIONS . . .: 0

B Results for Velocities 0.8-1.4 m/s

B1 Case 1: U=0.8 m/s

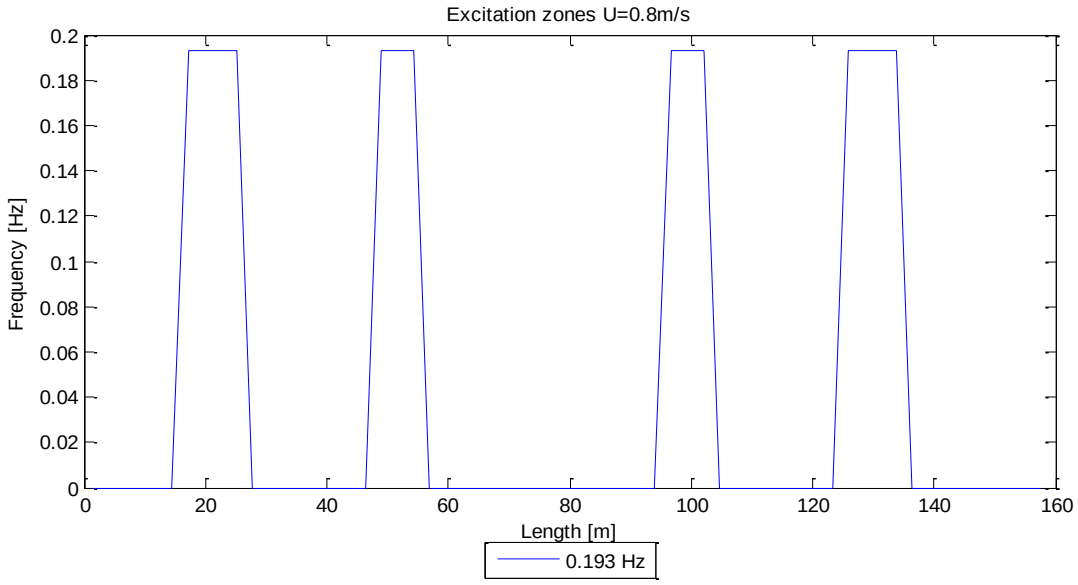

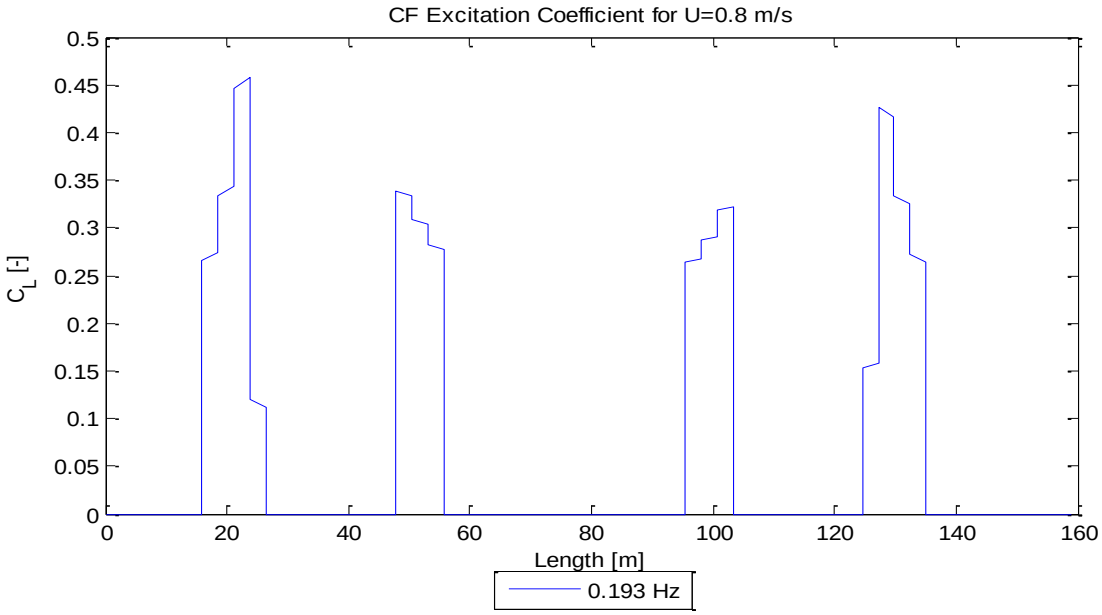

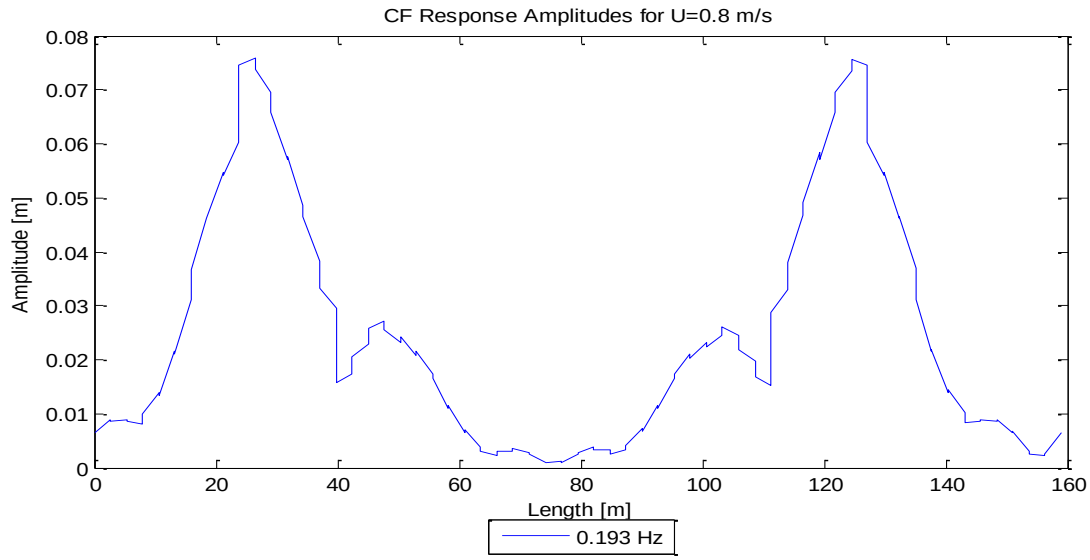
CF Response Amplitudes for U=0.8 m/s
Amplitude [m]
0.08
0.07
0.06
0.05
0.04
0.03
0.02
0.01
0
0
20
40
60
80
100
120
140
160
Length [m]
0.193 Hz

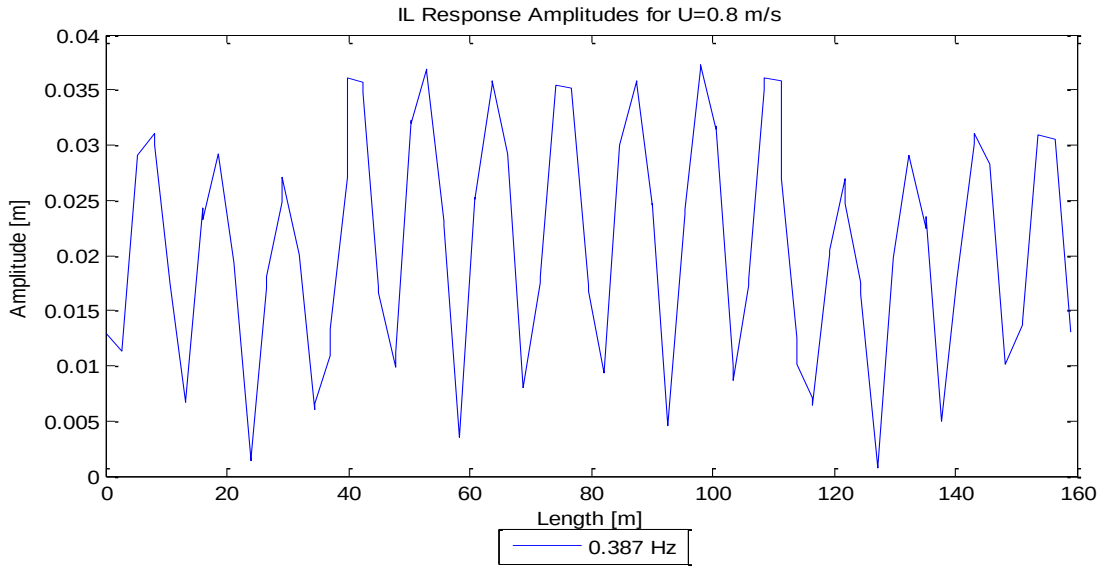
IL Response Amplitudes for U=0.8 m/s
Amplitude [m]
0.04
0.035
0.03
0.025
0.02
0.015
0.01
0.005
0
0
20
40
60
80
100
120
140
160
Length [m]
0.387 Hz

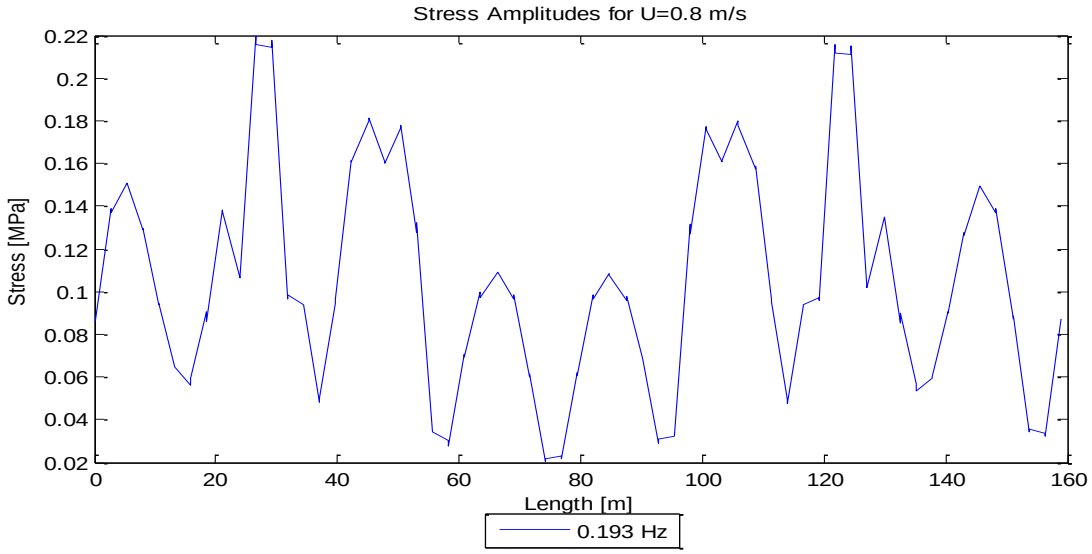
Stress Amplitudes for U=0.8 m/s
Stress [MPa]
0.22
0.2
0.18
0.16
0.14
0.12
0.1
0.08
0.06
0.04
0.02
0
20
40
60
80
100
120
140
160
Length [m]
0.193 Hz

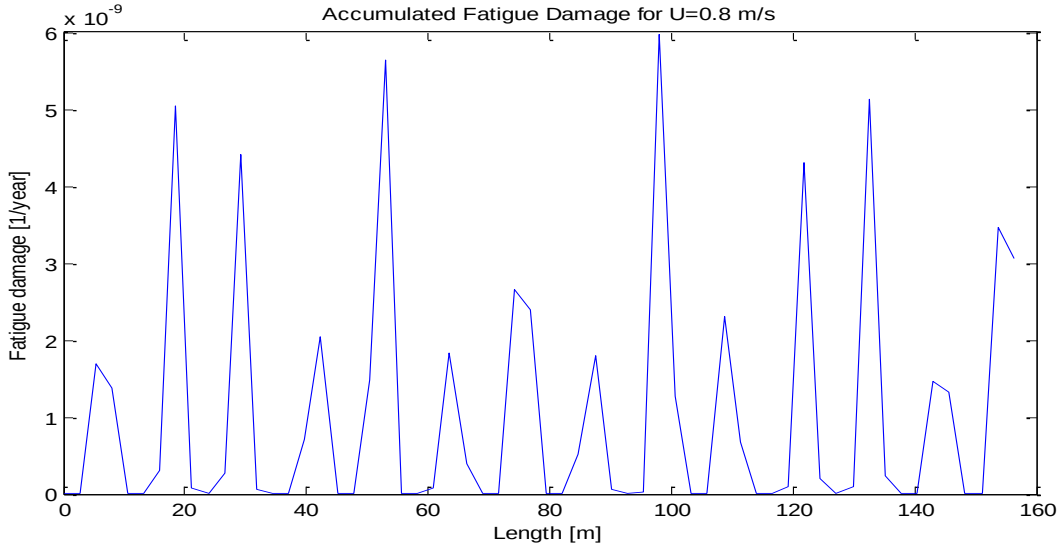
Accumulated Fatigue Damage for U=0.8 m/s
x 10^-9
Fatigue damage [1/year]
6
5
4
3
2
1
0
0
20
40
60
80
100
120
140
160
Length [m]

B2 Case 2: U=0.9 m/s

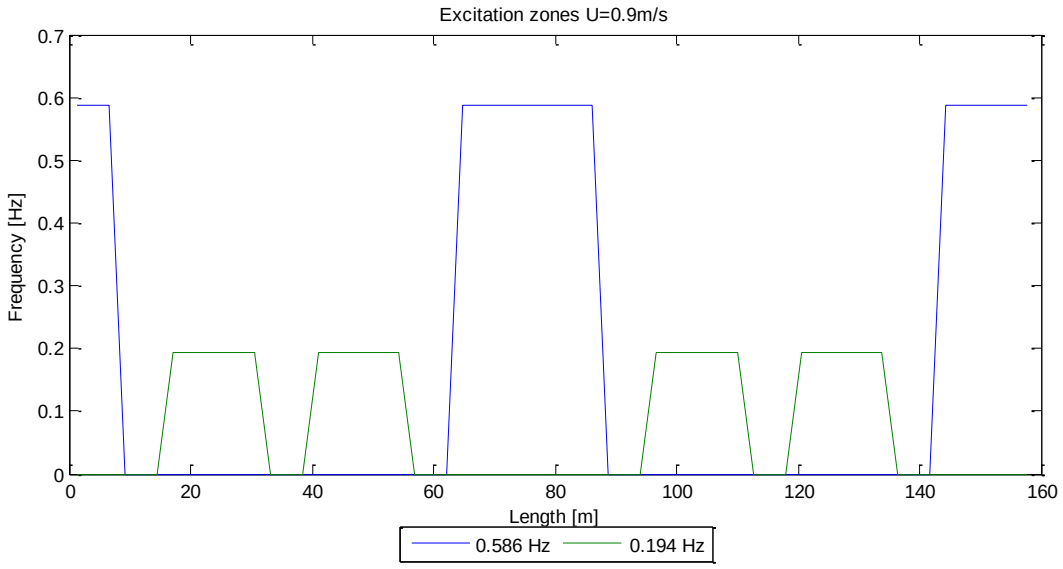

Table 0-1 Excitation frequencies for U=0.9 m/s

Frequency number	Frequency [Hz]	Duration [%]
2	0.586	75.0
1	0.194	25.0

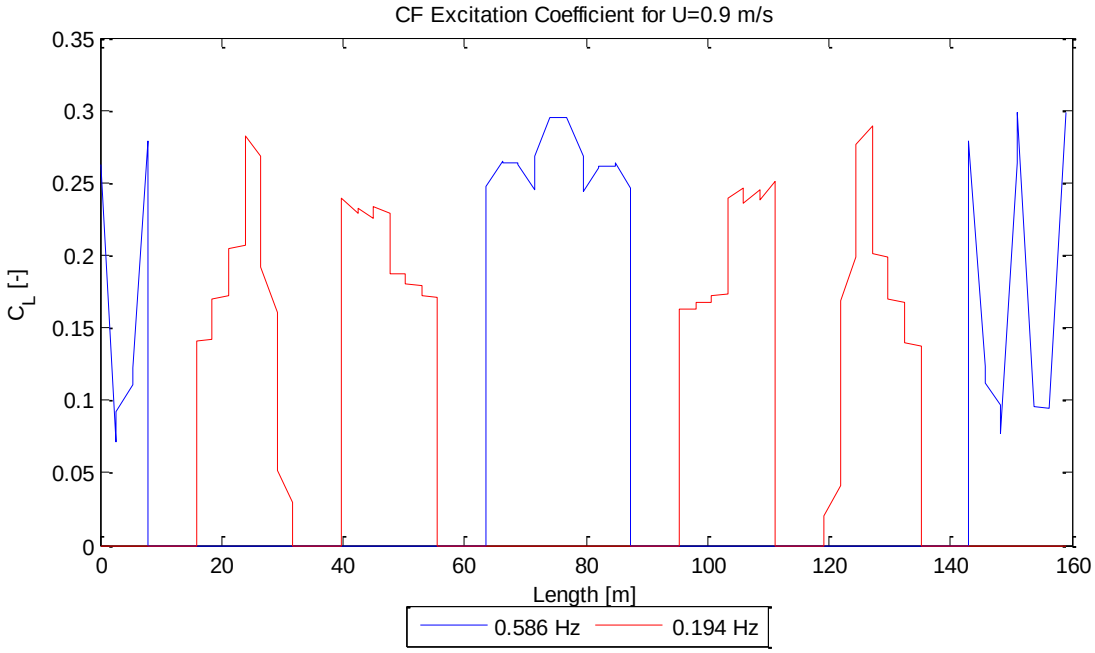

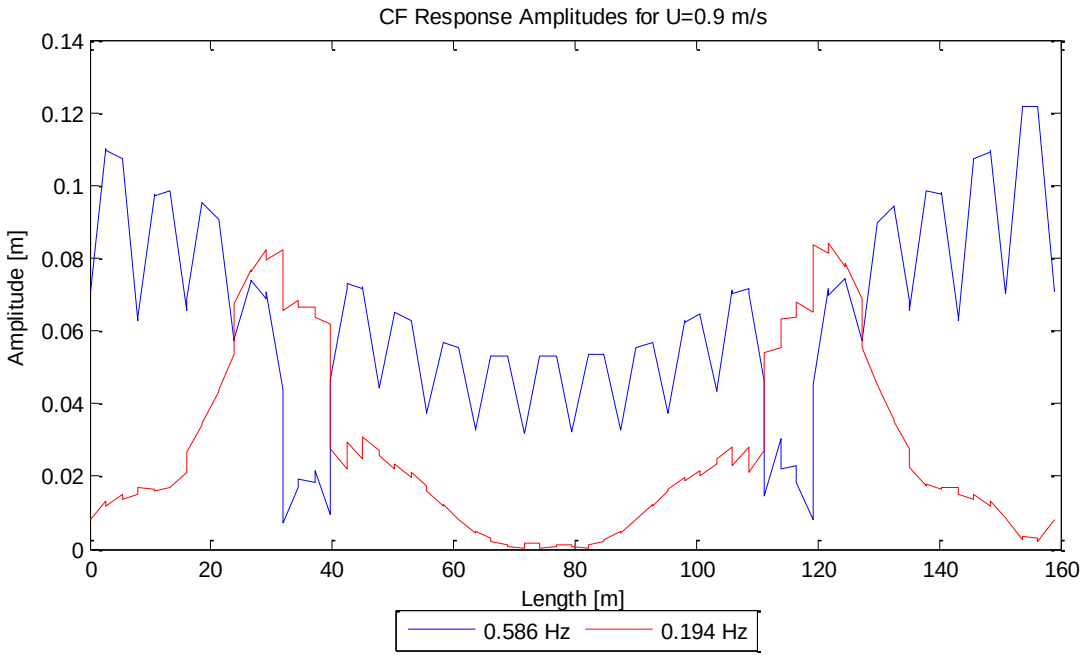
CF Response Amplitudes for U=0.9 m/s
Amplitude [m]
Length [m]
0.586 Hz
0.194 Hz

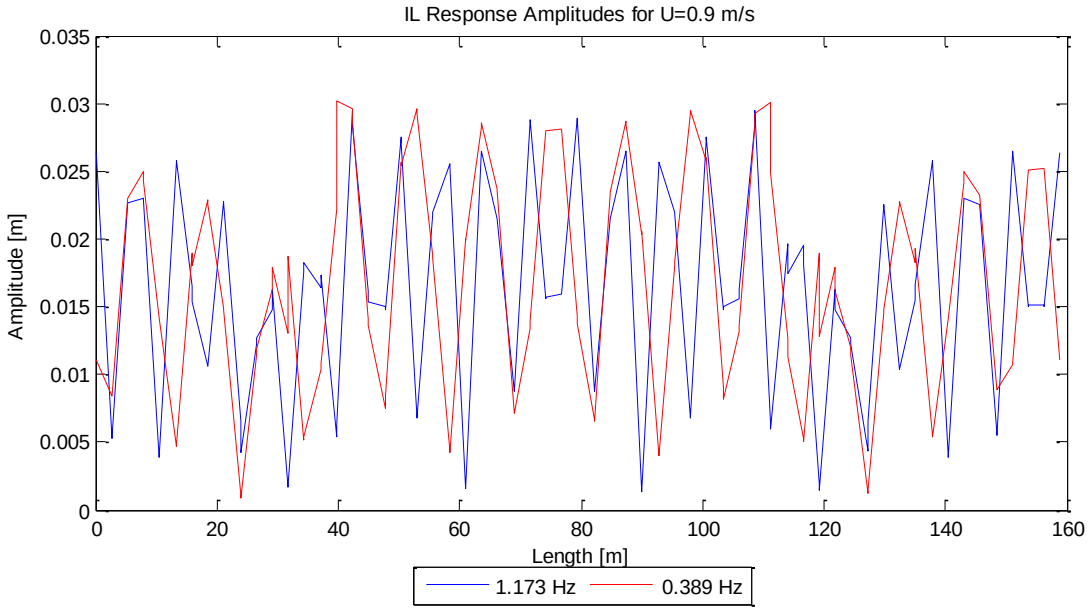
IL Response Amplitudes for U=0.9 m/s
Amplitude [m]
Length [m]
1.173 Hz
0.389 Hz

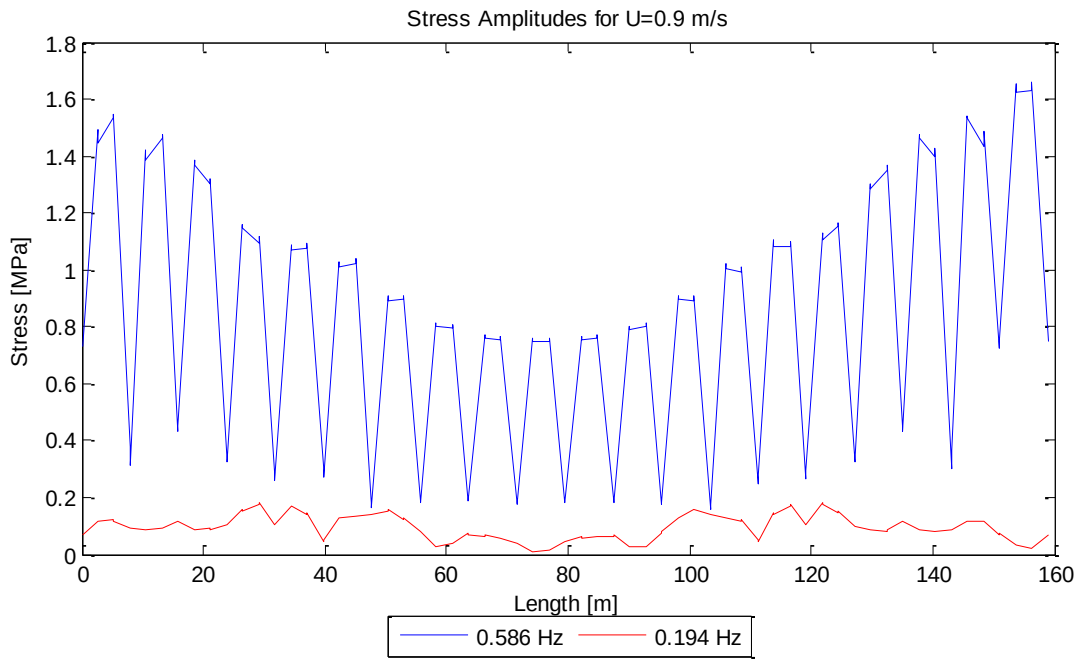
Stress Amplitudes for U=0.9 m/s
Stress [MPa]
Length [m]
0.586 Hz
0.194 Hz

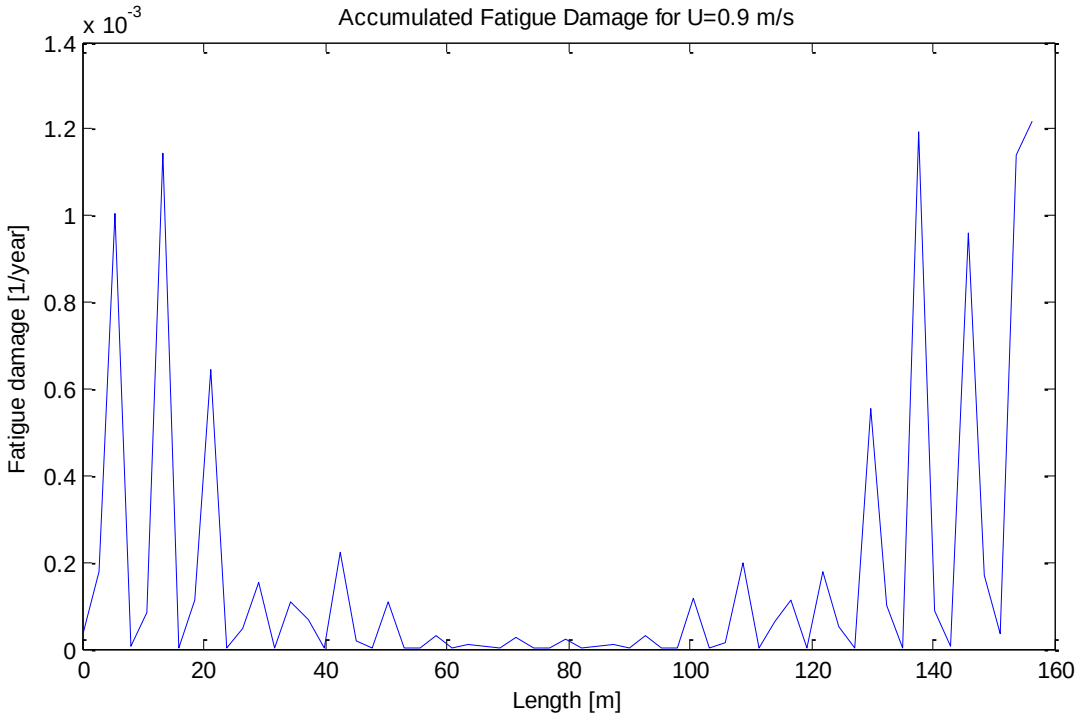
Accumulated Fatigue Damage for U=0.9 m/s
x 10^-3
Fatigue damage [1/year]
Length [m]

B3 Case 3: U=1.0 m/s

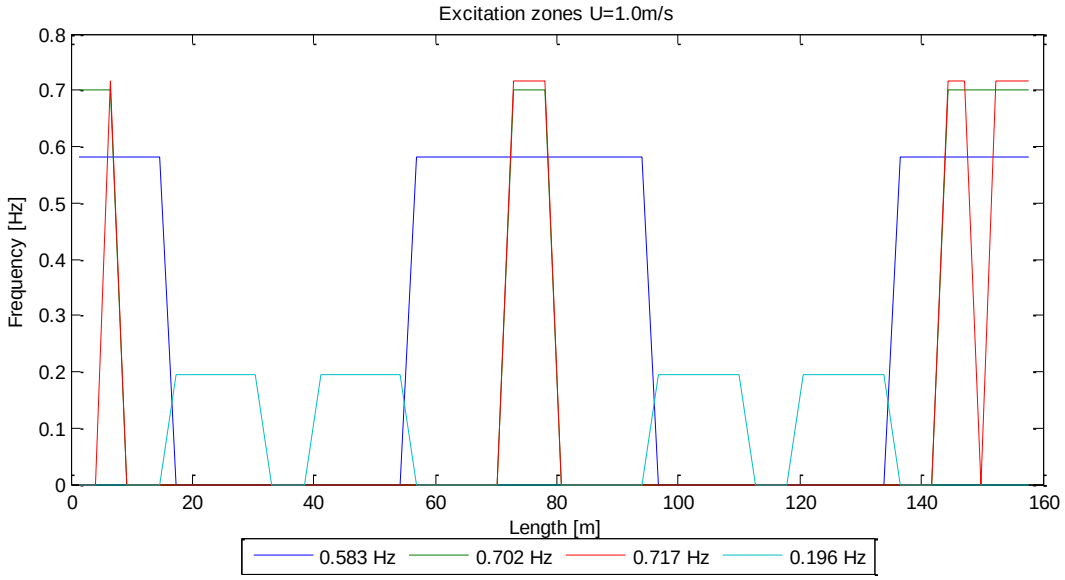

Table 0-2 Excitation frequencies for U=1.0 m/s

Frequency number	Frequency [Hz]	Duration [%]
2	0.583	59.2
3	0.702	18.4
4	0.717	12.9
1	0.196	9.5

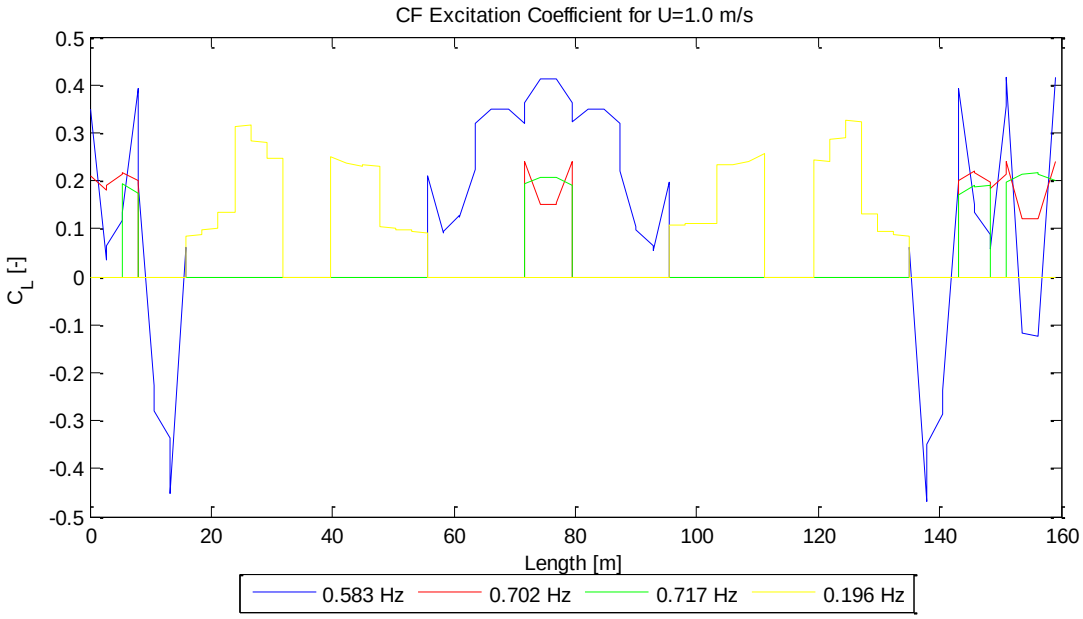
CF Excitation Coefficient for U=1.0 m/s
C_L [-]
0.5
0.4
0.3
0.2
0.1
0
-0.1
-0.2
-0.3
-0.4
-0.5
0
20
40
60
80
100
120
140
160
Length [m]
0.583 Hz
0.702 Hz
0.717 Hz
0.196 Hz

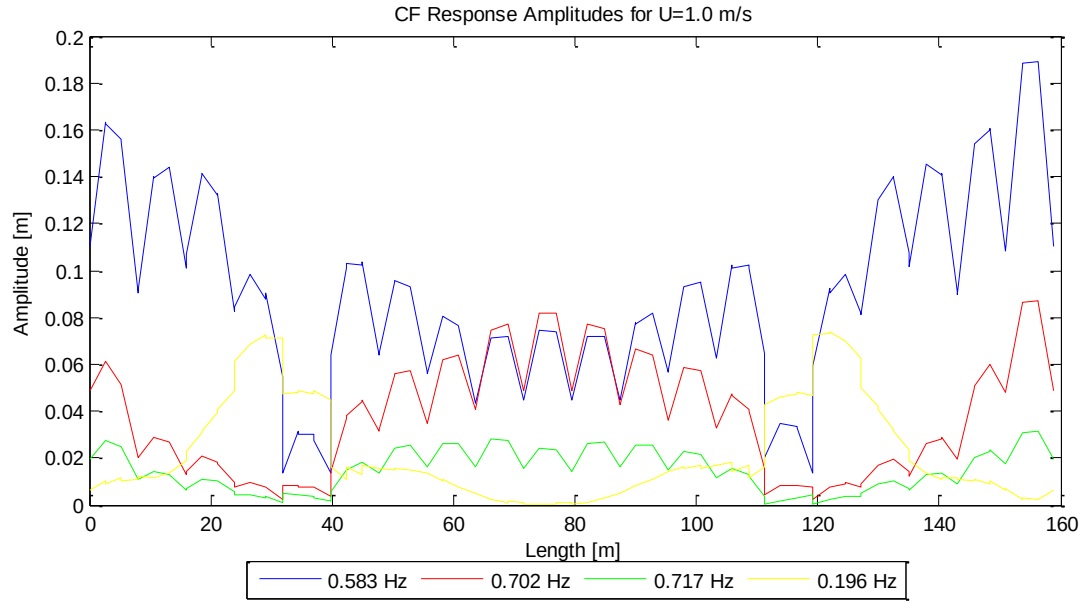
CF Response Amplitudes for U=1.0 m/s
Amplitude [m]
0.2
0.18
0.16
0.14
0.12
0.1
0.08
0.06
0.04
0.02
0
0
20
40
60
80
100
120
140
160
Length [m]
0.583 Hz
0.702 Hz
0.717 Hz
0.196 Hz

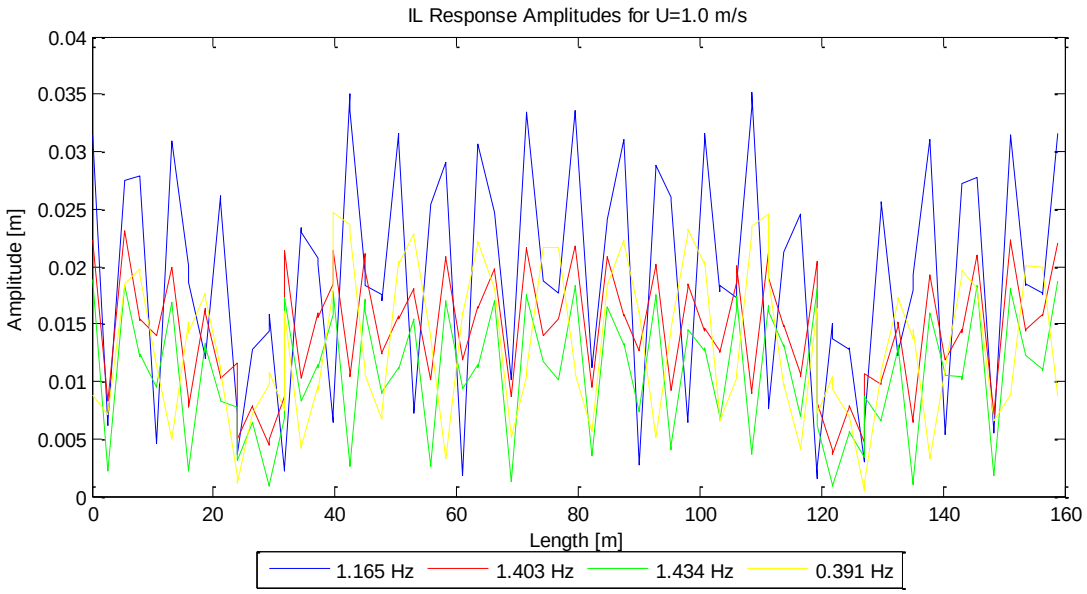
IL Response Amplitudes for U=1.0 m/s
Amplitude [m]
0.04
0.035
0.03
0.025
0.02
0.015
0.01
0.005
0
0
20
40
60
80
100
120
140
160
Length [m]
1.165 Hz
1.403 Hz
1.434 Hz
0.391 Hz

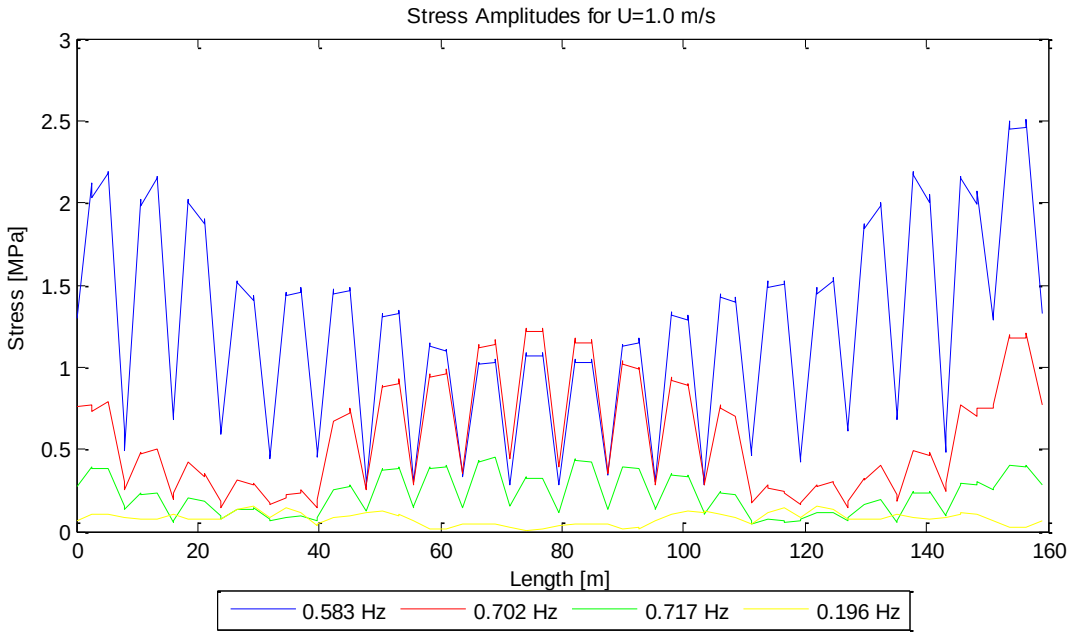
Stress Amplitudes for U=1.0 m/s
Stress [MPa]
3
2.5
2
1.5
1
0.5
0
0
20
40
60
80
100
120
140
160
Length [m]
0.583 Hz
0.702 Hz
0.717 Hz
0.196 Hz

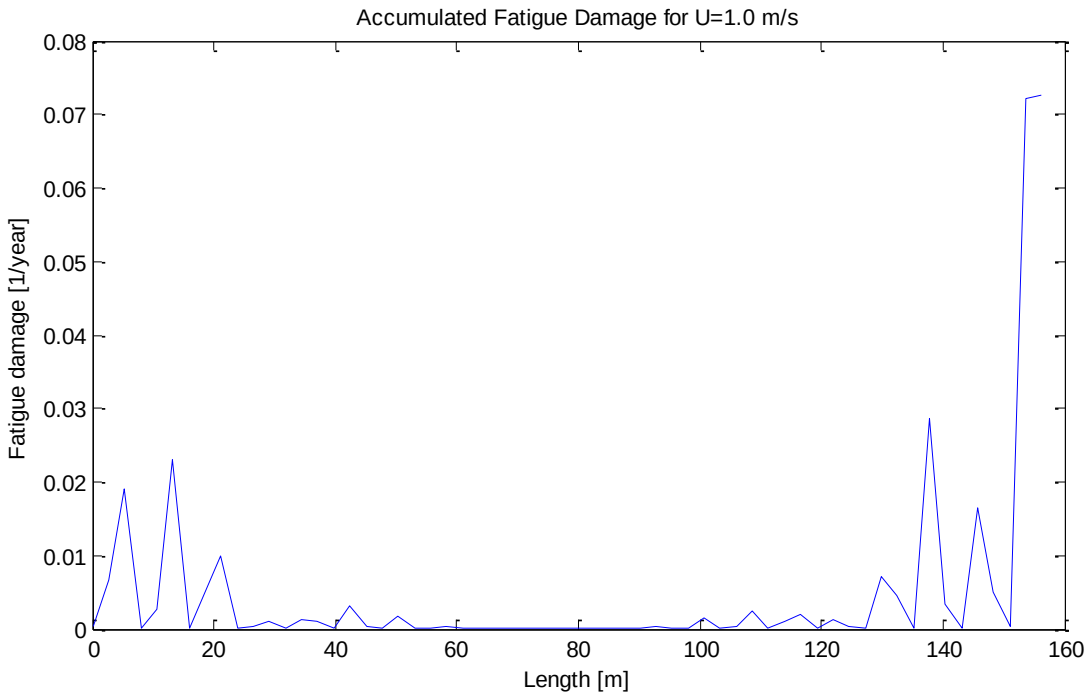
Accumulated Fatigue Damage for U=1.0 m/s
Fatigue damage [1/year]
Length [m]
0.08
0.07
0.06
0.05
0.04
0.03
0.02
0.01
0
0
20
40
60
80
100
120
140
160

B4 Case 4: U=1.1 m/s

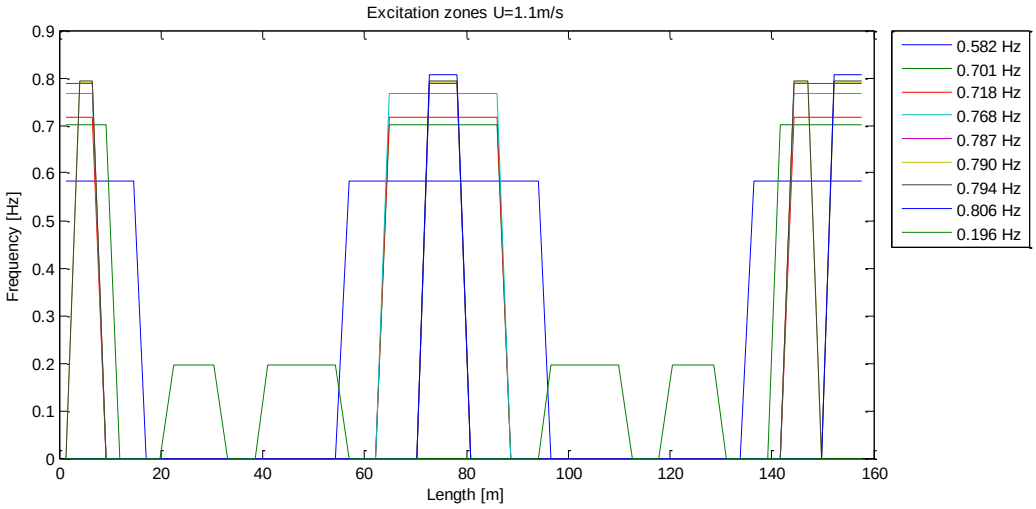

Table 0-3 Excitation frequencies for U=1.1 m/s

Frequency number	Frequency [Hz]	Duration [%]
2	0.582	31.7
3	0.701	16.9
4	0.718	14.9
5	0.768	11.3
6	0.787	7.3
7	0.790	6.1
8	0.794	6.0
9	0.806	3.5
1	0.196	2.3

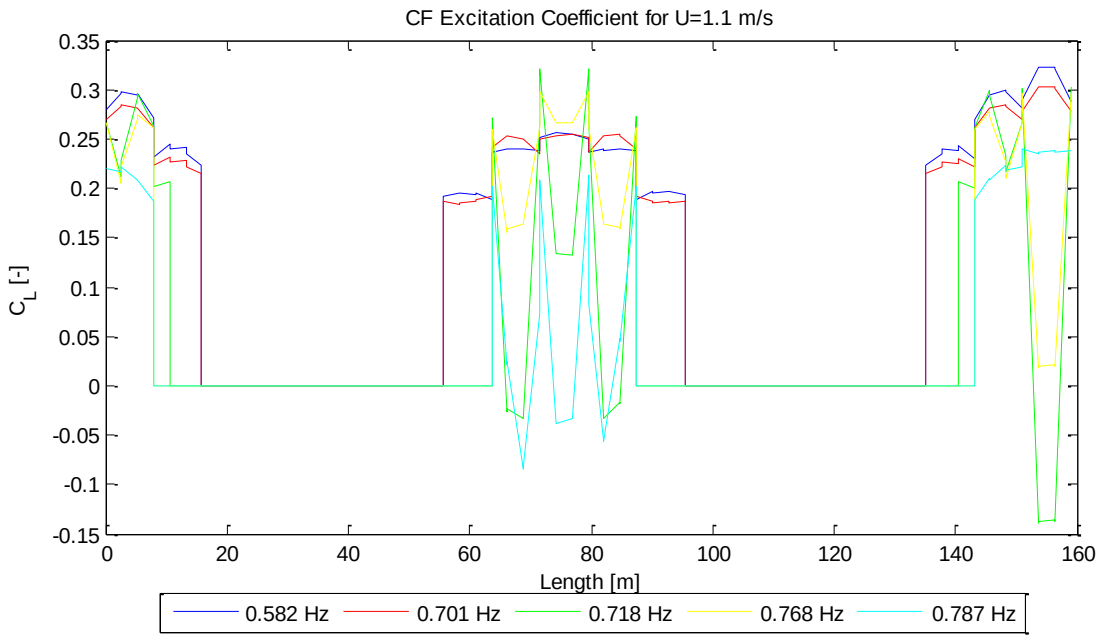
CF Excitation Coefficient for U=1.1 m/s
C_L [-]
Length [m]
0.582 Hz
0.701 Hz
0.718 Hz
0.768 Hz
0.787 Hz

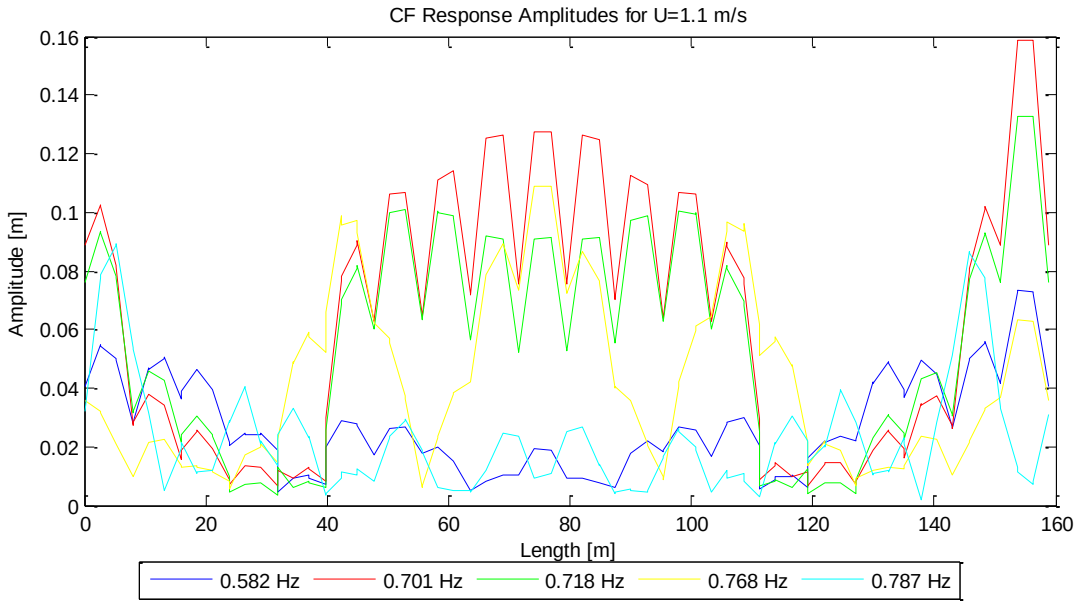
CF Response Amplitudes for U=1.1 m/s
Amplitude [m]
Length [m]
0.582 Hz
0.701 Hz
0.718 Hz
0.768 Hz
0.787 Hz

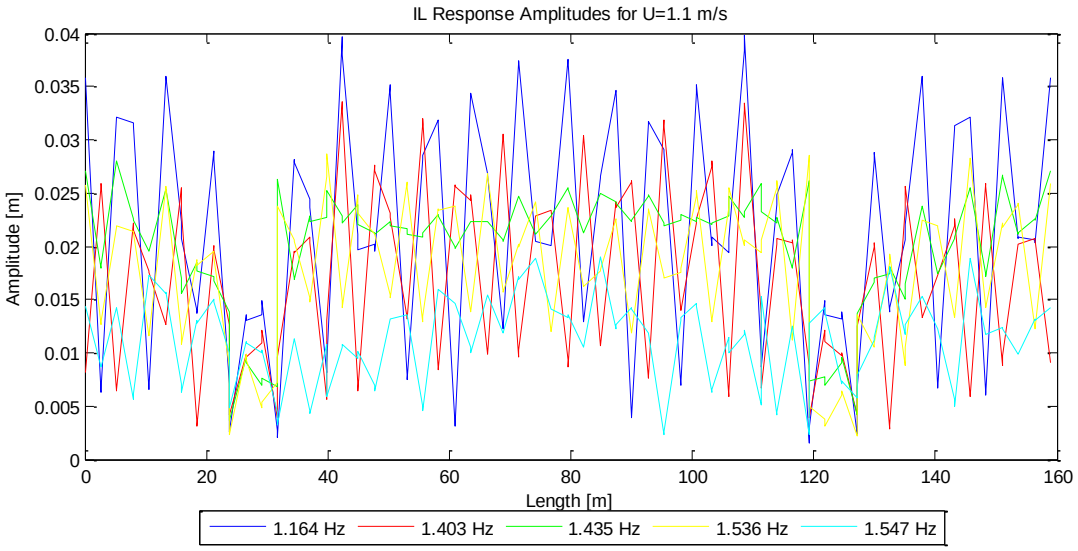
IL Response Amplitudes for U=1.1 m/s
Amplitude [m]
0.04
0.035
0.03
0.025
0.02
0.015
0.01
0.005
0
0
20
40
60
80
100
120
140
160
Length [m]
1.164 Hz
1.403 Hz
1.435 Hz
1.536 Hz
1.547 Hz

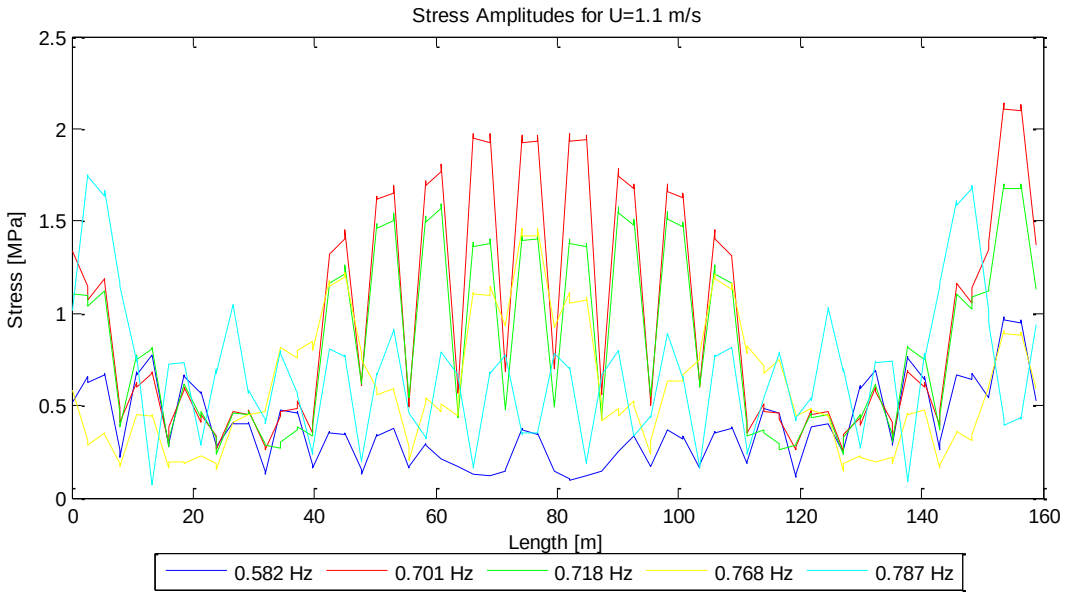
Stress Amplitudes for U=1.1 m/s
Stress [MPa]
2.5
2
1.5
1
0.5
0
0
20
40
60
80
100
120
140
160
Length [m]
0.582 Hz
0.701 Hz
0.718 Hz
0.768 Hz
0.787 Hz

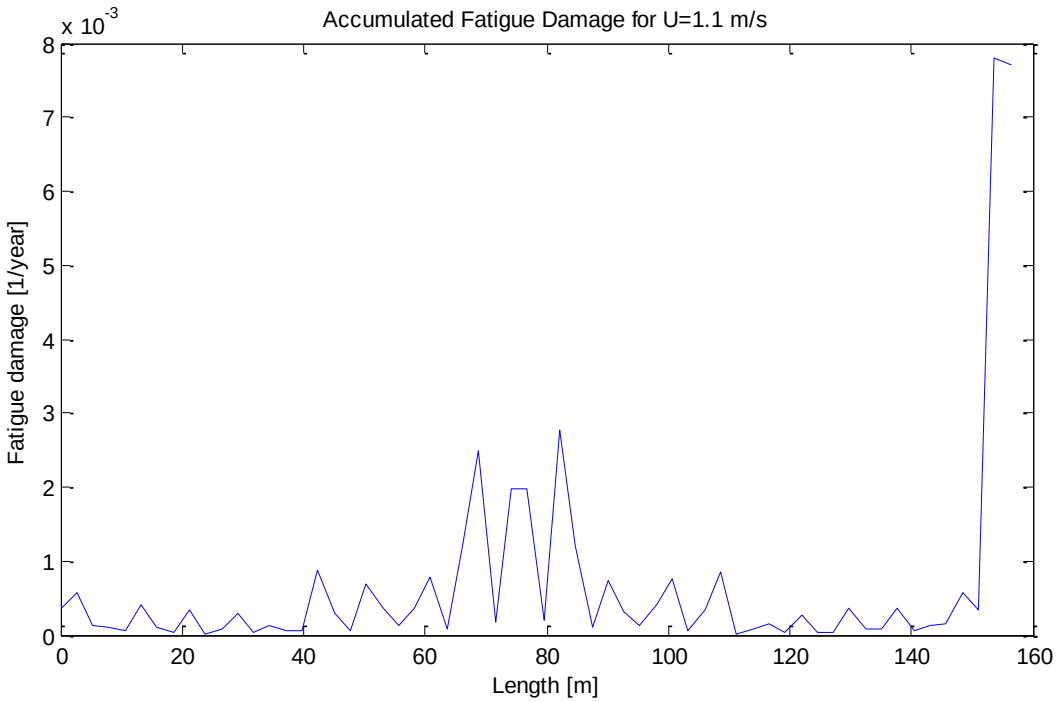
Accumulated Fatigue Damage for U=1.1 m/s
x 10^-3
Fatigue damage [1/year]
Length [m]
0
1
2
3
4
5
6
7
8
0
20
40
60
80
100
120
140
160

B5 Case 5: U=1.2 m/s

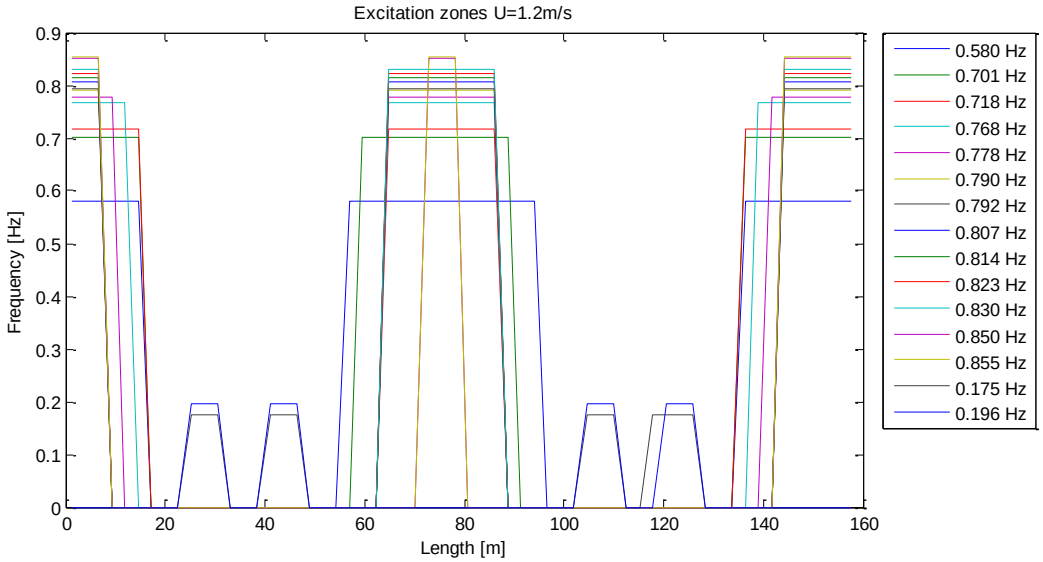

Table 0-4 Excitation frequencies for U=1.2 m/s

Frequency number	Frequency [Hz]	Duration [%]
3	0.580	17.2
4	0.701	11.6
5	0.718	10.5
6	0.768	8.2
7	0.778	7.6
8	0.790	6.8
9	0.792	6.7
10	0.807	6.3
11	0.814	6.1
12	0.823	5.8
13	0.830	5.6
14	0.850	3.7
15	0.855	3.6
1	0.175	0.3
2	0.196	0.2

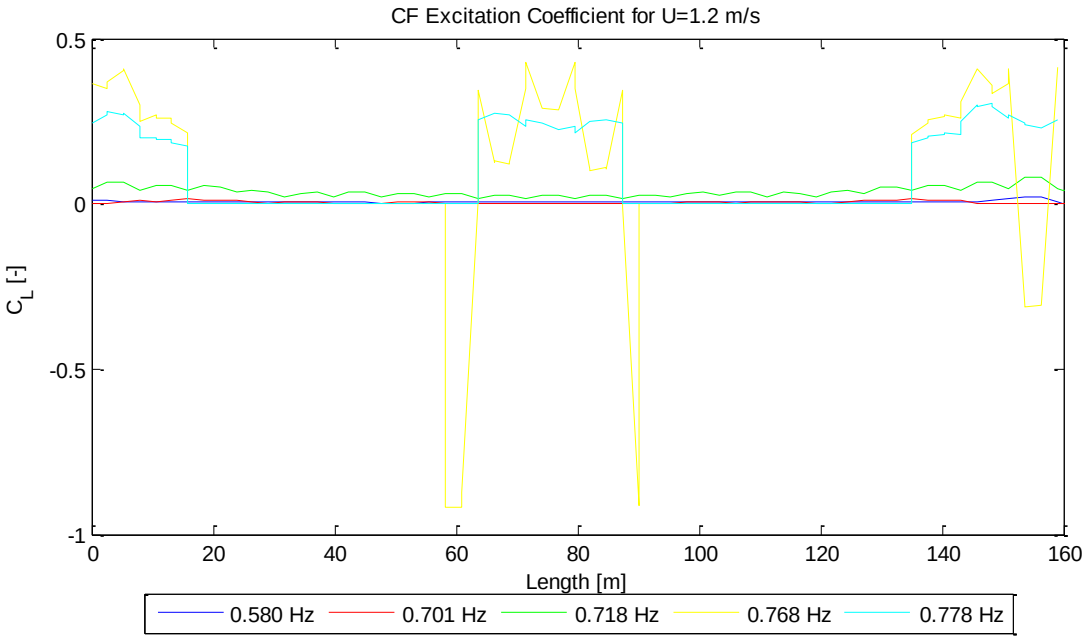
CF Excitation Coefficient for U=1.2 m/s
0.5
0
-0.5
-1
C_L [-]
0
20
40
60
80
100
120
140
160
Length [m]
0.580 Hz
0.701 Hz
0.718 Hz
0.768 Hz
0.778 Hz

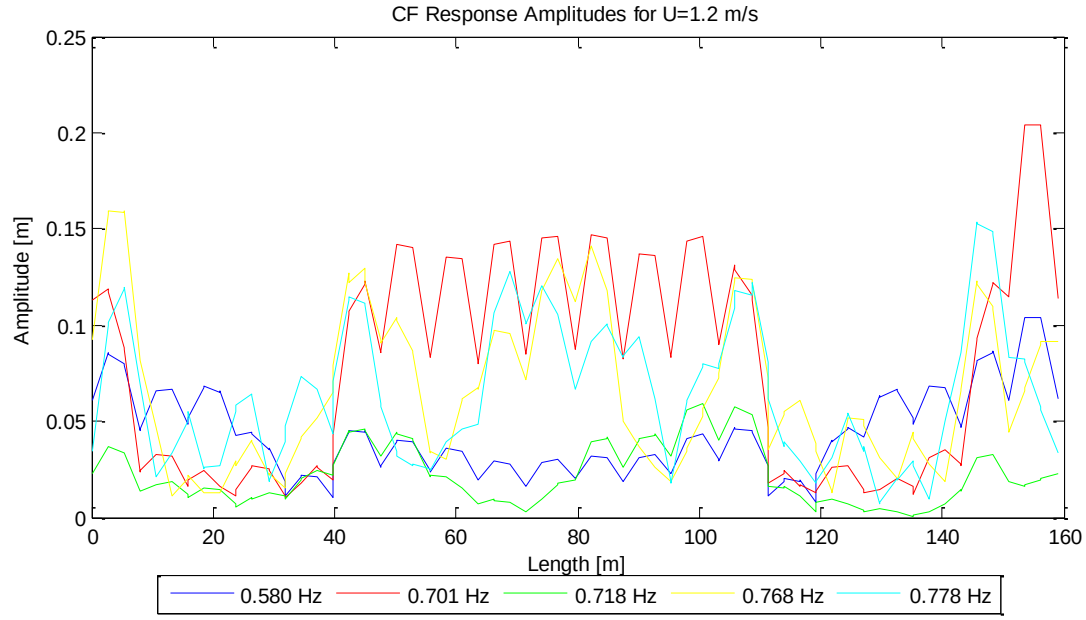
CF Response Amplitudes for U=1.2 m/s
0.25
0.2
0.15
0.1
0.05
0
Amplitude [m]
0
20
40
60
80
100
120
140
160
Length [m]
0.580 Hz
0.701 Hz
0.718 Hz
0.768 Hz
0.778 Hz

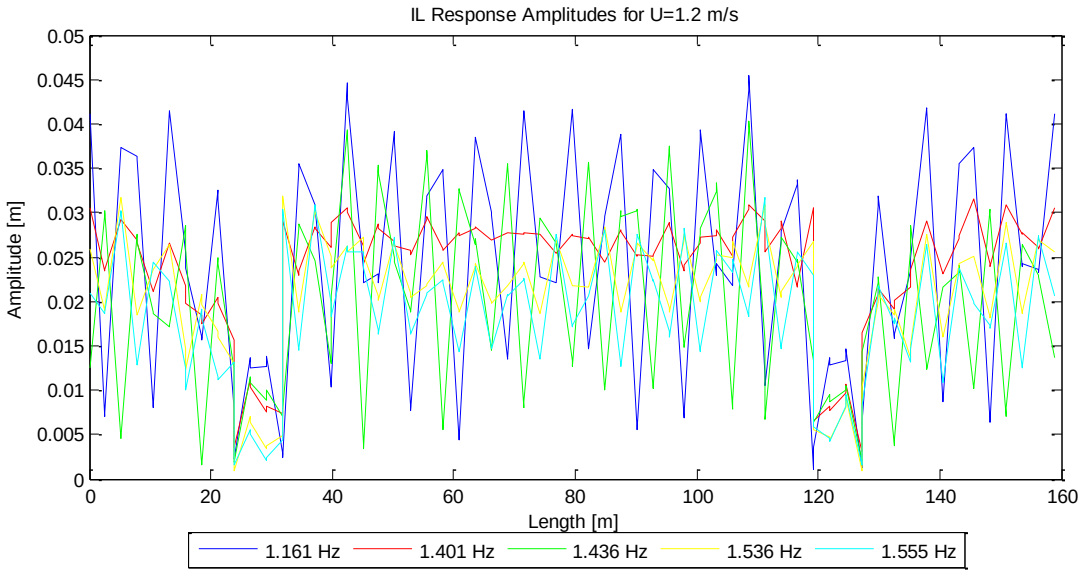
IL Response Amplitudes for U=1.2 m/s
Amplitude [m]
Length [m]
1.161 Hz
1.401 Hz
1.436 Hz
1.536 Hz
1.555 Hz

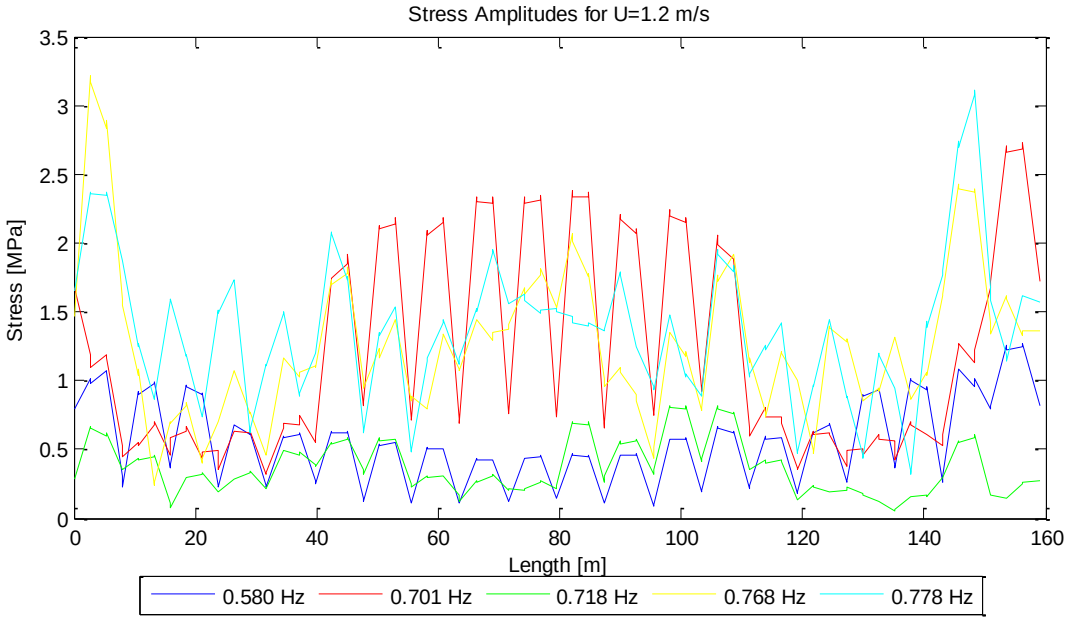
Stress Amplitudes for U=1.2 m/s
Stress [MPa]
Length [m]
0.580 Hz
0.701 Hz
0.718 Hz
0.768 Hz
0.778 Hz

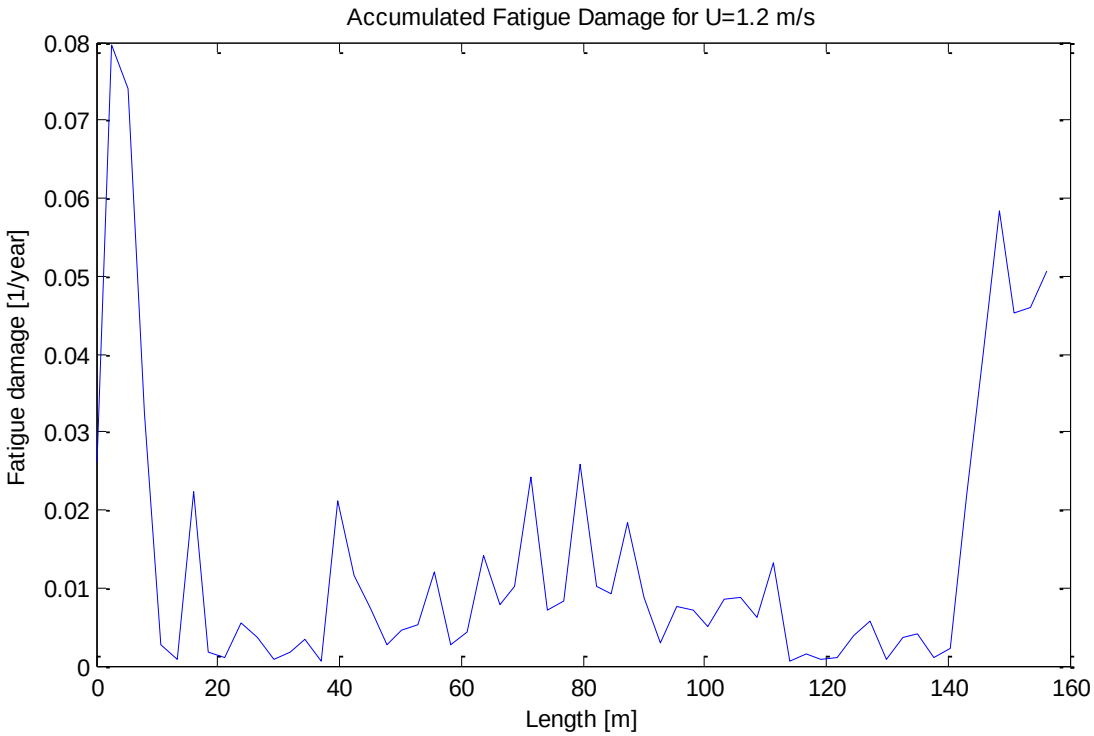
Accumulated Fatigue Damage for U=1.2 m/s
Fatigue damage [1/year]
Length [m]
0.08
0.07
0.06
0.05
0.04
0.03
0.02
0.01
0
0
20
40
60
80
100
120
140
160

B6 Case 6: U=1.3 m/s

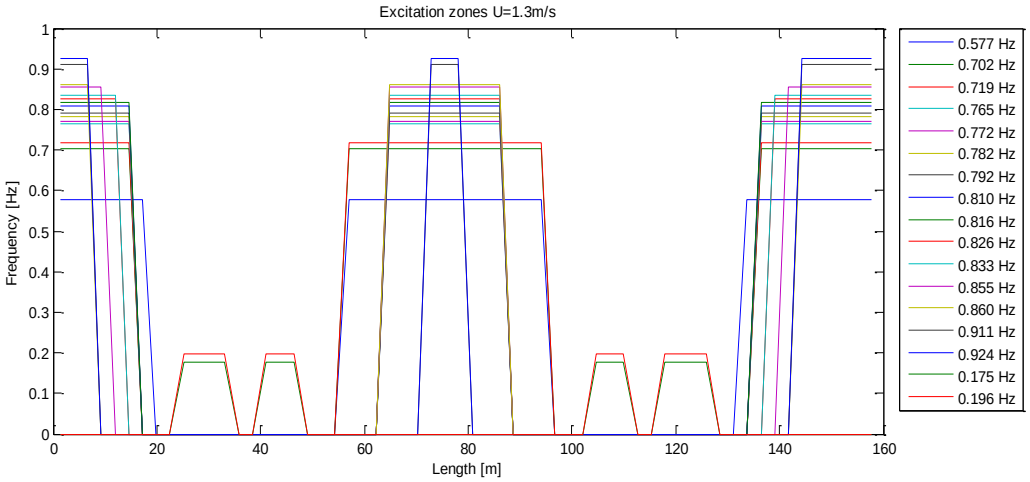

Table 0-5 Excitation frequencies for U=1.3 m/s

Frequency number	Frequency [Hz]	Duration [%]
3	0.577	14.3
4	0.702	9.6
5	0.719	9.1
6	0.765	7.4
7	0.772	7.2
8	0.782	7.0
9	0.792	6.8
10	0.810	6.3
11	0.816	6.2
12	0.826	5.7
13	0.833	5.6
14	0.855	4.9
15	0.860	4.5
16	0.911	2.7
17	0.924	2.5
1	0.176	0.2
2	0.196	0.2

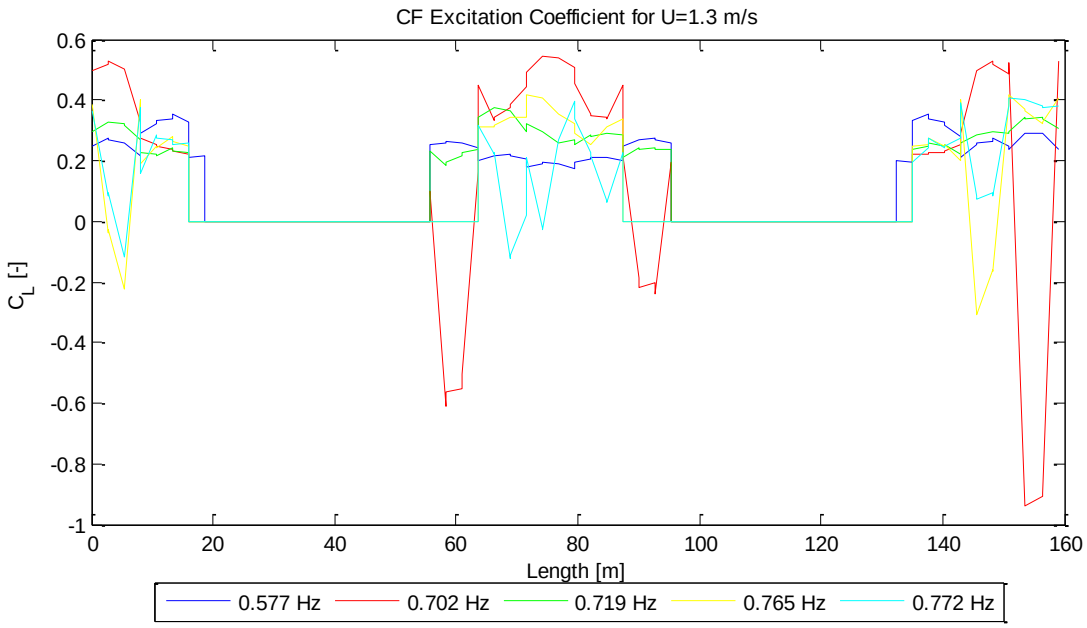
CF Excitation Coefficient for U=1.3 m/s
C_L [-]
Length [m]
0.577 Hz
0.702 Hz
0.719 Hz
0.765 Hz
0.772 Hz

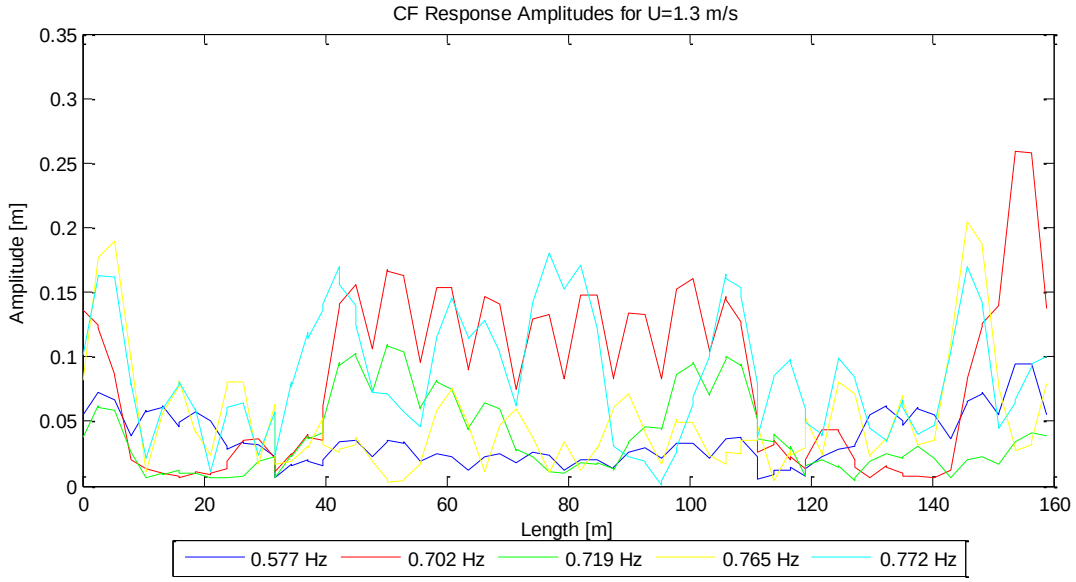
CF Response Amplitudes for U=1.3 m/s
Amplitude [m]
Length [m]
0.577 Hz
0.702 Hz
0.719 Hz
0.765 Hz
0.772 Hz

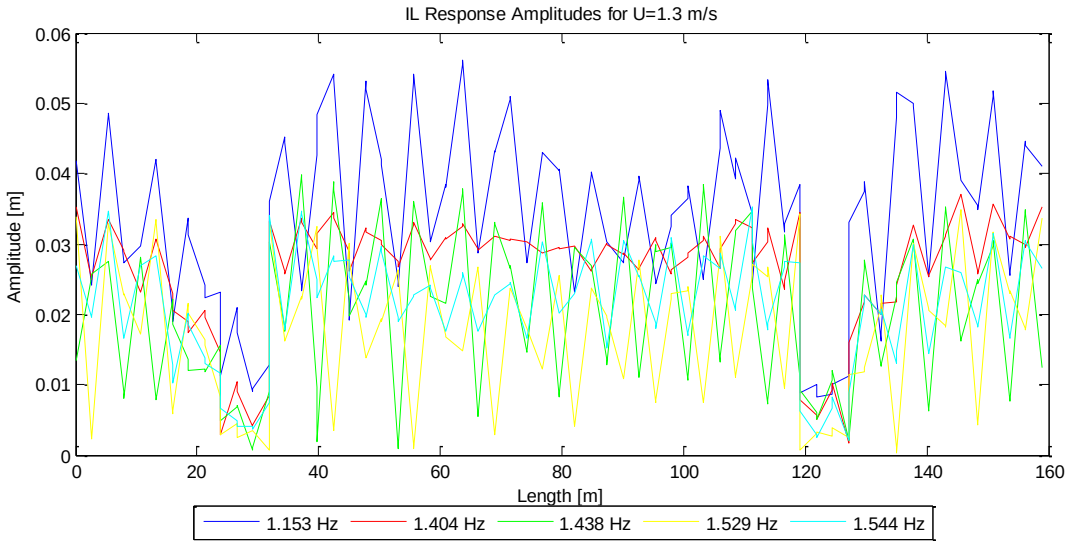
IL Response Amplitudes for U=1.3 m/s
Amplitude [m]
Length [m]
1.153 Hz
1.404 Hz
1.438 Hz
1.529 Hz
1.544 Hz

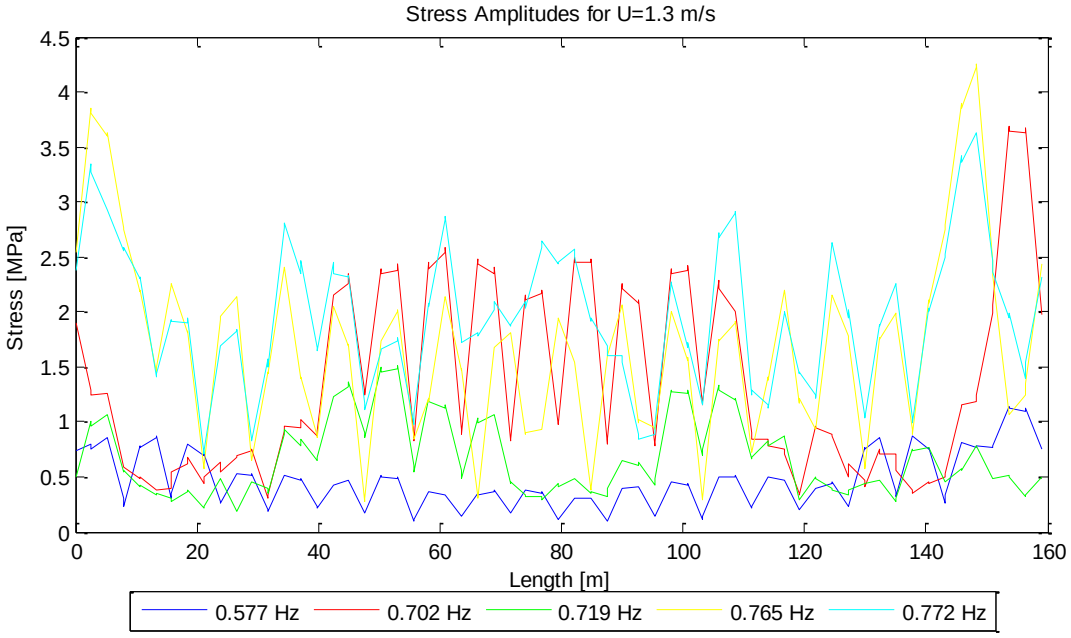
Stress Amplitudes for U=1.3 m/s
Stress [MPa]
Length [m]
0.577 Hz
0.702 Hz
0.719 Hz
0.765 Hz
0.772 Hz

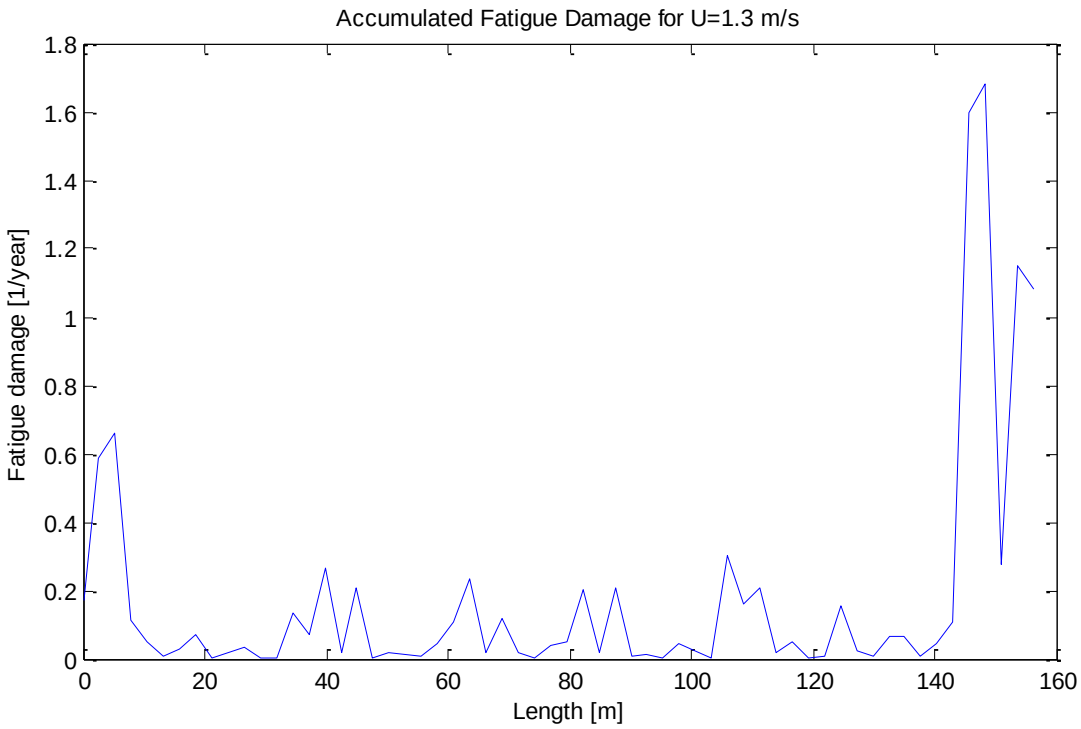
Accumulated Fatigue Damage for U=1.3 m/s
Fatigue damage [1/year]
Length [m]
0
0.2
0.4
0.6
0.8
1
1.2
1.4
1.6
1.8
0
20
40
60
80
100
120
140
160

B7 Case 7: U=1.4 m/s

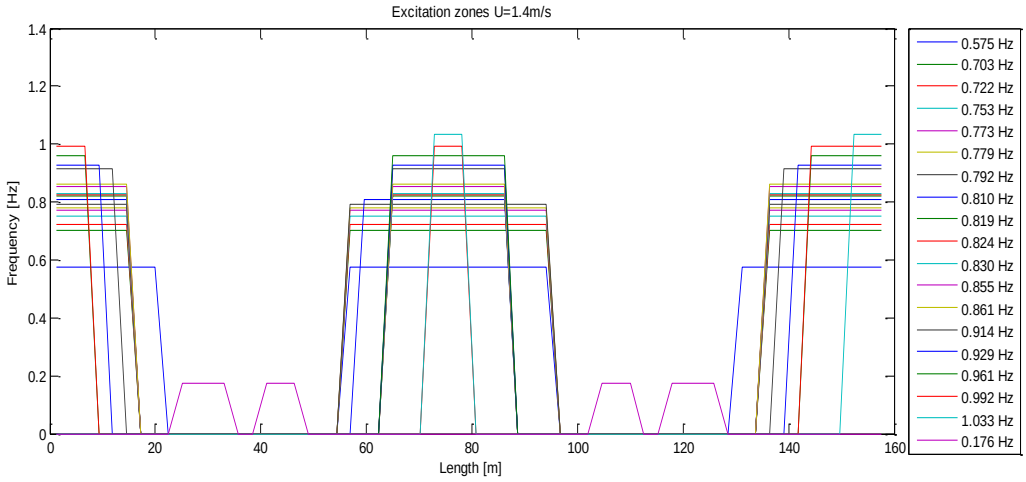

Table 0-6 Excitation frequencies for U=1.4 m/s

Frequency number	Frequency [Hz]	Duration [%]
3	0.575	12.1
4	0.703	8.0
5	0.722	7.7
6	0.753	7.1
7	0.773	6.8
8	0.779	6.6
9	0.792	6.4
10	0.810	5.8
11	0.819	5.6
12	0.824	5.5
13	0.830	5.4
14	0.855	5.0
15	0.861	4.9
16	0.914	3.9
17	0.929	3.5
18	0.961	2.9
19	0.992	1.9
20	1.033	0.8
1	0.176	0.1
2	0.197	0.1

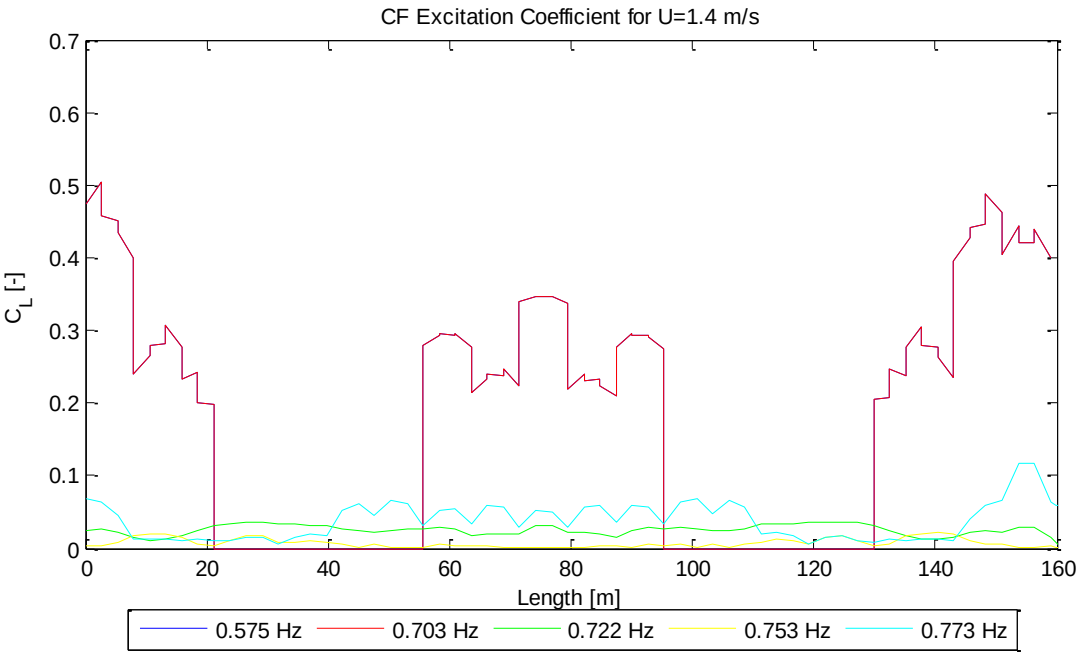
CF Excitation Coefficient for U=1.4 m/s
C_L [-]
Length [m]
0.575 Hz
0.703 Hz
0.722 Hz
0.753 Hz
0.773 Hz

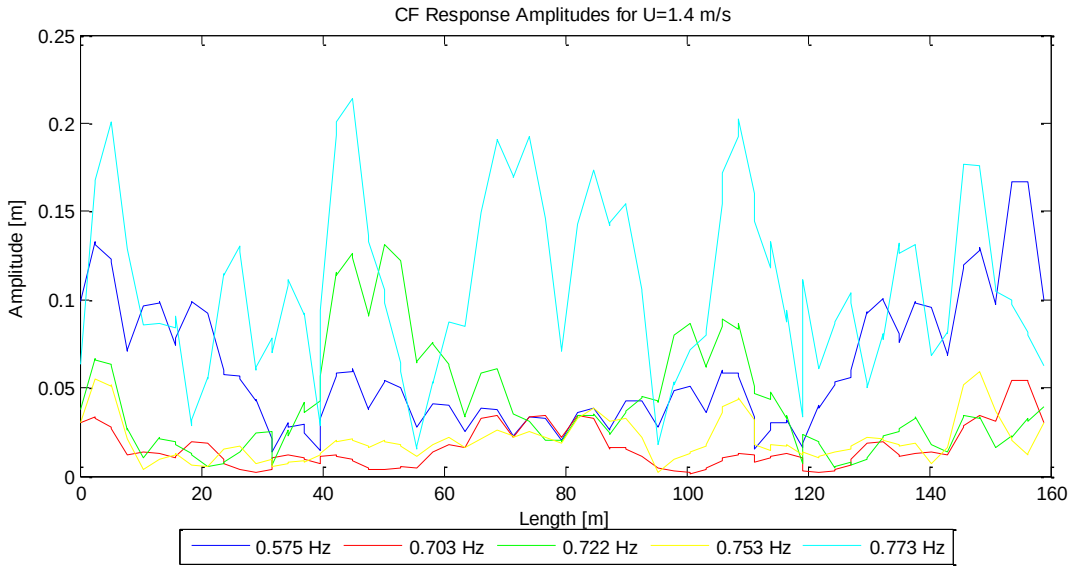
CF Response Amplitudes for U=1.4 m/s
Amplitude [m]
Length [m]
0.575 Hz
0.703 Hz
0.722 Hz
0.753 Hz
0.773 Hz

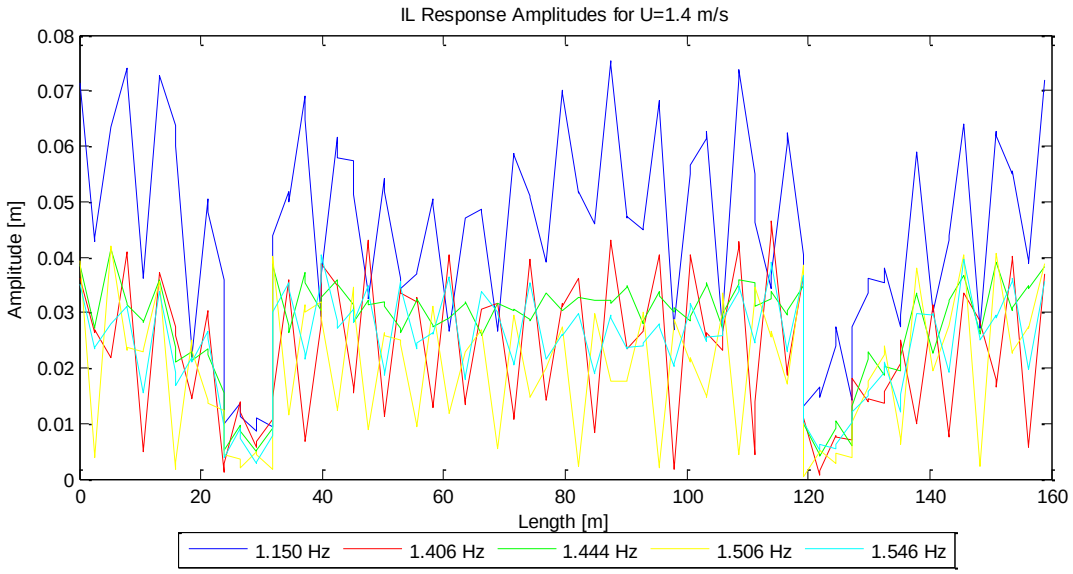
IL Response Amplitudes for U=1.4 m/s
Amplitude [m]
Length [m]
1.150 Hz
1.406 Hz
1.444 Hz
1.506 Hz
1.546 Hz

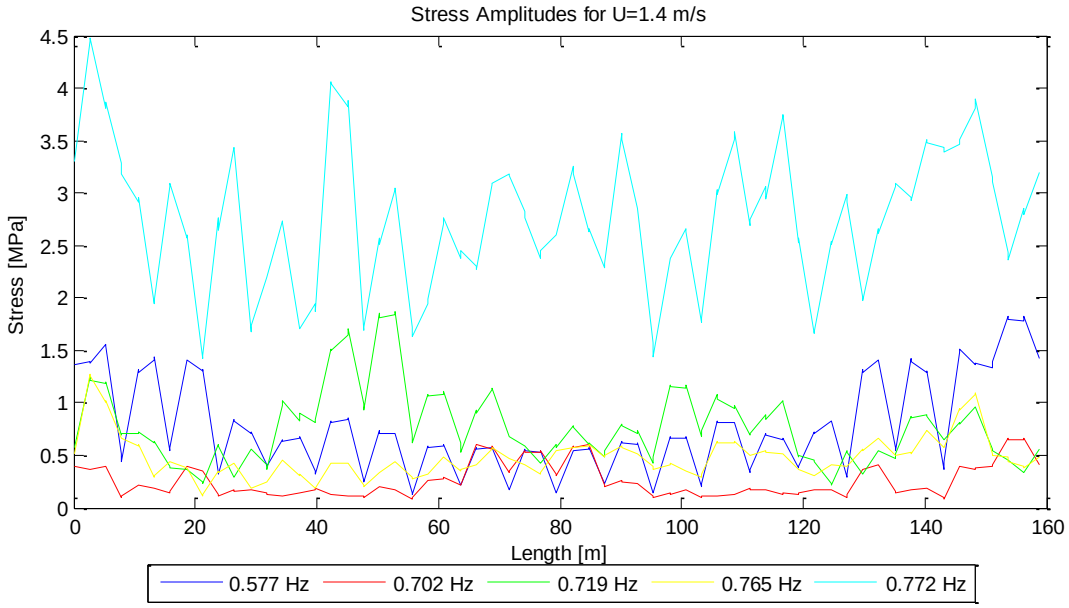
Stress Amplitudes for U=1.4 m/s
Stress [MPa]
Length [m]
0.577 Hz
0.702 Hz
0.719 Hz
0.765 Hz
0.772 Hz

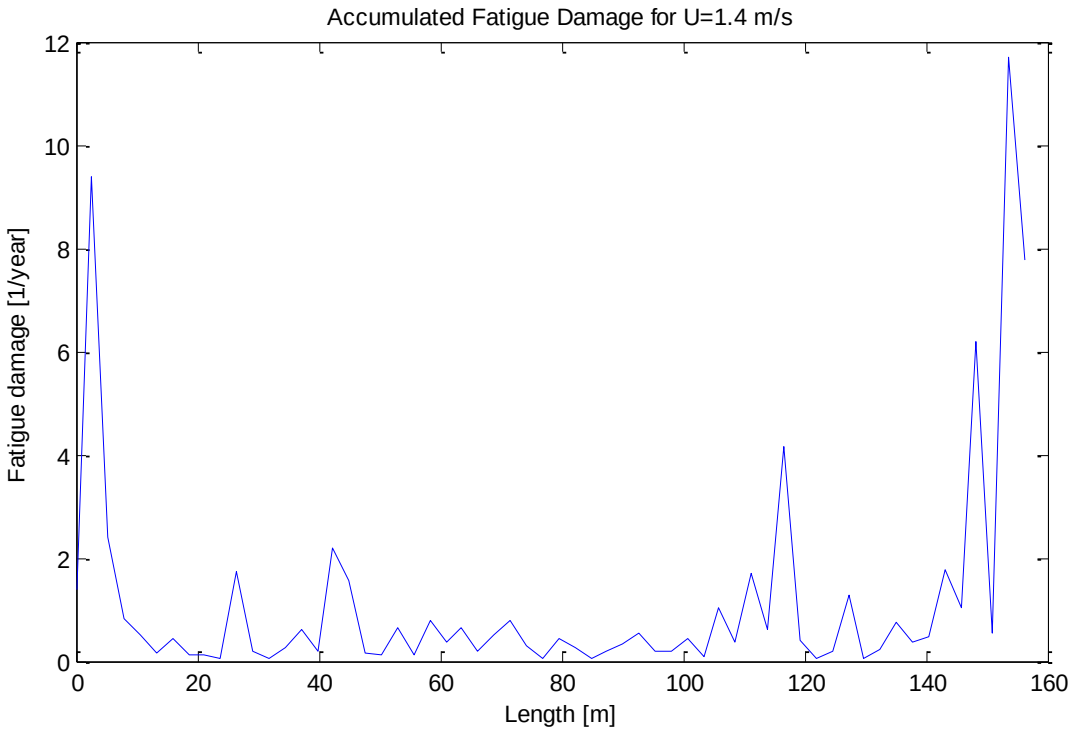
Accumulated Fatigue Damage for U=1.4 m/s
Fatigue damage [1/year]
Length [m]
0
2
4
6
8
10
12
0
20
40
60
80
100
120
140
160

C Problems with VIVANA

VIVANA has recently been implemented in SIMA. Several problems with the software have occurred during the period of working on this thesis. Many problems were solved when a new version of SIMA (3.1.1.12020) was released in beginning of March 2015. Problems were still discovered in the current version. Some of them are listed below, and they were all reported to MARINTEK.

User manual:

The SN curve description is no longer valid and should be updated.

Current:

$$Slope = \frac{\log N_2 - \log N_1}{\log S_2 - \log S_1} \qquad (slope\ is\ always\ negative)$$

Should be changed to:

$$Slope = \frac{\log N_1 - \log N_2}{\log S_2 - \log S_1} \qquad (slope\ is\ always\ positive)$$

Time sharing, fatigue calculation:

For the consecutive analysis option (time-sharing), it is not possible to specify elements of the structure to calculate fatigue. This is possible in the concurrent (space sharing) option. However, if an element is specified in the space sharing option, and the analysis is changed to time-sharing, the analysis will be interrupted, and a cryptic error message will appear. To solve this, the elements specified in the space sharing fatigue calculation were removed, and the analysis was changed back to time-sharing.

Constant added mass:

There is a conflict between the added mass coefficients given for the cross sections in inpmod, and the constant added mass specified in VIVANA. To obtain a response frequency equal to the eigenfrequency for VIV response, the added mass coefficients in inpmod and VIVANA should be similar. It is not enough to only define a constant added mass in VIVANA.

In-line added mass:

When the added mass iterations for in-line response were performed, it occurred that the added mass range became negative, and the analysis was interrupted. This can probably be explained by different structure properties in the IL and CF direction.

Post processing:

Not possible to write results from VIVANA to .xls files.

Identification of active eigenfrequencies:

There is probably a problem with how VIVANA identifies possible excitation frequencies. This problem is likely to occur due to the ring structure. The ring structure has different properties than a normal riser, and VIVANA may not account for that.